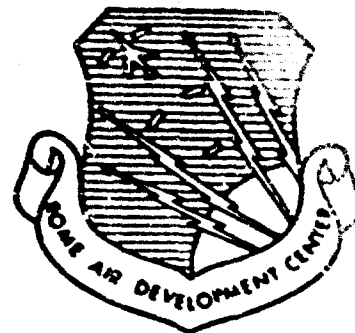


RADC-TR-64-543
Final Report



AD 615905

**FREQUENCY SELECTIVE LIMITER USING
NUCLEAR MAGNETIC RESONANCE**

Roger W. Orth
Darrell R. Jackson
Glenn B. Coughlan
(Boeing Company)

TECHNICAL REPORT NO. RADC-TR-64-543
April 1965

2 3 4.00 1.00 14.90

DDC
JUN 7 1965

**Communications Techniques Branch
Rome Air Development Center
Research and Technology Division
Air Force Systems Command
Griffiss Air Force Base, New York**

ARCHIVE COPY

**Best
Available
Copy**

PAGES _____
ARE
MISSING
IN
ORIGINAL
DOCUMENT

When US Government drawings, specifications, or other data are used for any purpose other than a definitely related government procurement operation, the government thereby incurs no responsibility nor any obligation whatsoever; and the fact that the government may have formulated, furnished, or in any way supplied the said drawings, specifications, or other data is not to be regarded by implication or otherwise, as in any manner licensing the holder or any other person or corporation, or conveying any rights or permission to manufacture, use, or sell any patented invention that may in any way be related thereto

If this copy is not needed, return to Rome Air Development Center, Attn: EMCTN-2, Griffiss AFB, New York, 13442.

**FREQUENCY SELECTIVE LIMITER USING
NUCLEAR MAGNETIC RESONANCE**

**Roger W. Orth
Darrell R. Jackson
Glenn B. Coughlan**

FOREWORD

This final technical report was prepared under Contract No. AF30 (602)-3407 by the Boeing Company, Aero-Space Division, Seattle, Washington.

The project engineer was John R. Martin, EMTN. The project number was 4519 and the task number was 451902.

This technical report has been reviewed and is approved.

Approved:

John R. Martin
JOHN R. MARTIN
Project Engineer

Approved:

T. P. Swanson
T. P. SWANSON
Colonel, USAF
Chief, Communications Division

FOR THE COMMANDER:

Irving J. Gabelman
IRVING J. GABELMAN
Chief, Advanced Studies Group

ABSTRACT

This report describes the experimental and theoretical investigation directed toward development of a frequency selective limiter using nuclear magnetic resonance. This effort was carried out from April 23 to November 26, 1964 and was supported by Rome Air Development Center under Contract AF 30(602)-3407.

The report reviews principles of operation of the device and describes developments carried out under the contract. The principal accomplishments were as follows: The circuit and quantum mechanical theory of the device was extended and refined. The magnetic properties required to obtain frequency selective limiting over a band of frequencies were determined. Expressions for insertion loss and limiting threshold were derived. The amount of intermodulation and signal suppression was calculated as a function of the interference and signal power levels and the frequency separation between them. The effectiveness of the limiter in suppressing several types of interfering signals was analyzed and an experimental model of a frequency selective limiter operating at 30 mc/sec was designed, constructed and tested.

The performance goals set in the contract were essentially reached with the exception of the bandwidth of the device. The experimental development indicated that great care must be taken to assure stability of the device; as a result of this laboratory work, several techniques have evolved which can reduce stability problems in future limiter designs.

The program confirmed that CW interference can be suppressed without significantly affecting a desired signal which is removed in frequency by only a few cycles per second. It was verified experimentally that the extreme case of limiting, in which an interfering signal was 30 db above a desired signal, required a frequency separation of no more than 64 cps between the two signals to assure negligible intermodulation and suppression of the desired signal.

TABLE OF CONTENTS

		<u>Page</u>
1.0	Introduction	1
2.0	Principle of Operation	3
	2.1 Types of Limiting	3
	2.2 Magnetic Resonance Phenomena	5
	2.3 Frequency Selective Limiting Circuit	8
3.0	Determination of Magnetic Properties	13
	3.1 Bandwidth Enhancement (reactive compensation)	17
	3.2 Physical Realization of Spin Distribution	17
	3.3 Imbalance Impedance of Re-Entrant Cavities	17
4.0	Circuit Theory	18
	4.1 Insertion Loss	18
	4.2 Optimum Cavity Design	20
	4.3 Saturation Level	24
5.0	Intermodulation	25
6.0	Analysis of Limiter Performance	30
	6.1 Steady State Analysis	30
	6.2 Transient Response	36
7.0	Experimental Results	39
	7.1 Bandwidth and Limiting Range	39
	7.2 Insertion Loss	45
	7.3 Saturation Level	45
	7.4 Selectivity and Intermodulation	48
	7.5 Limiter Configuration	52

	<u>Page</u>
8.0	
Conclusions and Recommendations	56
Bibliography	58
Appendices	59

APPENDICES

		<u>Page</u>
I	Imbalance Impedance of Re-Entrant Cavity	59
II	Optimum Cavity Design	66
III	Diffusion Effects	68
IV	Intermodulation	70
V	Coherent Interference Suppression	82
VI	Transient Response	90
VII	Characteristic of Absorbing Sample	108
VIII	Coupling to Sample	115
IX	Limiting Characteristics	119
X	Saturation Level	129
XI	Selectivity and Intermodulation	131
XII	Noise Figure of the Limiter	132

LIST OF ILLUSTRATIONS

<u>Figure</u>		<u>Page</u>
1	Comparison of Ordinary Limiter and Frequency Selective Limiter	4
2	Absorption Process	6
3	Variation of Resonant Absorber Resistance with Current	9
4	Typical Limiter Circuit	10
5	Absorption with Shifted Particle Resonances	12
6	Relative Imbalance Impedance due to Spins in a Uniform Magnetic Field	14
7	Resistive and Reactive Bridge Imbalance for Rectangular and Compensated Distributions	15
8	Cavity and DC Field Configuration	16
9	Relative Magnitude of Imbalance of Coaxial Cavity due to Spin System	22
10	Re-entrant Cavity Circuit	20
11	Equivalent Circuit	20
12	Thevin Equivalent Circuit	21
13	Insertion Loss vs. Bandwidth for Uncooled Limiter	23
14	Intermodulation Power with Two Large Signals	27
15	Intermodulation with One Signal below Saturation and One Signal above Saturation	28
16	Suppression of Small Signal in Vicinity of Large Signal	29
17	Model Signal and Interference Spectra	31
18	Improvement in Interference/Signal Ratio Using Limiter with cw Interference	33

<u>Figure</u>		<u>Page</u>
19	Output Interference/Signal Ratio vs. Interference Bandwidth	34
20	Envelope of FSL Output for Switched cw Input	38
21	Block Diagram of System used to Measure Reactive Imbalance (FSL Bandwidth)	40
22	Measured Reactive Imbalance	42
23	Experimental Limiting Curves	43
24	Block Diagram of System Utilized in Measuring Limiting Curves	44
25	DC Magnetic Field Contours	46
26	Block Diagram of System Used to Measure Insertion Loss	47
27	Block Diagram of System used to Measure Selectivity of FSL	49
28	Block Diagram of System used to Measure Intermodulation	50
29	Intermodulation vs. Frequency Separation	51
30	Frequency Selective Limiter	53
31	Complete Limiter Circuit	56
32	Magnetic Field Components in Rotating Frame	70
33	Pole-Zero Plot	76
34	Poles in S-Plane	97

LIST OF SYMBOLS

z	Outer radius of re-entrant cavity
a_1, a_2, a_3, a_4	Constants
A, A_1, A_2, A_3	Constants
b	Inner radius of re-entrant cavity
b_1, b_2	Constants
B, B_1, B_2	Constants
B_S	Signal Bandwidth
B_I	Interference Bandwidth
C_1, C_2	Constants
D	$\sqrt{\omega_{rf}^2 + \Delta\omega^2}$
D_1, D_2	Constants
D_a	$\sqrt{\omega_{rf}^2 + (\omega_a - \omega)^2}$
D_b	$\sqrt{\omega_{rf}^2 + (\omega_b - \omega)^2}$
e	2.71828
\mathcal{E}	Mean square error
f_0	Larmor frequency
f_m	Modulation frequency of jamming signal
$S(\omega)$	Spin distribution function
$G_0(\omega)$	Signal power spectral density
$G_I(\omega)$	Interference power spectral density
$h(t^2)$	Inverse Fourier transform of $H(\omega)$
H_0	DC magnetic field
H_1	RF magnetic field at ω_1
H_2	RF magnetic field at ω_2
H_c	DC magnetic field at center of re-entrant cavity
H_{rf}	RF magnetic field
$H_{(s)}$	Limiter transfer function

j	$\sqrt{-1}$
k	Boltzman's constant
l	Mean free path between collisions
L	Length of re-entrant cavity
m	Mobility
$m_x(s), m_y(s), m_z(s)$	Laplace transforms of magnetization components
\vec{M}	Magnetization vector
M_0	Saturation magnetization
M_x, M_y, M_z	Components of magnetization
$M_{xn}, M_{yn}, M_{zn}, M_{tn}$	Fourier components of the magnetization
N	Integer
P_1	Power at ω_1
P_2	Power at ω_2
P_K	Power at ω_K
P_I	Total interference power input
P_S	Total signal power input
P_T	Total power absorbed by spin system
P_{IO}/P_{SO}	Effective interference-to-signal ratio (output)
P_{sat}	Saturation power
P_{walls}	Wall losses in re-entrant cavity
Q	Quality factor
$Q(\omega)$	Approximate signal power spectral density
Q_0	Unloaded cavity Q
r	Radius
r_a	Absorber equivalent parallel resistance
r_0	Equivalent parallel resistance of cavity (copper loss)
r_{un}	Inter-nuclear spacing
R_a	Absorber equivalent series resistance
R_0	Equivalent series resistance of cavity (copper loss)
t	Time
T	Temperature

T_1	Longitudinal relaxation time (spin lattice relaxation time)
T_2	Transverse relaxation time (Inverse linewidth, small signal case)
T_{21}	Inverse linewidth seen at ω_1
T_{22}	Inverse linewidth seen at ω_2
$U_{(t)}$	Unit step
$v_1^i(t)$	i^{th} member of the input interference voltage ensemble
$v_s^i(t)$	i^{th} member of the input signal voltage ensemble
$v_o^i(t)$	i^{th} member of the output voltage ensemble
$v(t)$	$M_x(t) - M_o$
V	Limiter output voltage at ω
$\hat{x}, \hat{y}, \hat{z}$	Unit vectors
X_a	Absorber equivalent reactance
α	Constant
β	Constant
γ	Gyromagnetic ratio
δ	Frequency separation in radians
δ_{on}	Kronecker delta
$\delta(x)$	Dirac delta function
ϵ_r	Relative dielectric constant
η	Viscosity
μ_h	Nuclear magnetic moment
ρ	Spin density per unit volume
τ	$T_1 = T_2 = \tau$
ω	Frequency in radians
ω_a	Larmor frequency at lower edge of spin distribution
ω_b	Larmor frequency at upper edge of spin distribution
ω_o	γH_o
ω_c	γH_c
ω_{Hf}	γH_{Hf}
ω_k	Frequency of k^{th} interference component
Ω	A complex frequency parameter
Ω'	A normalized complex frequency parameter

EVALUATION

The contractual effort proved the feasibility of frequency selective limiting using nuclear magnetic resonance. The program refined the theory of operation and demonstrated the operation of a 30 MC frequency selective limiter.

The principal accomplishments were as follows:

(a) The magnetic properties required to obtain frequency selective limiting over a band of frequencies were determined.

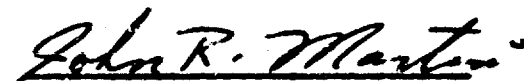
(b) Expressions for insertion loss and limiting threshold were determined. The insertion loss encountered was higher than the design goals. Proper impedance matching could account for some of this loss.

(c) The amount of intermodulation and signal suppression was calculated as a function of the interference, signal power levels and frequency separation. The contractual effort confirmed that CW interference can be suppressed without affecting a desired signal removed by two or three cycles. Small signal selectivity surpassed the design goals of the limiter. For large interfering signals 30 db above a desired signal required a frequency separation of 64 cycles to assure negligible intermodulation and suppression of desired signals.

(d) The contractual effort indicated that a problem area exists in the stability of the limiter. Stability can be corrected by better temperature control and the selection of material for capacitive loading of the cavity to assure maximum stability.

(e) The bandwidth of the limiter presented a problem in that obtaining a smooth DC magnetic gradient perpendicular to the limiter while maintaining a constant magnetic field in the longitudinal direction was impossible with the pole faces and cavity dimensions utilized. A 1.8 KC bandwidth was obtained and compared favorably with expectations.

Future programs should concentrate on reducing insertion loss, size, and increasing bandwidth and better stabilization. The frequency selective limiter concept could be utilized in any communications channel where vulnerability to CW interference may be a problem in or out of the pass band of information.



JOHN R. MARTIN
Aero Space Comm Unit
Narrow Band Trans Section
Communications Division

1.0 INTRODUCTION

This report presents a complete exposition of the development, both analytical and experimental, of a frequency selective limiter.

The Boeing Company has carried out research for two years on HF frequency selective limiters utilizing nuclear magnetic resonance and more recently on microwave limiters utilizing electron spin resonance. This work has been directed toward formulating the theory and establishing the feasibility of developing these devices.

The objective of the program carried out under this contract was to refine the theory and demonstrate the operation of a 30 mc frequency selective limiter with certain specified characteristics.

In the following section the principles of operation of such a limiter are discussed in moderate detail. Subsequent sections discuss the design and performance calculations for a frequency selective limiter. The report concludes with a description of the device and a discussion of experimental results obtained on a prototype frequency selective limiter. Finally, recommendations and conclusions are presented.

The frequency selective limiter in its various forms offers (1) protection against narrow band interference, and (2) a means of signal equalization in a multiple access repeater. In both these applications the unique characteristic of the frequency selective limiter is that it limits strong signals without generating significant intermodulation products.

The prototype frequency selective limiter developed under this contract is particularly suited to reduction of coherent interference. The use of such a device complements conventional spread-spectrum anti-jam techniques since many such systems are vulnerable to cw interference. For instance, if the power spectral density of a coded signal is not uniform over the signal bandwidth, jamming may be best achieved by concentrating the jamming power in the frequency region where maximum signal power exists. Also,

a spread-spectrum system can be jammed by cw signals strong enough to cause saturation of the receiver. In both of these situations the frequency selective limiter will provide substantial protection because it can selectively attenuate several large interfering signals within a communication channel while passing essentially all frequency components of small desired signals. Interfering signals will be automatically limited at any frequency within the system bandwidth. No a priori knowledge of the frequency of the interfering signal or signals is required, and, indeed, limiting will occur even though the interfering signal changes frequency.

2.0

PRINCIPLE OF OPERATION

2.1

Types of Limiting

The frequency selective limiter is an anti-interference device with the ability to selectively attenuate large signals while passing small desired signals. This action differs from that of ordinary limiters in which a strong interaction results in the generation of spurious power within the signal passband as well as possible suppression of the desired signal.

The disadvantages of conventional limiters are circumvented by the frequency selective limiter which utilizes a limiting mechanism which is extremely selective in frequency. This mechanism, using proton magnetic resonance, derives its selectivity from the extremely high Q (up to 10^6) of these resonances. With this new device it is possible to limit strong interfering signals within a communication channel without significantly affecting the desired signal. This has not been possible in the past.

The operation of an ideal frequency selective limiter is illustrated in Figs. 1A and 1C. These figures show the combined power spectrum of a weak signal (solid lines) and a strong interfering signal (dotted lines) before and after passage through an ideal frequency selective limiter. The operation of this limiter is such that any spectral component of the total input signal (desired signal plus interference) whose power exceeds the threshold level will be attenuated until its power is equal to the threshold power. Any spectral component that lies below the threshold is essentially unaffected and passed through the limiter without distortion. In contrast to this, Fig. 1B shows the effect of an ordinary limiter on a signal containing a large amount of interference. In this case, the interfering power is limited, but at the same time severe cross-modulation takes place between signal and interference.

In the example of Fig. 1C, the signal-to-interference ratio has been greatly improved after passage through the frequency selective limiter; in fact, a large increase in

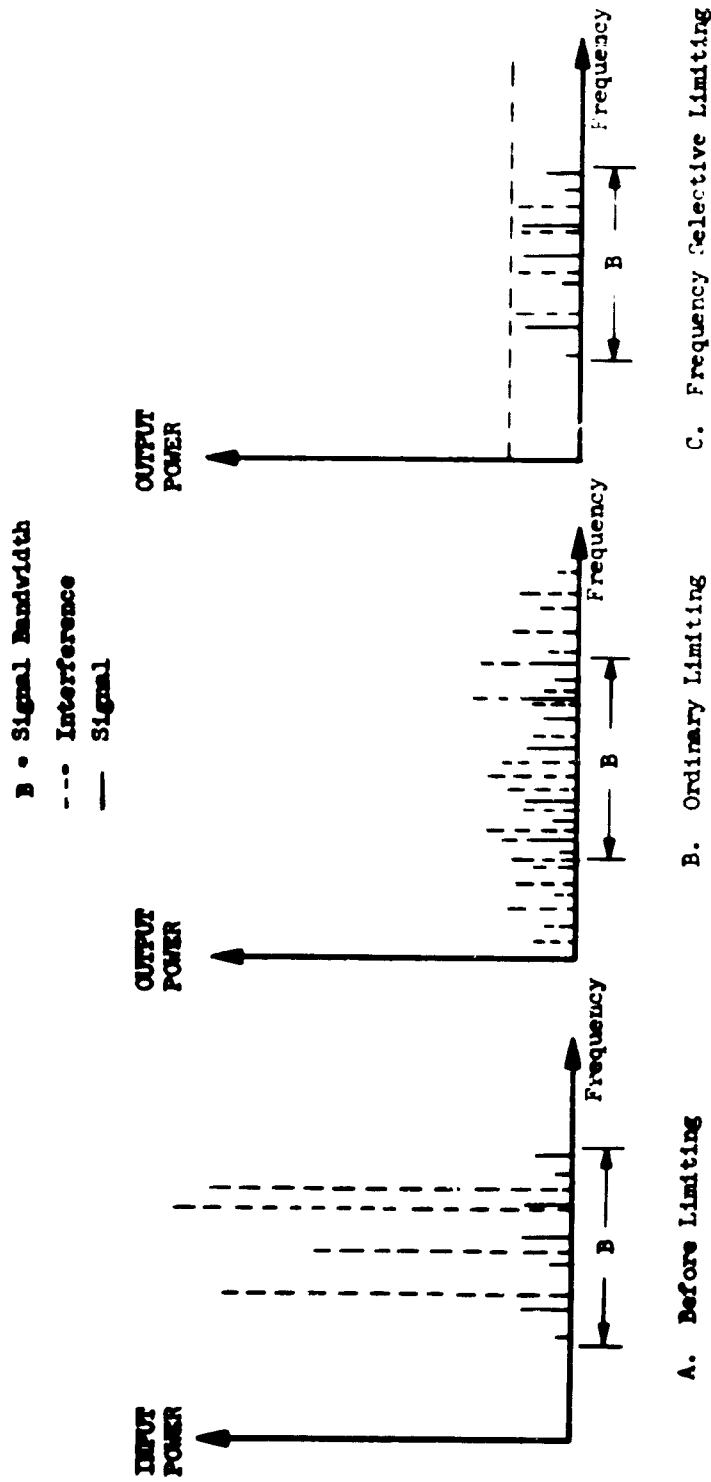


Fig. 1. Comparison of Ordinary Limiter and Frequency Selective Limiter

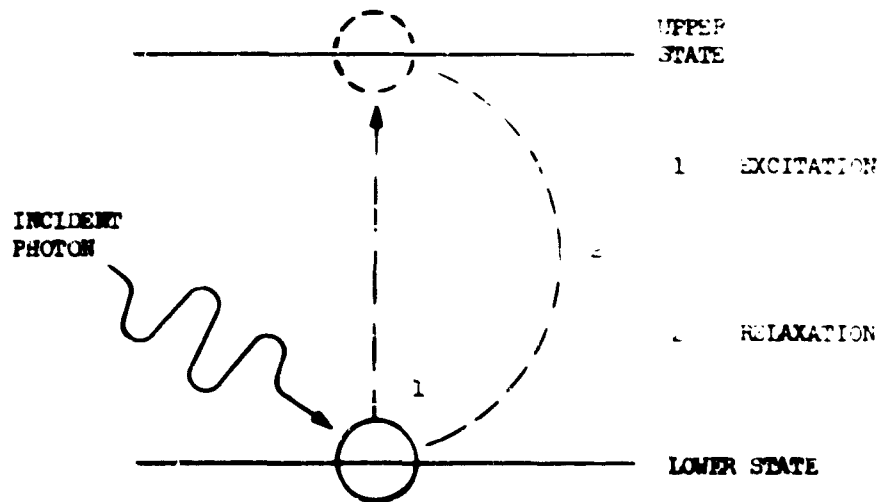


Fig. 2. Absorption Process

(hydrogen nucleus) in a sample of water will contribute its excess energy to the kinetic energy of surrounding water molecules. The energy transfer occurs randomly in an average time usually referred to as the spin-lattice relaxation time. The spin-lattice relaxation time might be measured experimentally by applying a pulse of photons and observing the time required for the system to return to thermal equilibrium with the bulk material.

Consider now the behavior of a system of such particles as a function of electromagnetic field strength. At low power levels, excitation of a particular electron or proton occurs only occasionally, because of the low density of incident photons. The absorbing particles will have ample time to return to thermal equilibrium between successive excitations, and as a result, the whole system will remain at thermal equilibrium. Under such conditions, absorbed power is proportional to incident power and the substance behaves as a linear resistive absorber. If, however, incident power is increased to a point where the mean time between excitations is less than the relaxation time, thermal equilibrium will be destroyed, and the absorptive ability of the substance will decrease. This decrease occurs because a greater number of particles now occupies the higher energy state where photon absorption is impossible. For power levels above threshold, the material behaves as a nonlinear absorber whose loss tangent decreases as incident power increases.

There are a great number of materials that may be suitable for use as absorbers. For a material to exhibit proton resonance, it must contain hydrogen atoms in its molecular structure. Some common substances showing strong proton resonance and narrow line width are water, ethyl alcohol, kerosene, and transformer oil. The protons in heavier atoms do not resonate as individual units; rather the nucleus as a whole resonates. Since this resonance is usually much weaker than that due to "free" protons, it is not as suitable for this application. To achieve limiting, the absorbing material must be contained in a structure that resonates electrically at the natural absorption frequency of the material. For a given incident power,

photon density is very high in such a structure, greatly enhancing the absorptive ability of the substance. This resonator may be represented as a series coil-capacitor combination, as shown in Fig. 3. At resonance this circuit may be represented by a nonlinear resistor whose resistance (R_a) decreases with current for currents above some threshold value. In Fig. 3, the effective resistance is illustrated as a function of current. A more rigorous description of magnetic resonance would show that there is a reactance associated with absorption as well as a resistance. This reactance may be ignored under certain conditions, so only R_a will be considered here. (The effects of the reactance are discussed in Section 3.0.)

It must be emphasized that the resonance is very selective in nature and the center frequency is established by the external dc magnetic field. The discussion thus far has described a nonlinear circuit element. The frequency selective limiter circuit which uses this element will now be described.

2.3 Frequency Selective Limiting Circuit

The frequency selective limiter circuit is basically an r-f bridge, one arm of which contains an absorbing substance. To ensure symmetry, the opposing bridge arm is constructed identically, even to the point of containing a substance identical to that of the absorbing arm. The only difference is that this dummy arm is not immersed in a dc magnetic field. A typical limiter circuit is shown in Fig. 4. Two identical resonant circuits are shown. The absorption resistance, R_a , in the absorber arm unbalances the bridge. Thus, at low signal levels where the resistance is linear, the signal at the output of the bridge will be linearly proportional to the input signal. However, as the input signal level increases to the point where R_a begins to decrease in value, the bridge will approach a balanced condition and the output signal will be limited. To obtain this performance it is necessary that the resonant frequency of the absorption cell correspond to the frequency of the applied signal; otherwise the reactances associated with the absorption cell mask R_a .

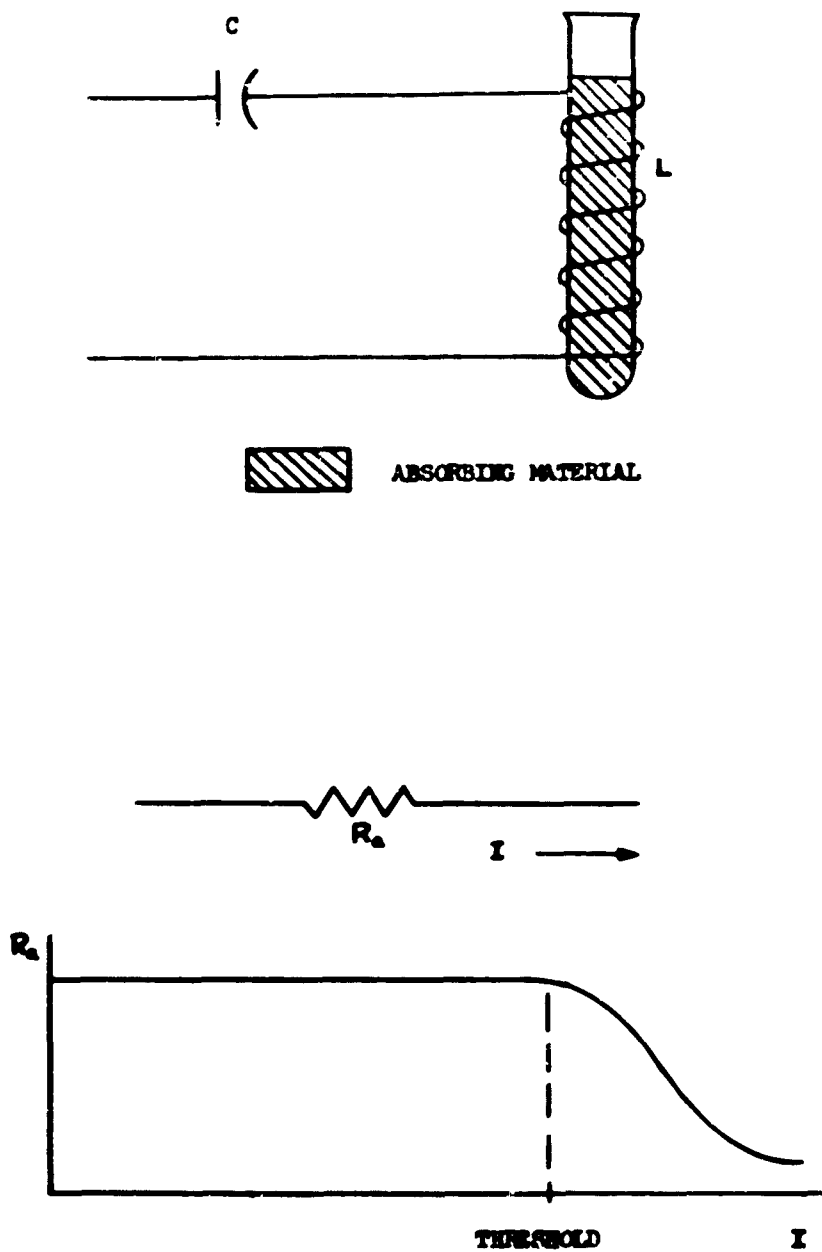


Fig. 3. Variation of Resonant Absorber Resistance with Current.

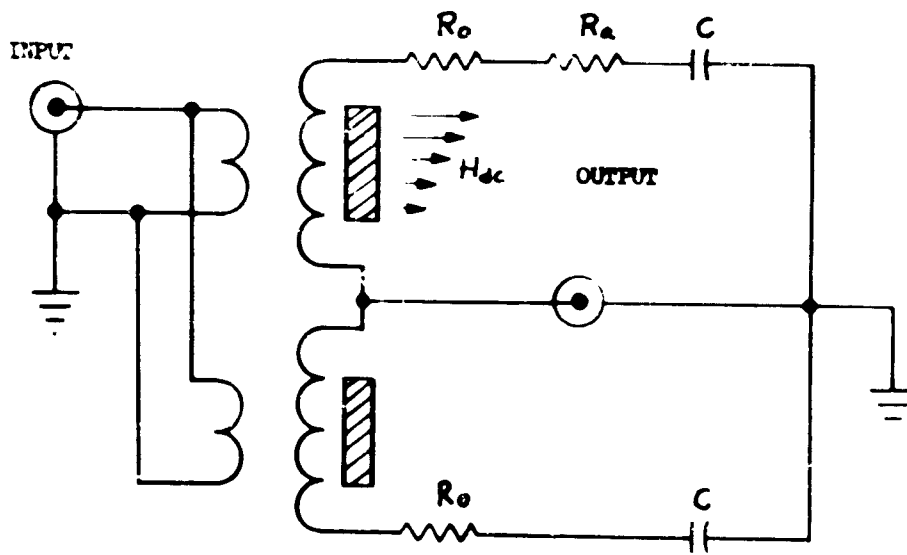


Fig. 4. Typical Limiter Circuit

This circuit will function as an ordinary limiter with no frequency selectivity. That is, if two signals are introduced, they will interact strongly whenever one or both exceed the threshold level, because both outputs depend on the changing magnitude of R_a . An obvious way to achieve partial frequency selectivity would be to combine a large number of narrow-band limiters. If the center frequencies of these limiters were staggered suitably over a band of frequencies, selective limiting would occur within this band. Frequency selectivity would be determined by the bandwidth of the individual circuits, i. e., two signals would not interact as long as their frequency difference exceeded this bandwidth.

A more practical way of achieving the same result is to shift the natural frequencies of the absorbing particles so that each one absorbs at a slightly different frequency. Each particle, with the external circuitry, can then be considered as a separate limiter functioning over the natural bandwidth (line width) of the proton resonance. The total bandwidth of the device will be determined by the frequency shift imposed on the absorbing particles (see Fig. 5).

Frequency shift can be accomplished quite simply by immersing the absorber in a non-uniform magnetic field. This scheme is based on the following relation between resonant frequency, f_0 , and magnetic field strength, H_0 :

$$f_0 = \frac{\gamma}{2\pi} H_0 \quad (1)$$

where

$$\gamma = 2.675 \times 10^4 \text{ rad/sec/gauss for proton resonance.}$$

The resonant frequency is directly proportional to the dc magnetic field strength. A field strength of 7050 gauss corresponds to a resonant frequency of 30 mc for proton resonance. The selectivity of the limiter depends upon the resonance line width of the absorbing material (approximately 1 cycle per second for many liquids). However, the bandwidth depends upon the dc magnetic field inhomogeneity.

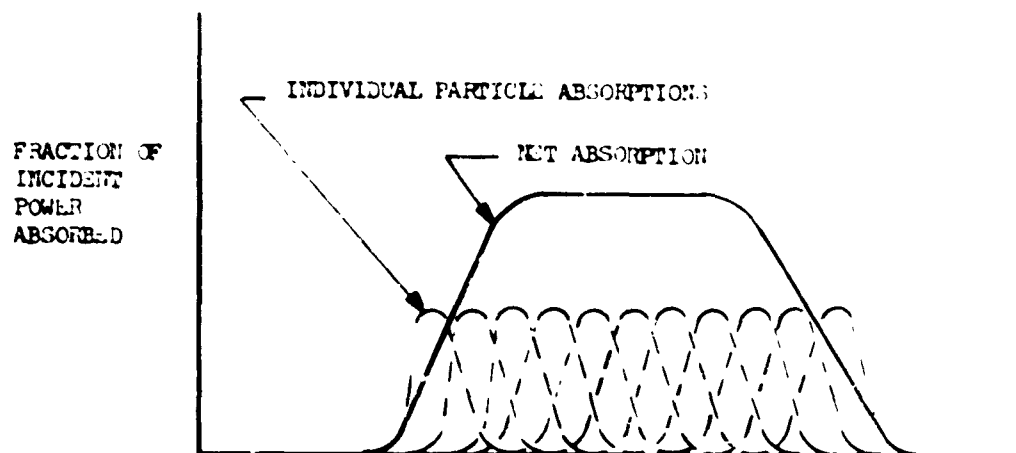


Fig. 5. Absorption with Shifted Particle Resonances

3.0 DETERMINATION OF MAGNETIC PROPERTIES

In the previous section it was mentioned that when magnetic resonance occurs, a reactive as well as a resistive imbalance occurs in the limiter bridge circuit. The reactive imbalance is zero only at the precise center of the magnetic resonance. At frequencies increasingly removed from the center of the resonance, the reactive imbalance increases rapidly.

Limiting is accomplished by the saturation, or decrease, in the resistive imbalance with increasing r-f power level. The reactive imbalance also decreases with increasing power level; however, saturation of the reactive imbalance requires substantially higher r-f power levels than are required to saturate the resistive imbalance. Thus, to achieve limiting at reasonable signal levels, the reactive bridge imbalance must be eliminated at all frequencies within the desired bandwidth of the limiter. The degree to which this "reactive compensation" can be achieved, determines the practical bandwidths over which frequency selective limiting can be obtained. This section is devoted to describing the magnetic properties required to eliminate the reactive imbalance over the required bandwidth. These properties are discussed in Appendix VII.

For a homogeneous dc magnetic field, the real and imaginary parts of the imbalance impedance, Z_a , are plotted in Fig. 6.

As described in the previous section, immersing the spin system in a non-uniform magnetic field results in an inhomogeneously broadened resonance line. For the case of a constant gradient dc magnetic field and a uniform number of spins per unit frequency interval, the reactive and resistive imbalances are shown in Fig. 7. The spreading in the frequency domain is apparent. If limiting over some frequency range between ω_1 and ω_2 is desired, the reactive imbalance must be reduced to a very small value over this same frequency range. Otherwise, the reactive bridge imbalance will "mask" the reduction in resistive imbalance caused by saturation.

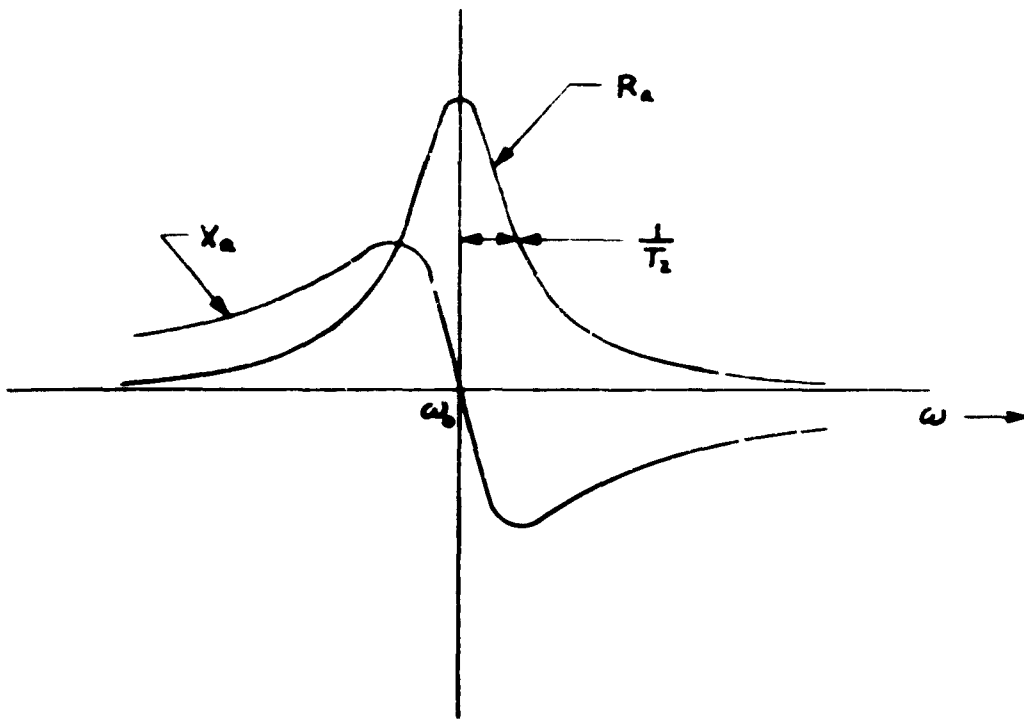


Fig. 6. Relative Bridge Imbalance Impedance due to
Spins in a Uniform Magnetic Field

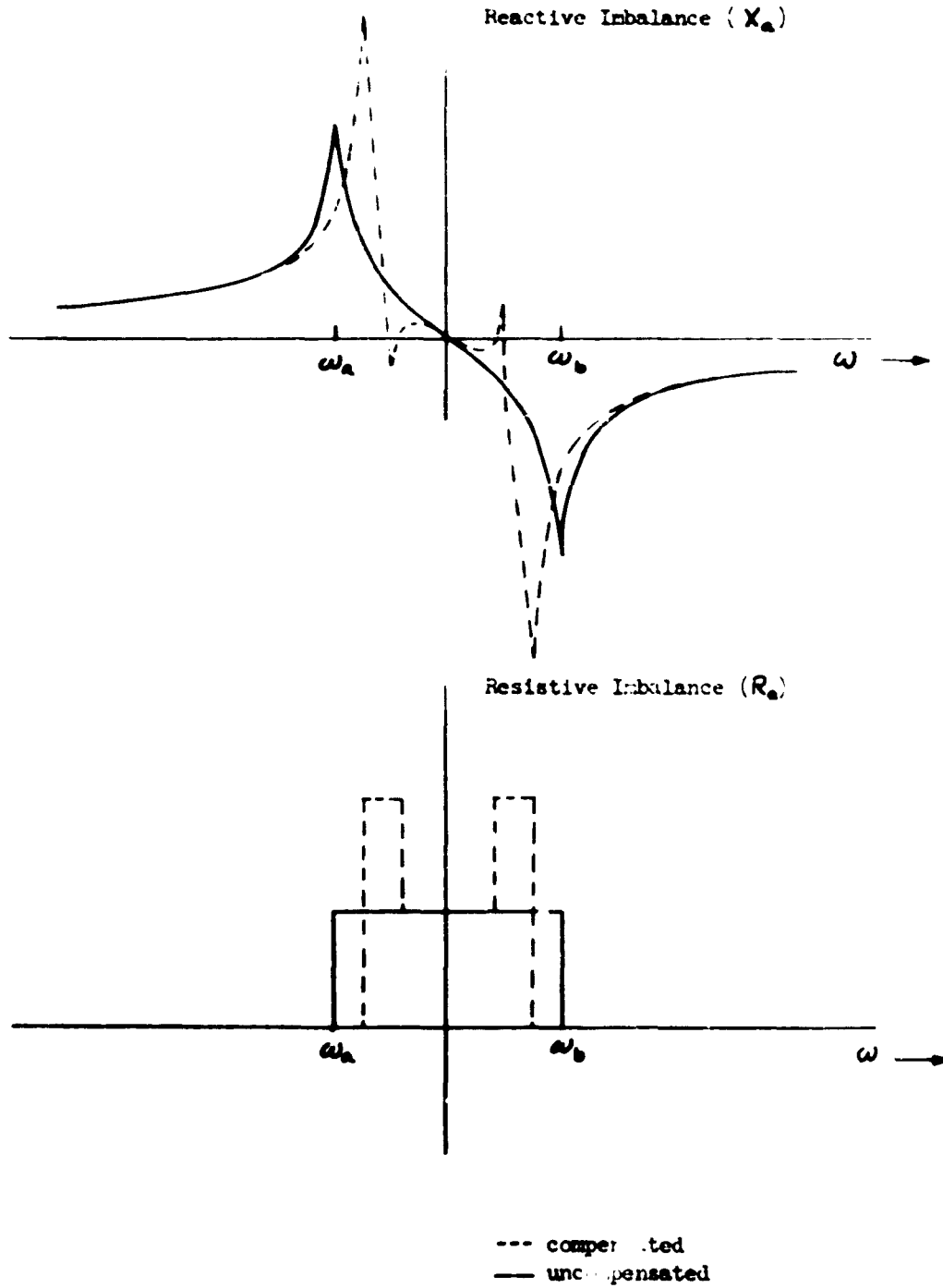


Fig. 7. Resistive and Reactive Bridge Imbalance for Rectangular and Compensated Distributions

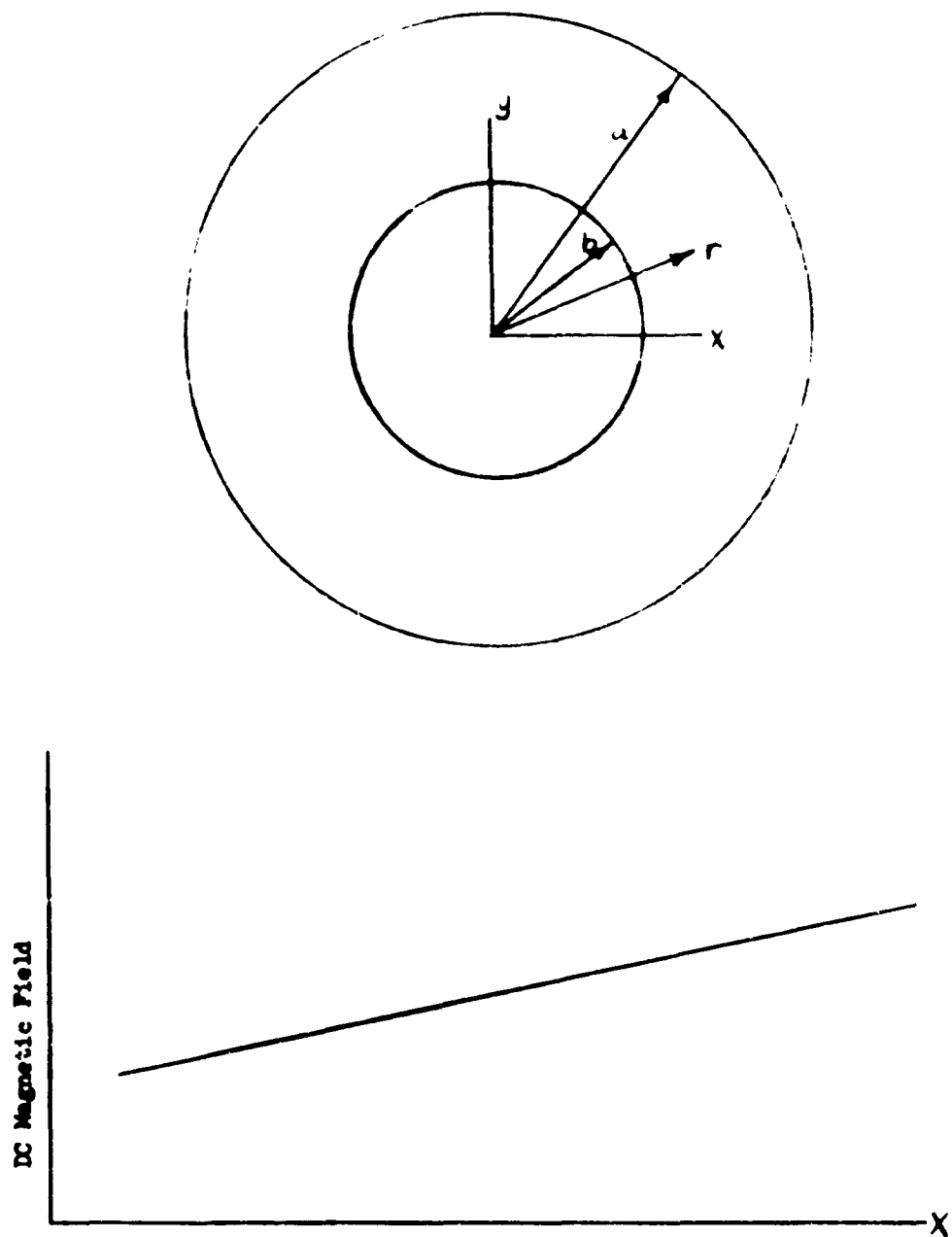


Fig. 8. Cavity Cross Section and DC Field Configuration

3.1 Bandwidth Enhancement (Reactive Compensation)

The approach used to reduce reactive imbalance over the desired limiter bandwidth is discussed in Appendix IX. This approach to reactive compensation involves a shaping of the absorber volume to achieve a distribution of spins per unit frequency interval which is peaked near the band edges. The distribution shown in Figure 7 is discussed on page 24 of Appendix I and is shown to double the useful limiter bandwidth compared to a uniform spin distribution.

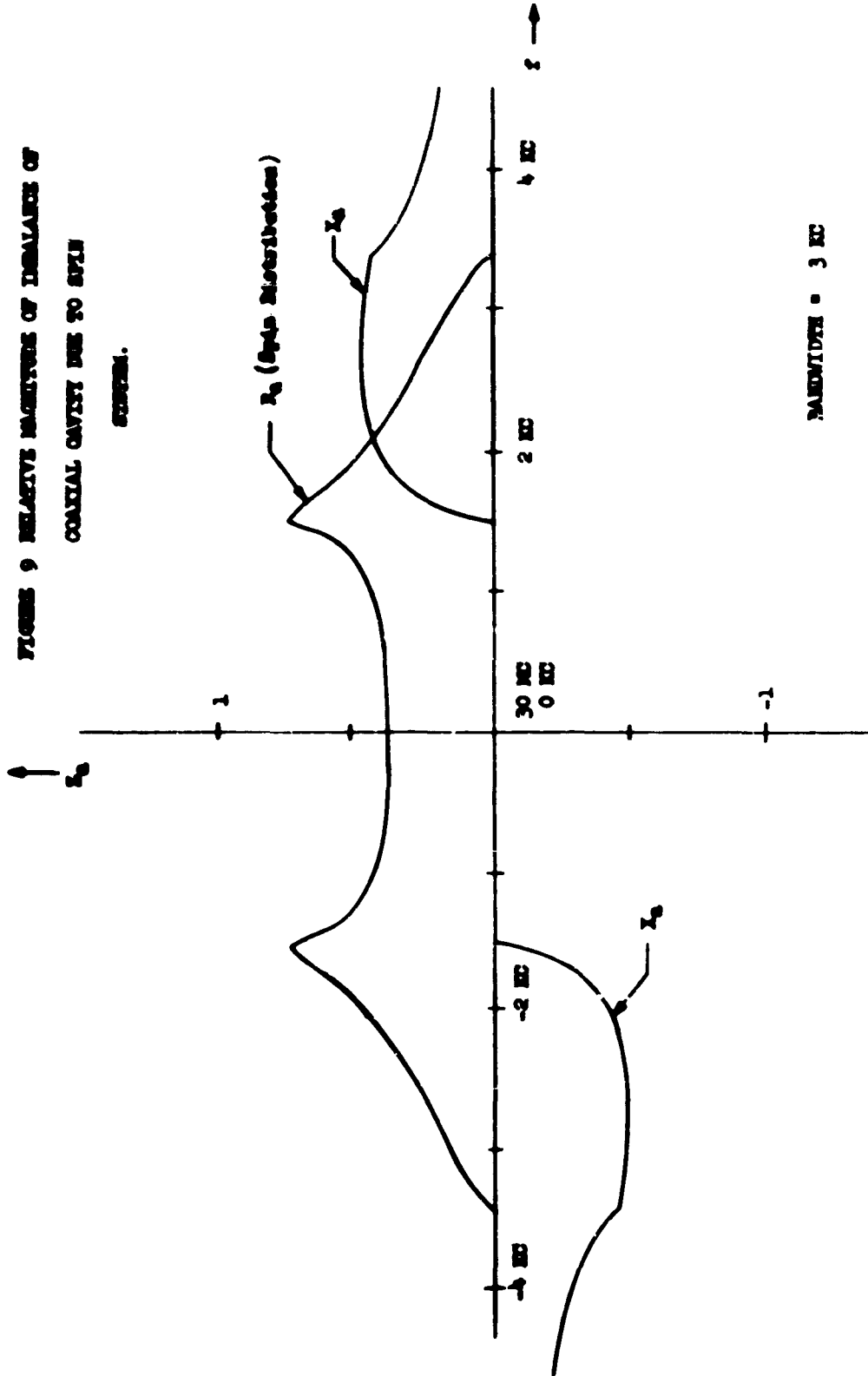
3.2 Physical Realization of Spin Distribution

A spin distribution superior to that shown in Figure 7 can be obtained by using a re-entrant cavity filled with absorbing material. If the dc magnetic field is parallel to the z-axis, and the field gradient is uniform along the x-axis, then the position along the x-axis is equivalent to frequency. It can be seen that the highest concentration of spins per unit frequency interval will occur for values of x equal to the center conductor radius. The resulting spin distribution is shown in Figure 9. This distribution is peaked near the band edges, as desired.

3.3 Imbalance Impedance of Re-Entrant Cavities

The impedance imbalance characteristics of the cavities used in the limiter model is calculated in Appendix I. The results are indeed quite striking as can be seen from Figure 9, the theoretical reactance imbalance is zero for all frequencies between the two peaks of the spin distribution function. The practical significance of this is that the magnetic field variation across the cavity center conductor determines the useful limiter bandwidth. Comparison of Figures 7 and 9 (solid curve) shows the theoretical improvement in useful limiter bandwidth using this reactive compensation technique. As discussed in Section 4.2, parameters consistent with a 3 kc bandwidth were selected for the model.

FIGURE 9 RELATIVE MAGNITUDE OF IMBALANCE OF
COAXIAL CAVITY DUE TO SFLN
SYSTEM.



BANDWIDTH = 3 MC

NOTE -- THE SFLN DISTRIBUTION AND R_0
HAVE THE SAME SHAPE

4.0 CIRCUIT THEORY

4.1 Insertion Loss

The complete re-entrant cavity circuit is given in Fig. 10. The equivalent circuit shown in Fig. 11 will be used to calculate insertion loss and saturation level. In this figure, r_a represents the power absorption of the spin system. It will be assumed that

$$r_a \gg r_o$$

i. e. . that the cavity wall losses far exceed the power absorbed by the spin system. Neglecting r_a in comparison to r_o , the impedance looking into the output terminals is found to be

$$Z_{out} = \frac{1}{2} \left(\frac{1}{j\omega C_2} + r_o + j\omega L_2 + j\omega M_2 \right)$$

If C_2 is adjusted to tune out the reactance caused by L_2 and M_2 , then

$$Z_{out} = \frac{1}{2} r_o.$$

The tuning condition for C_2 is

$$\omega^2 = \frac{1}{C_2(L_2 + M_2)}.$$

Setting $R_L = \infty$, and $r_a = \infty$, the current circulating through the secondary of the transformer with the input signal source connected is given by

$$I = \frac{j\omega M V_0}{r_o R_g + 2\omega^2 M_1^2 + r_o \left(\frac{1}{j\omega C_1} + j\omega L_1 \right)}.$$

If C_1 is chosen so that

$$\omega^2 = \frac{1}{L_1 C_1},$$

the circulating current, I , will be maximized, and equal to

$$I = \frac{j\omega M_1}{r_o R_g + 2\omega^2 M_1^2}.$$

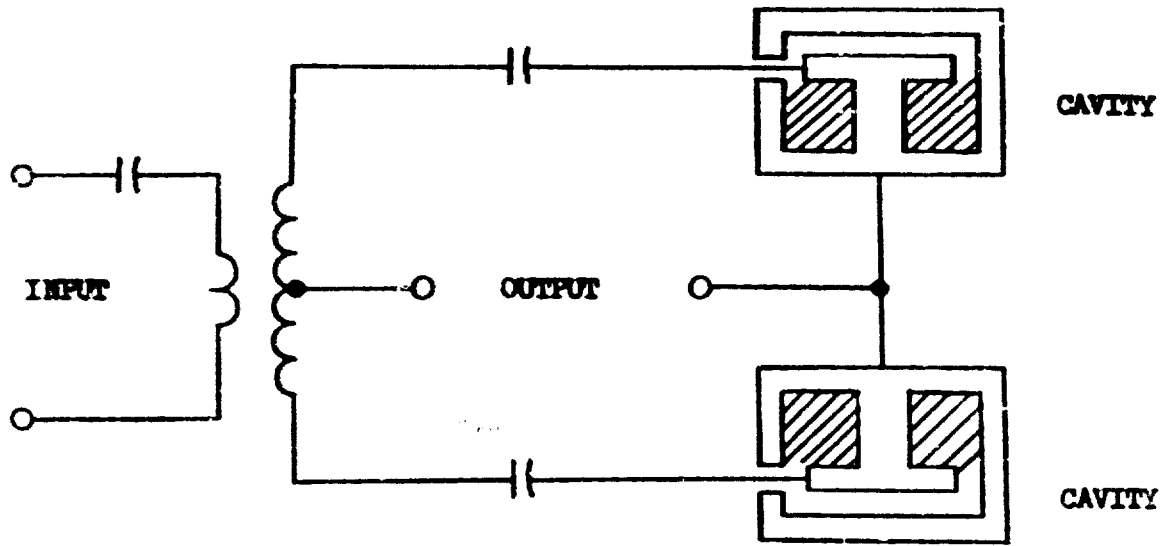


FIGURE 10 RE-ENTRANT CAVITY CIRCUIT

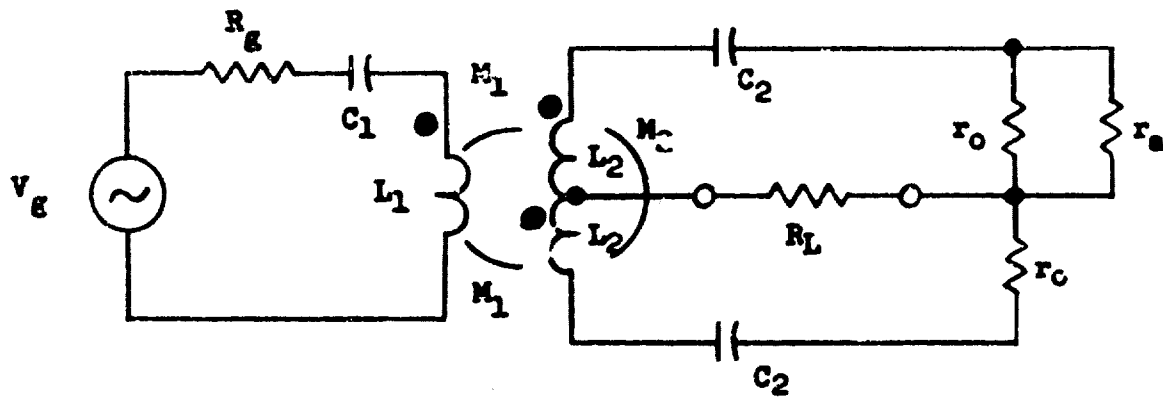


FIGURE 11 EQUIVALENT CIRCUIT

It is important that circuit parameters be adjusted so as to maximize I . If the circulating current is a maximum, the imbalance voltage produced by the introduction of the imbalance resistance, r_a , will also be maximum. I will attain its greatest value when the input impedance of the bridge is matched to the generator impedance, R_g . The value of mutual inductance, M_1 , needed to attain this match can be found by setting

$$\frac{\partial I}{\partial M_1} = 0.$$

This leads to the condition

$$M_1 = \frac{1}{\omega} \sqrt{\frac{r_0 R_g}{2}},$$

for which

$$I = \frac{j V_g}{2\sqrt{2} \sqrt{r_0 R_g}}.$$

If r_a is placed in parallel with r_0 , a change in resistance of ΔR ohms will occur.

$$\Delta R = r_0 - \frac{r_0 r_a}{r_a + r_0} \cong \frac{r_0^2}{r_a}$$

The bridge imbalance voltage with the output open circuited will be $I \Delta R$ volts.

$$V_{open} = \frac{j r_0^2 V_g}{2\sqrt{2} r_a \sqrt{r_0 R_g}}$$

The Thevenin equivalent of the bridge is shown below in Fig. 12.

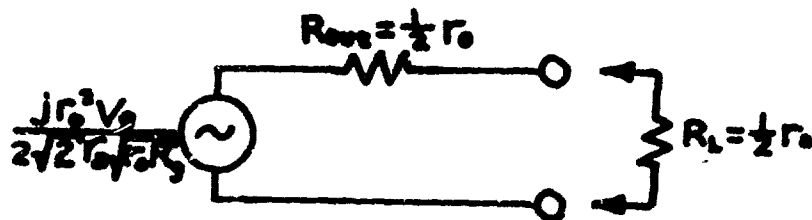


Fig. 12. Thevenin Equivalent Circuit

From this equivalent circuit, insertion loss is found to be

$$L_S = \frac{V_g^2 / 4R_g}{V_{open}^2 / 4R_{end}} = 4 \frac{r_a^2}{r_o^2} \quad (2)$$

For a typical limiter with 3 kc bandwidth, operating at 30 mc and at room temperature, $\frac{r_a}{r_o} = 100$. According to equation (2), this gives an insertion loss of 46 db. The ratio r_a/r_o is the reciprocal of the ratio R_a/R_o discussed in Appendix VIII. This is because R_a is the effective series resistance of the inductor due to NMR absorption while r_a is the equivalent shunt resistance for a parallel resonant circuit. Using the dependence of R_a/R_o upon frequency and bandwidth as developed in Appendix VIII, insertion loss versus bandwidth curves can be plotted for the re-entrant cavity circuit. (See Fig. 13.)

4.2 Optimum Cavity Design

In order to achieve the minimum small-signal insertion loss, as shown in the previous section, the ratio of power lost in the spin system to power lost in the wall of the cavity must be maximized. The wall losses for a TEM mode in a short coaxial line are compared in Appendix II to the power absorbed by the spin system. For a given ratio of cavity length to outer radius, the insertion loss can be minimized by proper choice of the ratio of outer to inner cavity radii. For convenience, the ratio of length to outer radius was chosen to be 2; the optimum ratio of outer to inner radii in this case is found to be 2.24

The cavity length was restricted by the 2 inch gap between magnet pole pieces. Taking this restriction and the considerations above into account, the cavity dimensions were determined. These are shown in Appendix II.

This analysis for an optimum re-entrant cavity has placed no restriction on the saturation level or line width which the designer may choose.

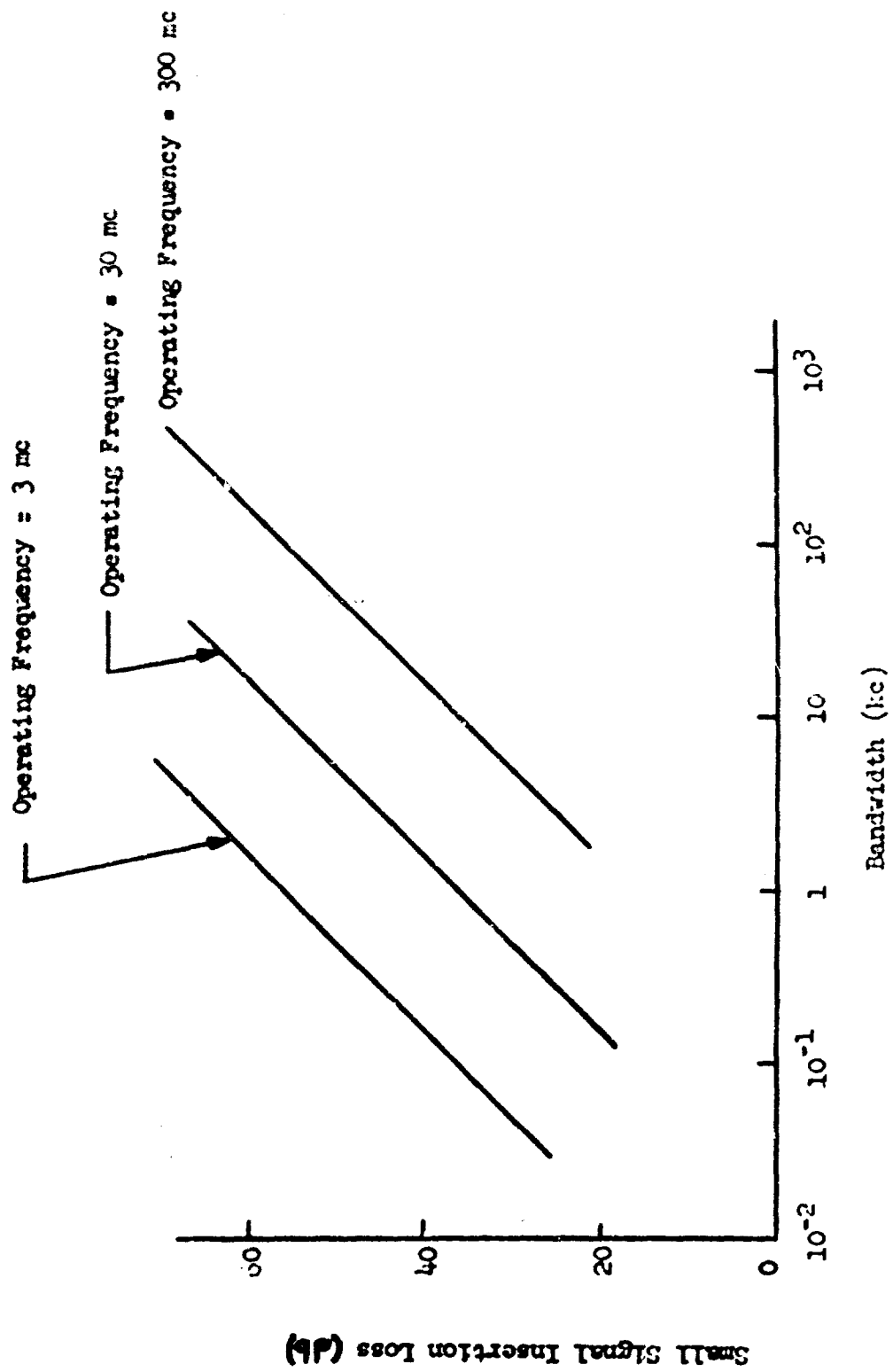


Fig. 13. Insertion Loss vs. Bandwidth for Uncooled Limiter

In some cases, saturation level and selectivity may be altered by two types of diffusion. One effect is the Brownian motion in which unsaturated spins move from a region of dc magnetic field corresponding to the interference signal frequency to a field corresponding to a frequency more than one line width removed. This results in saturating more than the necessary number of spins and results in a higher saturation level. The other effect is one of spin diffusion by the process of mutual spin flips and has a similar effect on the saturation level.

The problem of Brownian motion is considered in Appendix III. For a frequency selective limiter with a selectivity on the order of one cycle and a bandwidth of 3 kc, the motional diffusion is found to be negligible.

Spin diffusion by mutual spin flips is also considered in Appendix III. With similar assumptions concerning the frequency selective limiter characteristics the spin propagation rate is only 1/29 of the selectivity per second and thus may also be neglected.

Since diffusion effects are negligible, the saturation level analysis given on page 74 of Appendix IV (which neglects diffusion effects) can be applied to the circuit of Figure 11. The saturation power (input threshold power) is found to be

$$P_{sat} = \frac{2\omega V}{\pi Q_0 \gamma^2 T_1 T_2} \quad (3)$$

where

T_1 = Spin lattice relaxation time

T_2 = Inverse line width

V = Total cavity volume

Q_0 = Unloaded cavity Q

For the experimental model, $Q_0 = 415$, $V = 50$ cc, $T_1 = T_2 = 0.075$ sec giving

$$P_{sat} = -34.5 \text{ dbm}$$

5.0 INTERMODULATION

To predict the limiter intermodulation characteristics, Bloch's equations were solved for the case of two applied signals having angular frequencies ω_1 and ω_2 and power levels P_1 and P_2 . Approximate solutions were obtained by using a Fourier series expansion for the components of magnetization in a coordinate system rotating in phase with one of the applied signals. The recursion relations found between the Fourier components of magnetization were solved approximately for two separate cases. These components were then integrated over the field inhomogeneity to determine the limiter output voltage. (See Appendix IV)

Case I:

If it is assumed that the two input signals are sufficiently spaced in frequency so that

$$T_2(\omega_2 - \omega_1) \gg \frac{\sqrt{P_1 P_2}}{P_{sat}} \quad (4)$$

where $T_2(\omega_2 - \omega_1)$ is the frequency separation in linewidths.

It is found that the only significant intermodulation products occur at the frequencies $2\omega_1 - \omega_2$ and $2\omega_2 - \omega_1$. The magnitudes of these products are

$$\frac{P_{2\omega_1 - \omega_2}}{P_{out}|_{P_2=0}} = \frac{P_1 P_2 (1 + \frac{P_1}{P_{sat}})}{4 T_2^4 (\omega_2 - \omega_1)^4 P_{sat}^2} \left[-\frac{1}{2} + \frac{1}{\sqrt{1 + P_1/P_{sat}}} + \frac{1}{2\sqrt{1 + P_2/P_{sat}}} \right] \quad (5)$$

and

$$\frac{P_{2\omega_2 - \omega_1}}{P_{out}|_{P_2=0}} = \frac{P_2^2 (1 + \frac{P_2}{P_{sat}})}{4 T_2^4 (\omega_2 - \omega_1)^4 P_{sat}^2} \left[-\frac{1}{2} + \frac{1}{2\sqrt{1 + P_1/P_{sat}}} + \frac{1}{\sqrt{1 + P_2/P_{sat}}} \right] \quad (6)$$

where $P_{out}|_{P_2=0}$ is the limiter output power at ω_1 , when no signal is present at ω_2 . Intermodulation power for this case varies inversely with the fourth power of frequency separation. If P_2 is well above saturation, power at the frequency $2\omega_2 - \omega_1$ will vary as the square of P_2 and will be the most significant product if $P_2 \gg P_1$.

Curves showing the variation of $P_2\omega_2 - \omega_1$ with frequency separation are shown in Fig. 14, for the case where $\frac{P_1}{P_{sat}} = 1$. For a limiter with 1 cps selectivity these curves show that intermodulation power will be at least 20 db below signal output power with a 50 cps separation providing P_2 is no more than 30 db above saturation.

Case II

If $P_1 \ll P_2$, as would be the case when a small desired signal is subjected to a large degree of coherent interference, it is found that the only significant intermodulation product occurs at $2\omega_2 - \omega_1$. Intermodulation level is illustrated in Fig. 15 as a function of frequency separation. From these curves, it can be concluded that no significant intermodulation power will be generated when a small signal mixes with a large signal in the limiter. The most important effect will be suppression of the small signal which occurs when the frequency separation is comparable to the selectivity. This effect is illustrated in Fig. 16. The presence of a large, saturating signal at ω_2 causes a "hole" of width $\frac{1}{T_2} \sqrt{1 + \frac{P_2}{P_{sat}}}$ to appear in the limiter pass-band. The effect of these "holes" upon output signals is discussed in Section 6 and in Appendix V.

FREQUENCY DIFFERENCES IN DIVERSITIES

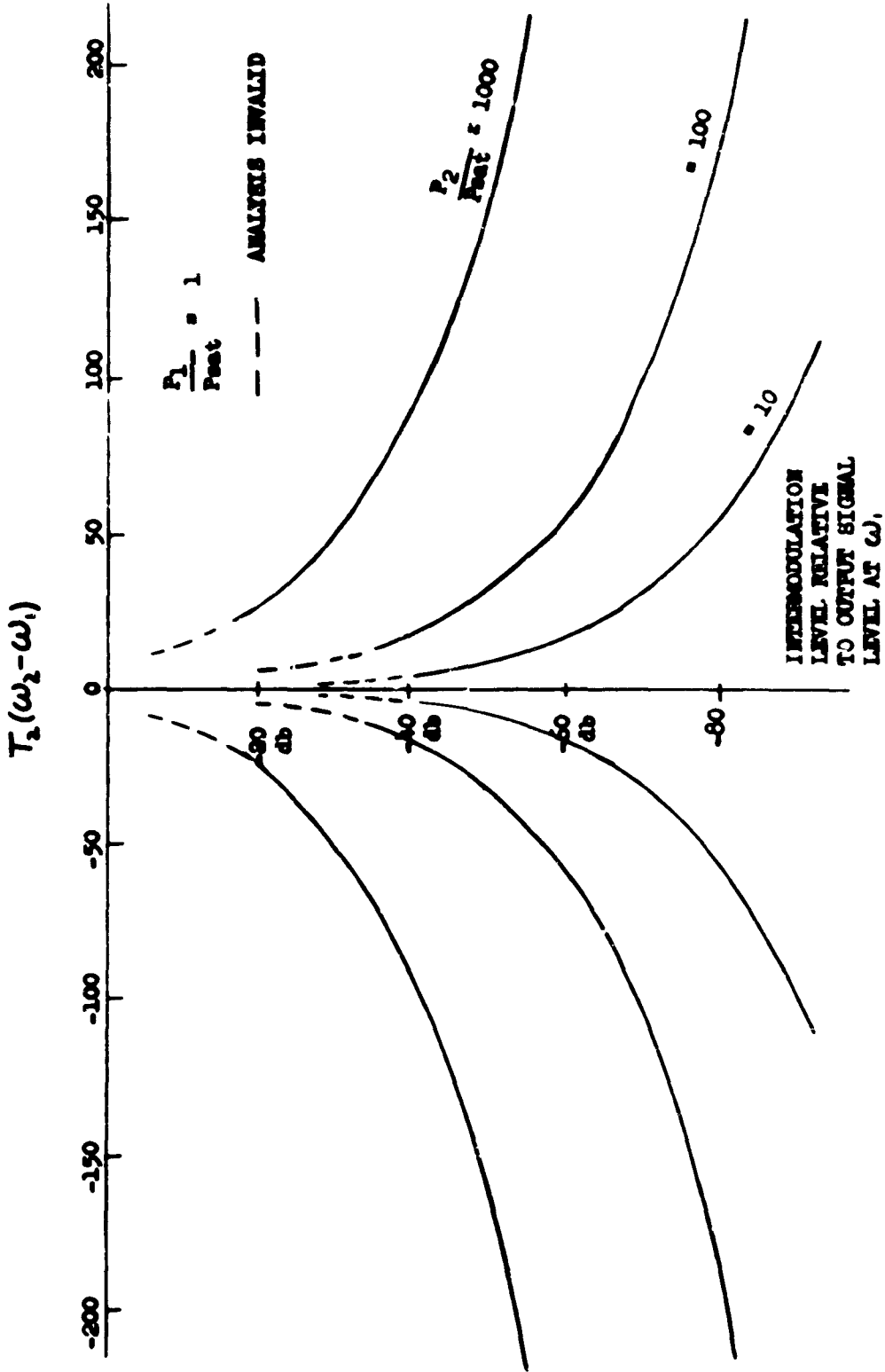


FIGURE 14 INTERMODULATION POWER WITH TWO LARGE SIGNALS

FREQUENCY RESPONSE IN LINEARIZATION

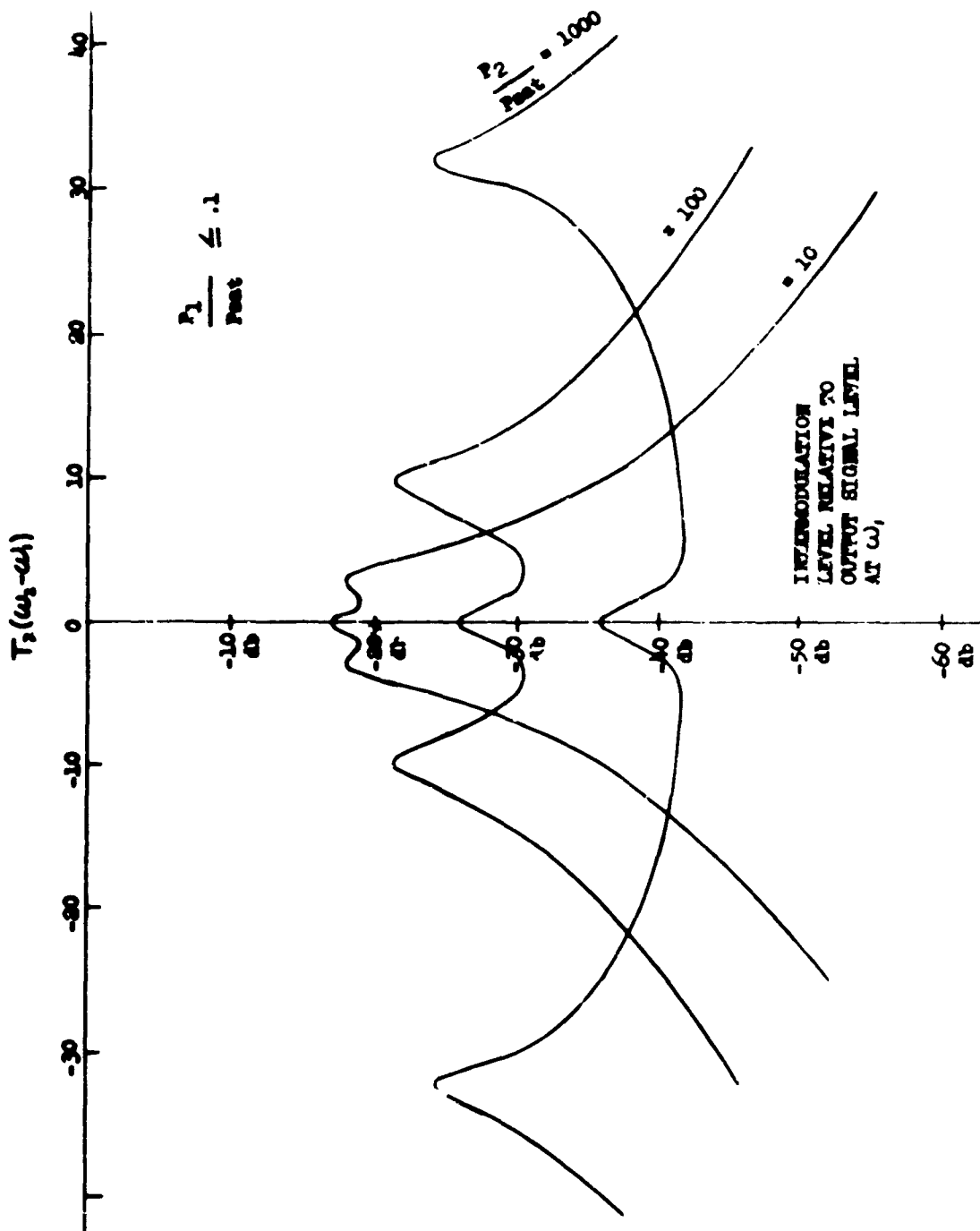


FIGURE 15 INTERMODULATION WITH ONE SIGNAL, BELOW SATURATION AND ONE SIGNAL ABOVE SATURATION

FREQUENCY RESPONSE IN LIMITING

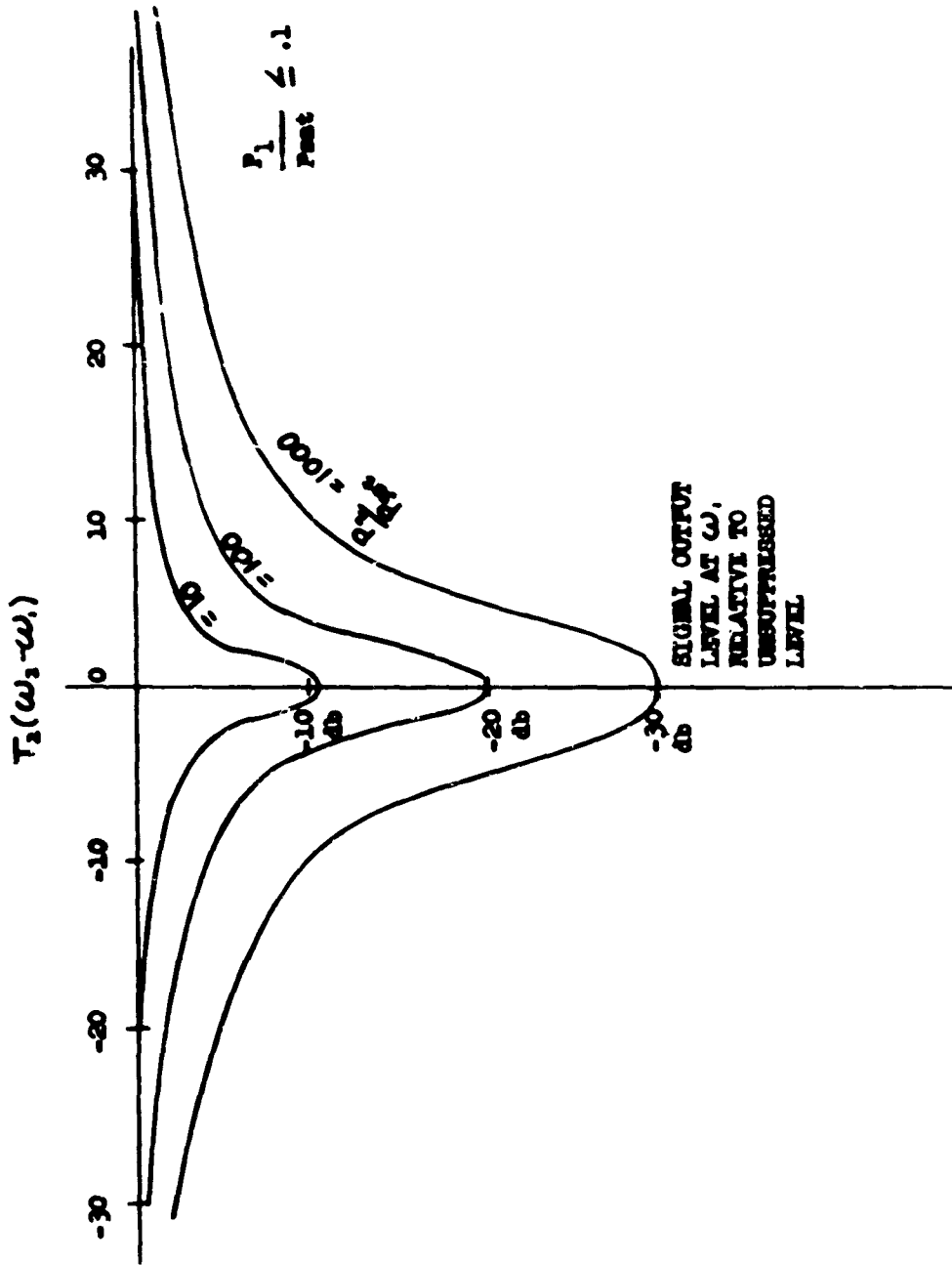


FIGURE 16 SUPPRESSION OF SMALL SIGNAL IN VICINITY OF LARGE SIGNAL

6.0 ANALYSIS OF LIMITER PERFORMANCE

In order to determine the effect of a frequency selective limiter on system performance, the steady state and transient response of the limiter has been studied for the following types of interference

- 1) CW
- 2) Frequency-swept CW
- 3) Pulsed CW
- 4) Noise

6.1 Steady State Analysis

In Appendix V, the error introduced in an arbitrary signal by coherent (unmodulated or periodically modulated) interference is calculated. This error is introduced in two ways: by the presence of interference power at the limiter output, and by the suppression of those portions of the desired signal spectrum which are close to the major spectral components of interference. An expression which permits the calculation of error once the power spectral densities of the signal and interference are known is given in Appendix V.

The basic properties of the limiter in various interference environments can be brought out by assuming simple rectangular spectrums for both the desired signal and the interference. As shown in Fig. 17 the signal bandwidth is denoted B_s , the interference bandwidth is denoted B_I , and the spacing of interference components is f_m , the modulation frequency.

Error is expressed in terms of an equivalent interference/signal ratio which is defined rigorously in Appendix V. For the model spectra shown in Fig. 17, this ratio is

$$\frac{\text{Interference Power Output}}{\text{Signal Power Output}} \cong M \left[\frac{1}{8T_2 B_s} \frac{(P_I/P_{det}N)^2}{\left(1 + \frac{P_I}{N P_{det}}\right) \left[1 + \left(\frac{P_I}{N P_{det}}\right)^2\right]^{1/2}} \frac{P_s/NB}{1 + \frac{P_I}{N P_{det}}} \right] \quad (7)$$

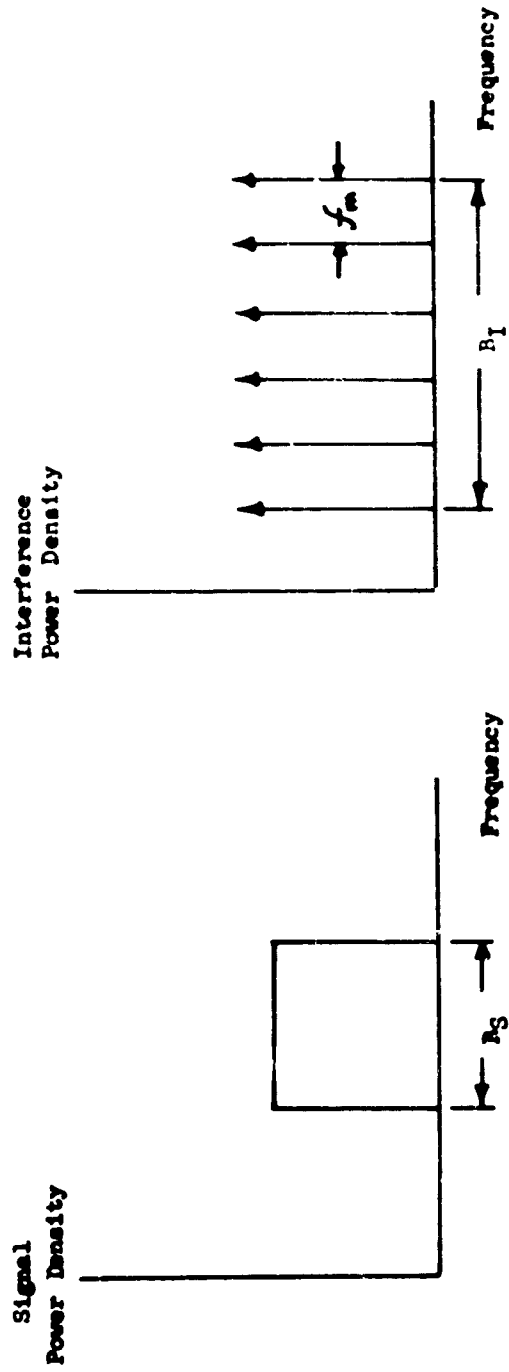


Fig. 17. Model Signal and Interference Spectra

where

N - Number of components of interference power

M - Number of components of interference power which fall within
the signal passband

P_I - Interference power level at input

P_S - Signal power level at input

The above expression is plotted as a function of input interference/signal ratio in Fig. 18. A signal bandwidth of 3 kc and a selectivity of 1 cps has been assumed.

Fig. 19 shows the effect of variations in B_I and f_m upon the error between desired and actual signals. Equivalent interference/signal ratio is plotted as a function of interference bandwidth, B_I , with modulation frequency, f_m , as a parameter. An input interference/signal ratio of 20 db is assumed, so that when no limiter is used, the output interference/signal ratio is 20 db for $B_I < B_S$ and decreases linearly as B_I increases beyond the signal bandwidth ($B_I > B_S$). When no limiter is used, the equivalent interference/signal ratio is independent of modulation frequency, but with the limiter this ratio decreases sharply as f_m increases. This is because the interfering power is concentrated in fewer in-band spectral components which can be effectively limited.

Using the information contained in Figs. 18 and 19, generalizations can be drawn about the performance of the limiter in a variety of interference environments.

1) CW Interference

Fig. 18, with $M = N = 1$ shows the improvement (in equivalent interference/signal ratio) which results when the limiter is used. Improvements up to 30 db are possible, with the greatest improvement occurring at high input interference levels.

2) Frequency-Swept CW

This case can be treated approximately by taking f_m to be the fundamental frequency of the periodic modulation and B_I to be the frequency deviation. Fig. 19 shows that the worst case occurs when frequency deviation is equal to the signal

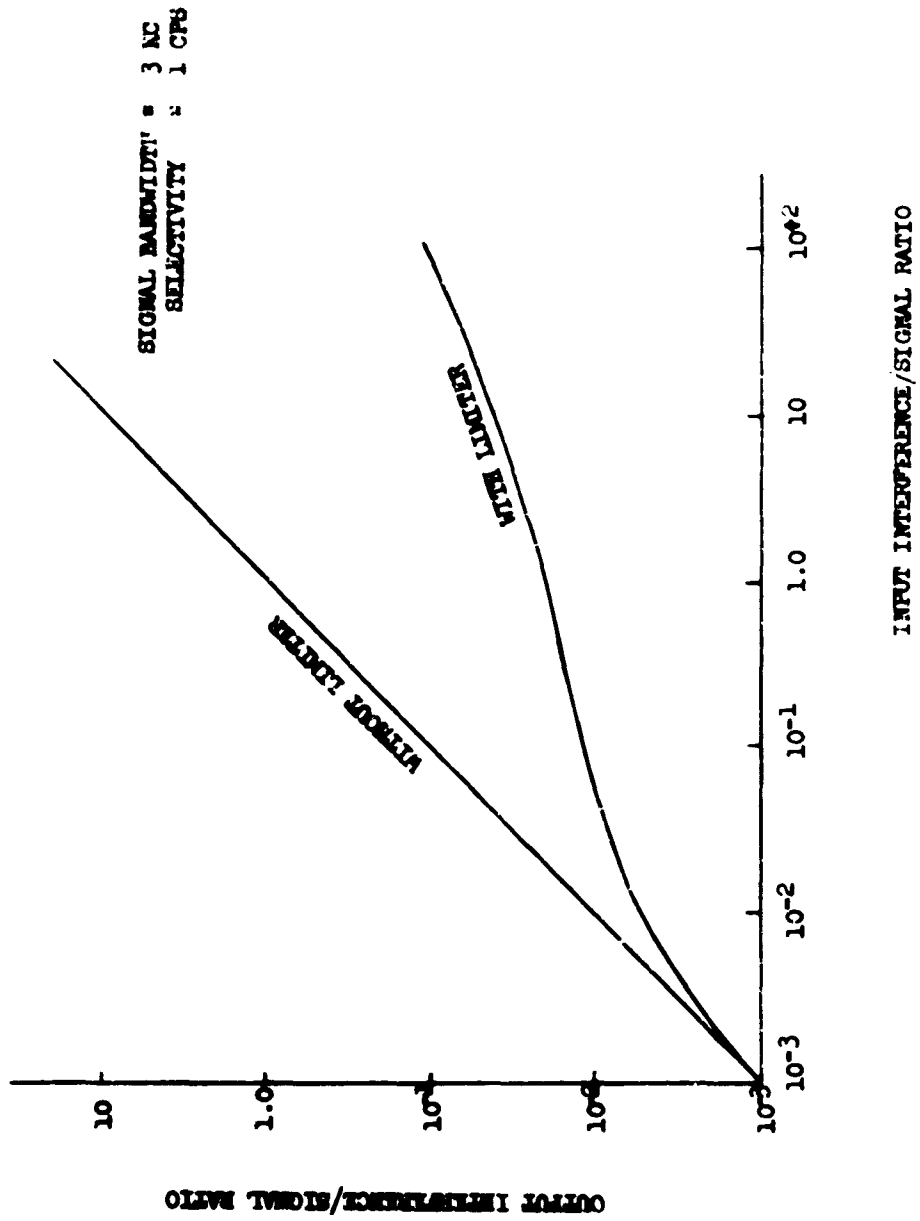
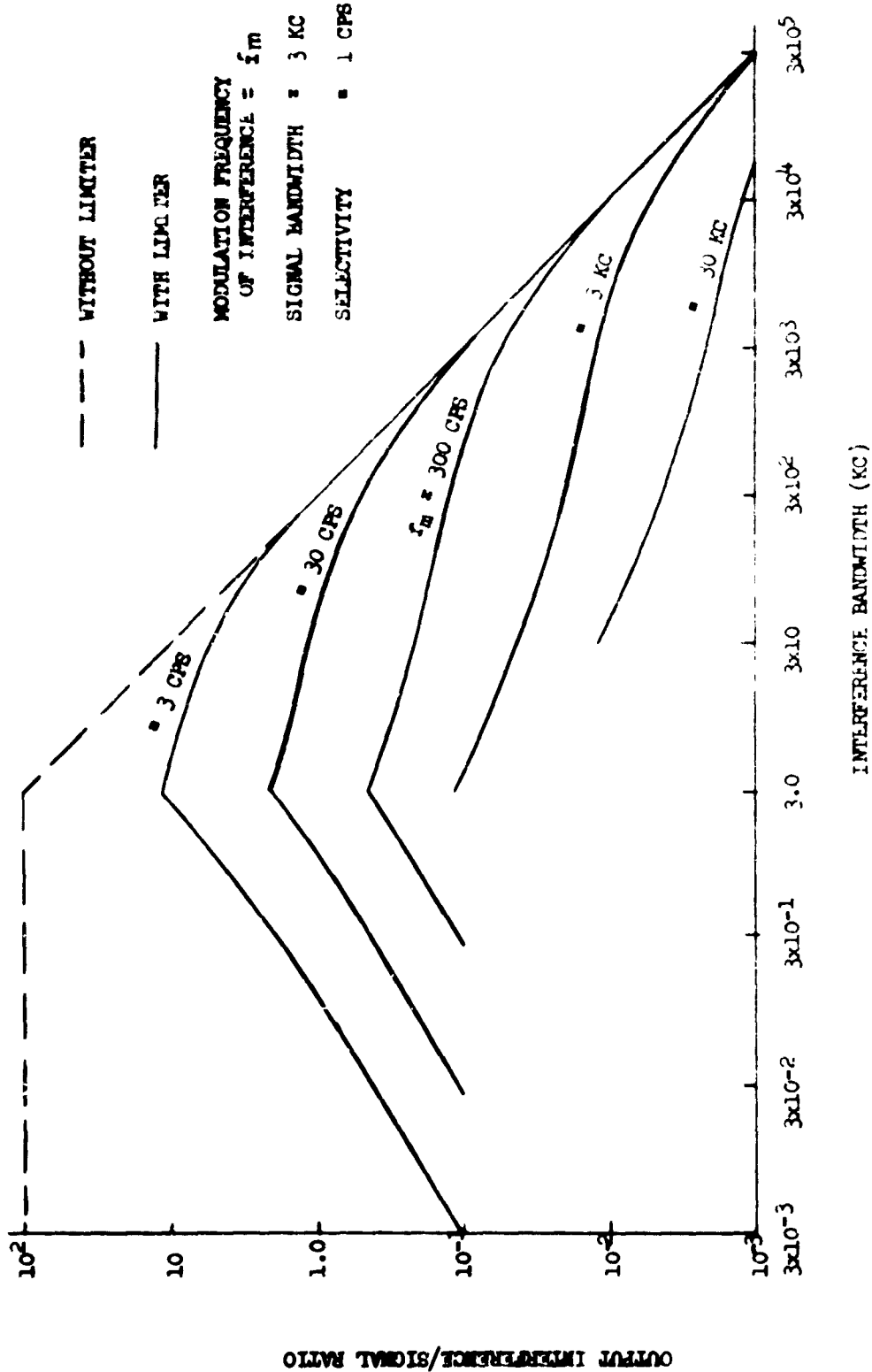


FIGURE 18 IMPROVEMENT IN OUTPUT INTERFERENCE/SIGNAL RATIO USING LIMITER WITH C-W INTERFERENCE



bandwidth and the modulation frequency is low. For modulation frequencies greater than 30 cps, however, equivalent interference signal ratio can be reduced 20 db and more.

3) Pulsed CW

For this case, f_m is taken to be the pulse repetition frequency, and B_1 is taken to be the inverse pulse width. The worst case occurs when inverse pulse width is equal to the signal bandwidth and the modulation frequency is low. For example with a repetition rate of 30 cps and a duty cycle of about 1%, equivalent interference signal ratio is improved by 20 db. If the duty cycle is increased, an even greater improvement occurs because the interference spectrum tends to concentrate in just a small portion of the signal bandwidth. If the duty cycle is made shorter than 1%, interference power is wasted outside the signal bandwidth, and equivalent interference/signal ratio again improves.

4) Noise

The operation of the limiter in a heavy noise environment has not been studied analytically; however, certain conclusions can be drawn by considering the case where the model spectrum is very dense, i. e., $f_m \rightarrow 0$. As can be seen from Fig. 19, the curves of interference/signal ratio versus B_1 tend toward the curve which applies when no limiter is used. This is an indication that, in a noise environment, the limiter behaves as a linear device, neither improving nor degrading interference/signal ratio. Because noise power is spread uniformly over the limiter bandwidth, saturation occurs only when sufficient noise power is available to saturate all the spins rather than just a small localized volume. For a limiter with a 3 kc bandwidth and 1 cps selectivity, the noise saturation power will be approximately 30 db greater than the cw saturation power.

If an accurate estimate of system performance is desired, more detailed information about the signal and interference power spectra can be inserted in equation (81) of Appendix V. If the signal and interference spectra tend to concentrate in the same areas, it will be found that the estimate of equivalent interference/signal ratio given

by Fig. 19 is somewhat optimistic. On the other hand, if the signal and interference spectra tend to concentrate in different areas, the equivalent interference/signal ratio will be smaller than predicted by Fig. 19.

6.2 Transient Response

The steady state analysis for coherent interference has been discussed in terms of the equivalent interference/signal ratio. The transient effects will now be considered by first establishing the effect of the limiter on a unit step of cw interference.

Starting from Bloch's equations, and using a Laplace transform method of solution as shown in Appendix VI, the frequency response of one magnetic resonant particle (more accurately, the response of a volume small enough so that H_0 can be considered uniform) was determined. To account for the inhomogeneously-broadened resonance, the frequency response of individual particles was integrated over the field inhomogeneity. The resulting transient response is found to provide an important contribution to the resistance imbalance only. Even if a rectangular distribution of spins with respect to frequency had not been assumed, the transient effects would be essentially the same and would be of minor importance in the reactance imbalance of the bridge. This major transient in the real part of the bridge imbalance impedance is found to be proportional to an exponentially decaying Bessel function as shown in equation (8).

$$\text{FSL output voltage} \propto \omega_{rf} e^{-\frac{t}{T_2}} J_0(\omega_{rf} t) + \left[\begin{array}{c} \text{small} \\ \text{correction} \\ \text{terms} \end{array} \right] \quad (8)$$

where

$J_0(x)$ = Zeroth order Bessel function

$$\omega_{rf} = \gamma H_{rf}$$

$$\gamma = T_1 = T_2$$

In Fig. 20 the transient output voltage of the bridge for a switched cw input is shown for two degrees of saturation. It is important to note that the transient signal leaving the bridge will decay in a time at least as short as τ . The relaxation time, τ , is 0.075 seconds for the experimental limiter, but can vary between 10^{-3} to 10 seconds, depending upon the absorber material. The major portion of the transient is limited in a time of $\frac{2.3}{\omega_{ns}}$. This means that the further the input signal level is above the saturation level, the less time is required for saturation of the absorber and subsequent reduction in bridge output.

The transient response for a unit step in any coherent interference can be discussed in terms of the above result by first determining the Fourier spectrum of the interference under consideration and treating the components individually. The spectral components in the interfering signal must be spaced at a distance greater than the chosen limiter selectivity.

Each spectral component of coherent interference signal will contribute a leakage spike of the form shown in Fig. 20. The leakage spike energy is proportional to

$$\text{Spike Energy} \propto \omega_{ns}^2 \int_0^{\infty} e^{-\frac{t}{\tau}} J_0^2(\omega_{ns} t) dt \quad (9)$$

The major contribution will occur in the first $\frac{2.3}{\omega_{ns}}$ seconds so that the spike energy is nearly proportional to

$$\text{Spike Energy} \propto \omega_{ns}^2 \int_0^{2.3} J_0^2(x) dx \quad (10)$$

for signals above the limiting threshold. This shows the spike leakage is proportional to ω_{ns}^2 .

The wave shapes shown in Fig. 20 were observed in the laboratory.

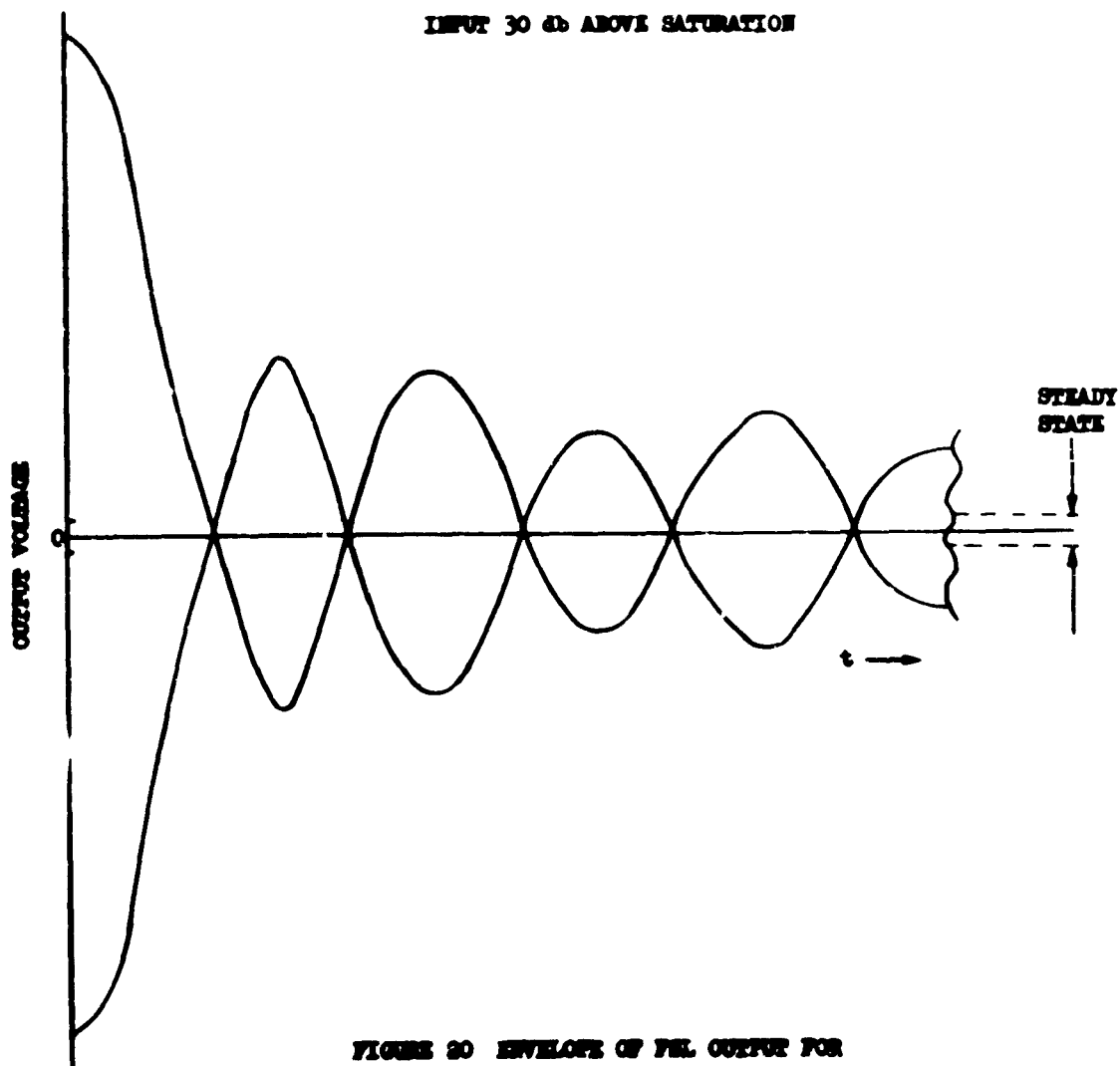
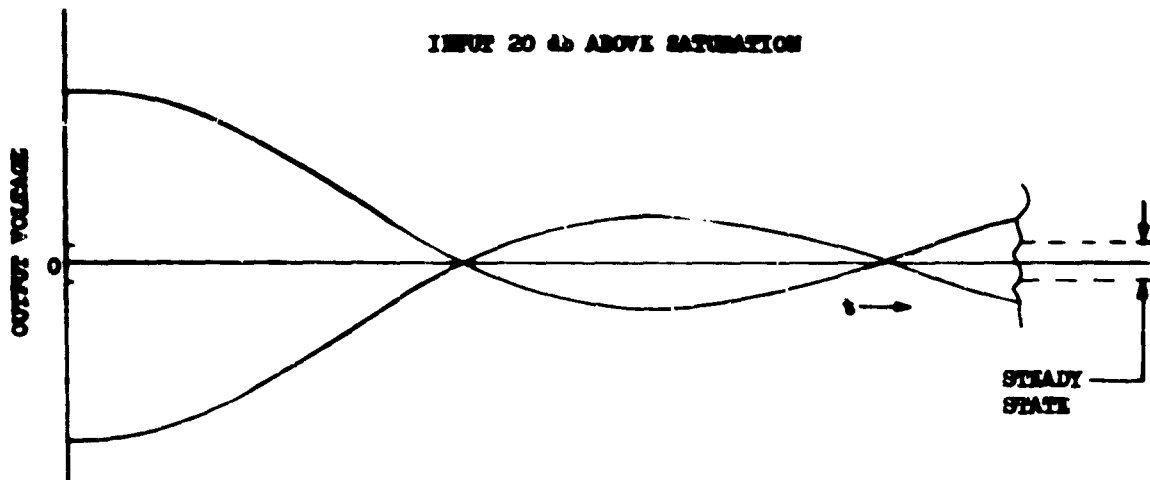


FIGURE 20 ENVELOPE OF PNL OUTPUT FOR SWITCHED ON INPUT

7.0

EXPERIMENTAL RESULTS

At the conclusion of this program the laboratory model frequency selective limiter exhibited the following characteristics:

	<u>Experimental Results</u>	<u>Design Goal</u>
Center Frequency	30 mc	30 mc
Bandwidth	18 kc	3 kc
Limiting Range	15-35 db	> 20 db
Insertion Loss	52 db	< 50 db
Saturation Level	-36 dbm	> -40 dbm
Small Signal Selectivity	2 cps	< 100 cps
Intermodulation (with 64 cps signal separation)	16 db below small signal output level	

Experimental techniques and results will be discussed in detail in this section and, finally, the limiter configuration will be described.

7.1 Bandwidth and Limiting Range:

The usable bandwidth of the limiter is determined by the range of frequencies over which reactive bridge imbalance is small. A block diagram of the setup used to measure reactive bridge imbalance is shown in Fig. 21. The dc magnetic field was moved through the resonance line in increments of approximately .1 gauss and output voltage (which is proportional to bridge imbalance impedance) was measured using a Stoddart NM-30 field intensity meter. The signal applied to the limiter was 40 db above saturation so that bridge imbalance was essentially reactive. After each increment in magnetic field, 5 seconds was allowed for the limiter to come to full saturation before reading the output voltage.

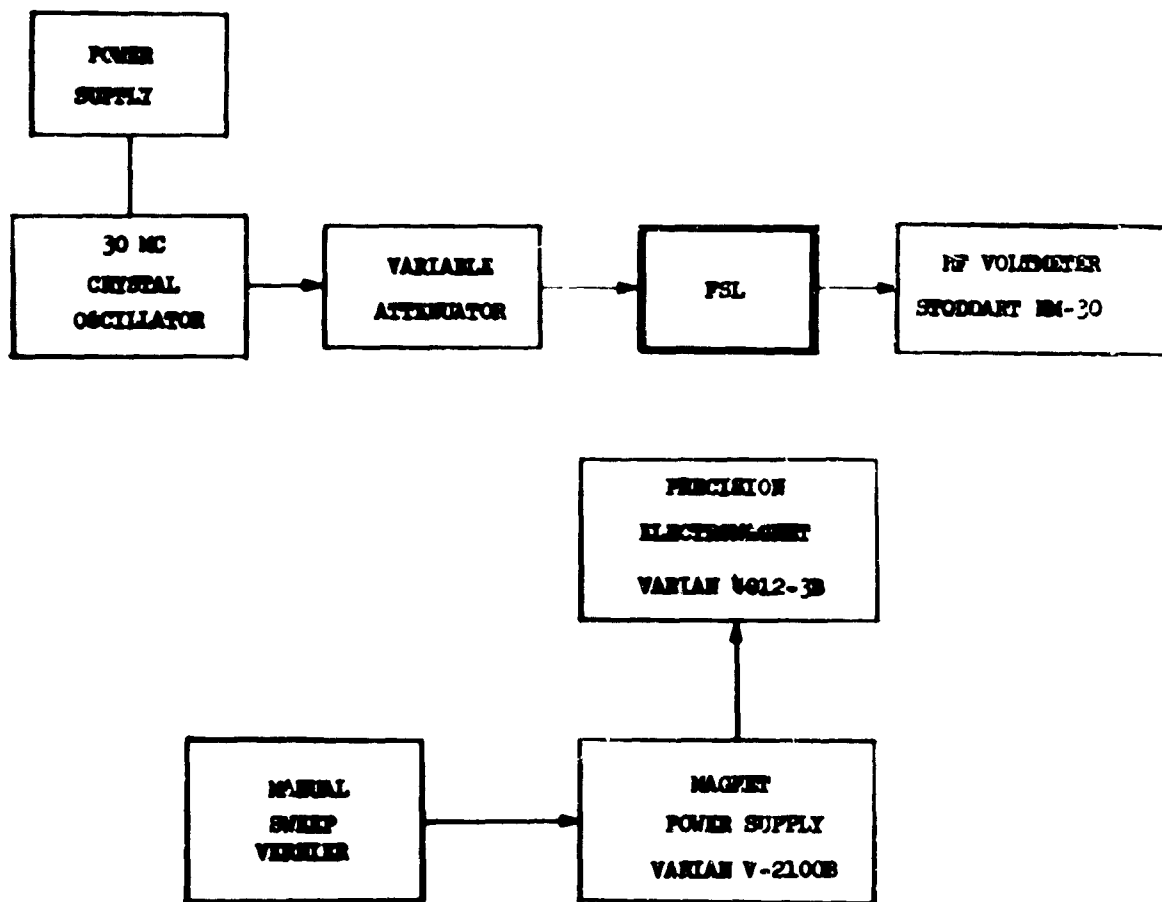


FIGURE 21 BLOCK DIAGRAM OF SYSTEM USED TO MEASURE REACTIVE IMPEDANCE (FSL BANDWIDTH)

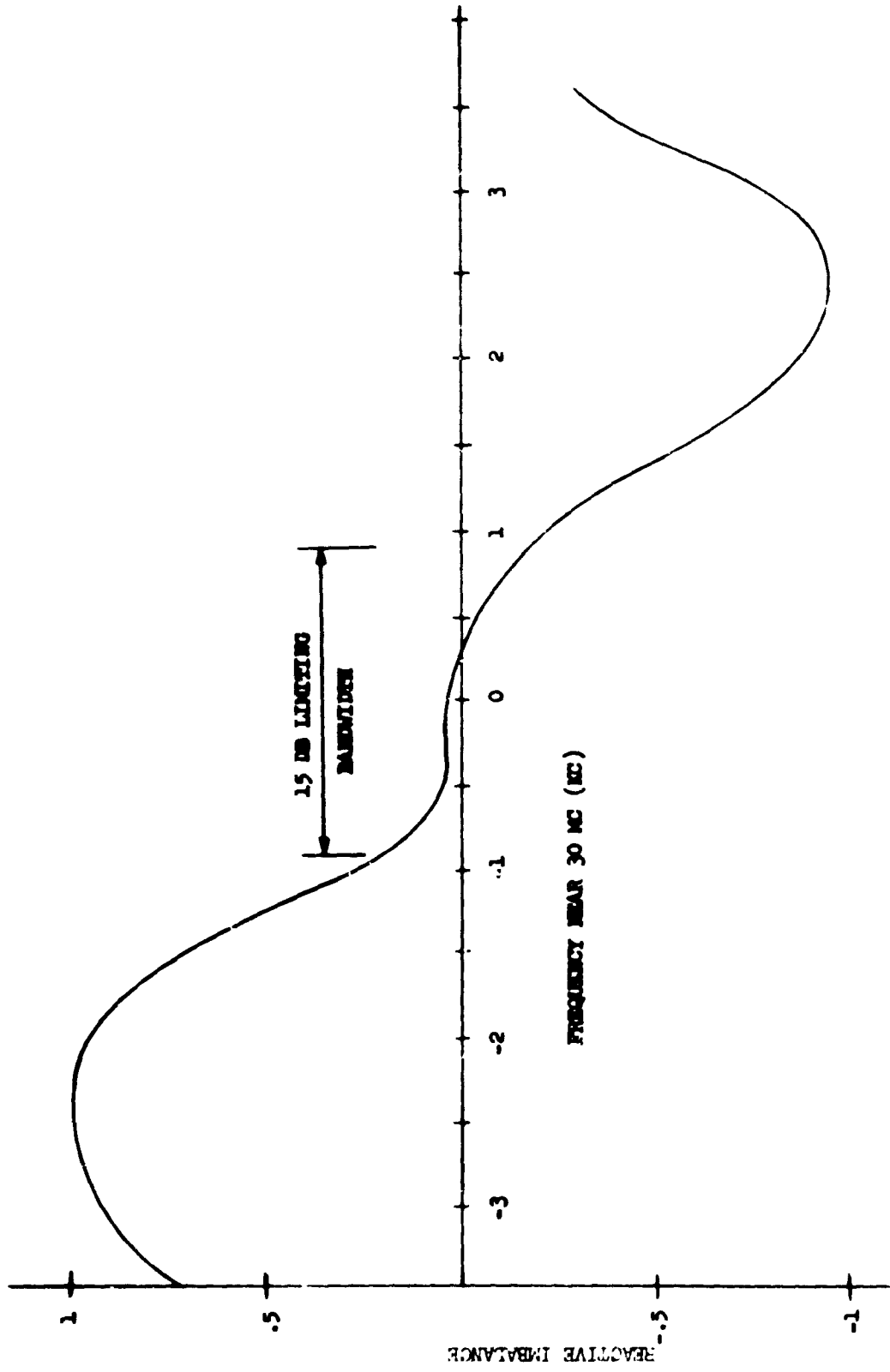


FIGURE 22 MEASURED REACTIVE IMBALANCE

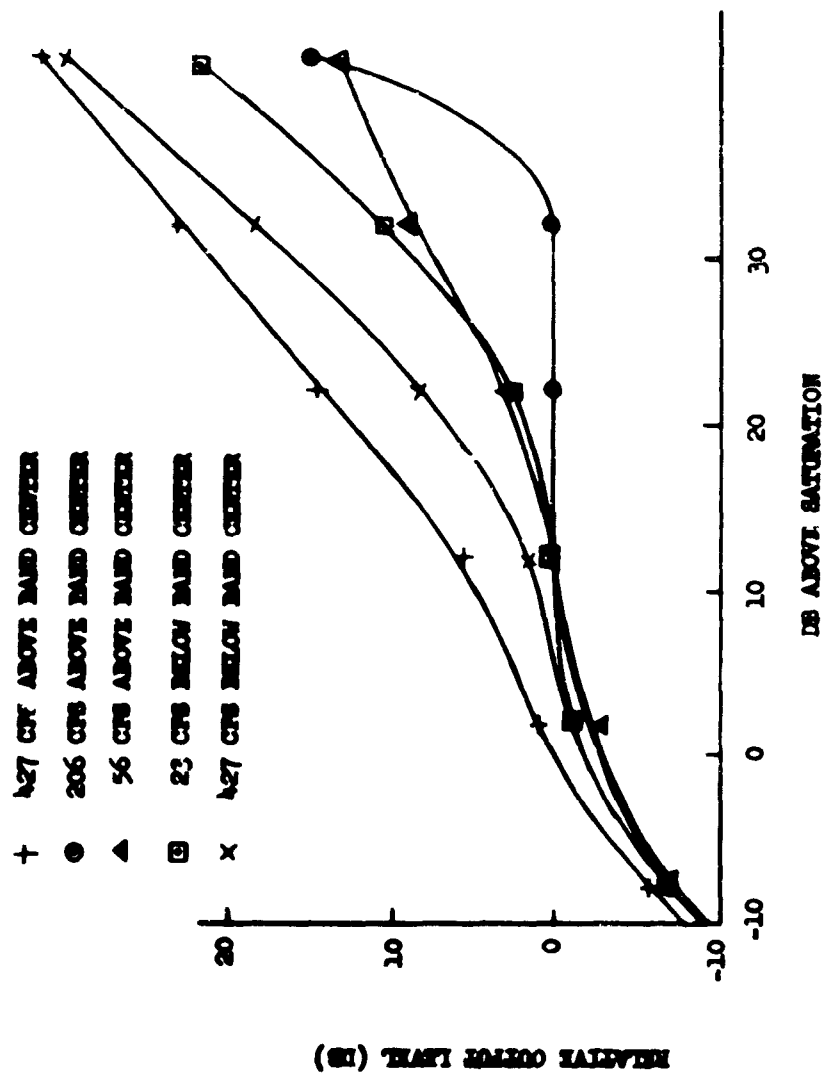


FIGURE 23 EXPERIMENTAL LIMITING CURVES

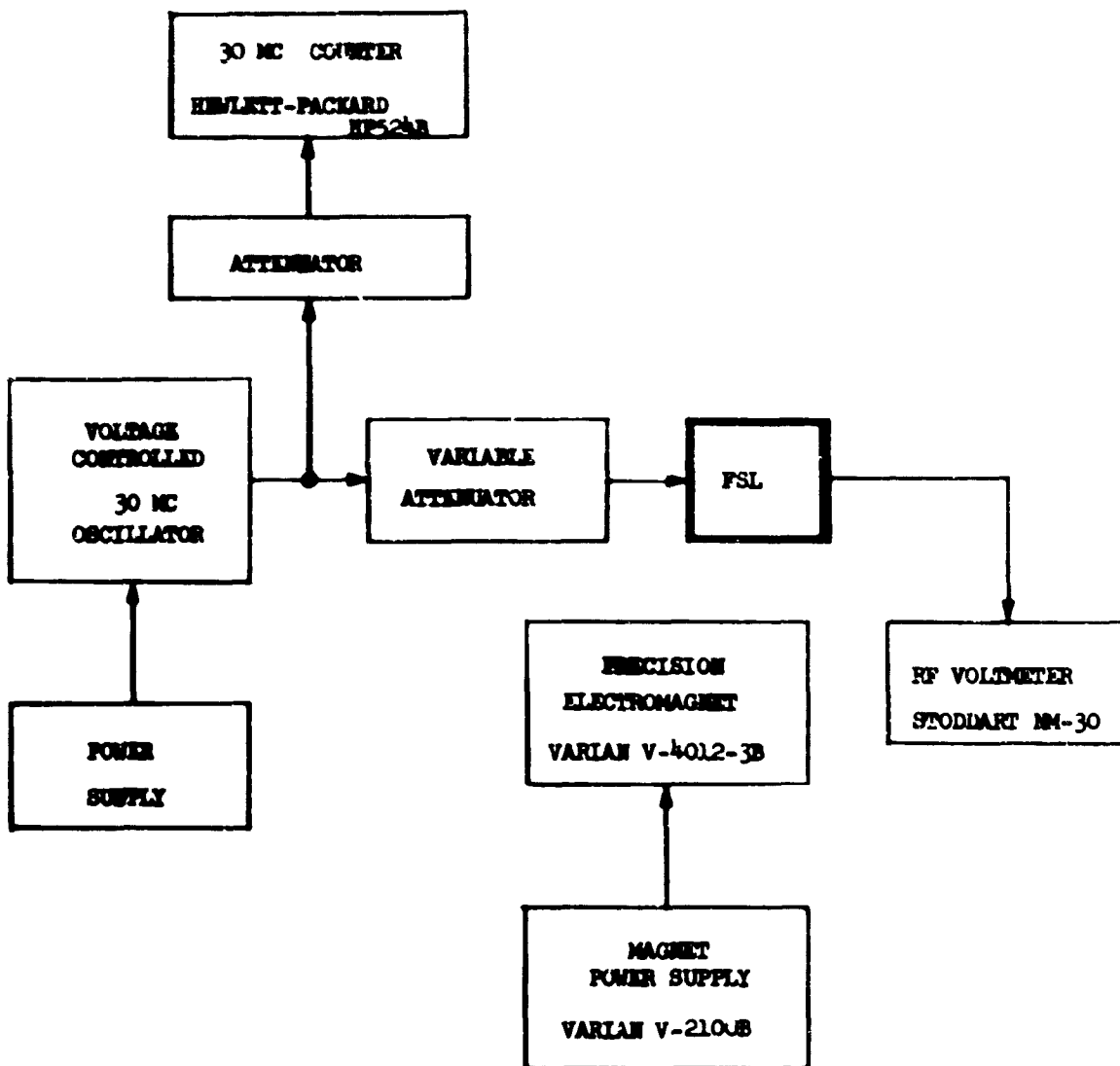


FIGURE 24 BLOCK DIAGRAM OF SYSTEM UTILIZED IN MEASURING LIMITING CURVES

The cavity position used for all experiments is indicated in Fig. 25. The total transverse field variation at this position is approximately 4.5 kc while the longitudinal variation is approximately 0.2 kc. If smaller overall cavity dimensions were used, or if specially shaped pole pieces were used, it is likely that a far closer approximation to the required field distribution could be obtained.

7.2 Insertion Loss

Insertion loss was measured using the setup shown in Fig. 26. A 30 mc signal from a 50 ohm source was passed through the limiter and into a 50 ohm r-f voltmeter (Stoddart NM 30-A preceded by a 10 db attenuator). Next, the limiter was bypassed completely, and attenuation was added to the signal source until the voltmeter reading was equal to that obtained with the limiter in the circuit. Insertion loss was found to be 52 db; this compares favorably with the theoretical figure of 46 db given in Section 4.1. Time restrictions made it impossible to match the input and output impedances to the measuring equipment. With proper impedance matching, the insertion loss could be reduced considerably.

7.3 Saturation Level

According to Section 4.3, the saturation level is given by

$$P_{\text{sat}} = \frac{24V}{\pi Q \gamma T_1 T_2} \quad \text{ergs/sec}$$

The cavity volume is 50 cc and its measured Q (unloaded) is 415. For the transformer oil used in the limiter,

$$T_1 = T_2 = 0.075 \text{ sec.}$$

This value was determined by finding the r-f magnetic field level at which the real part of magnetic susceptibility was reduced to $\frac{1}{\sqrt{2}}$ of its unsaturated value and using the saturation condition

$$\frac{1}{4} \gamma^2 H_s^2 T_1 T_2 = 1$$

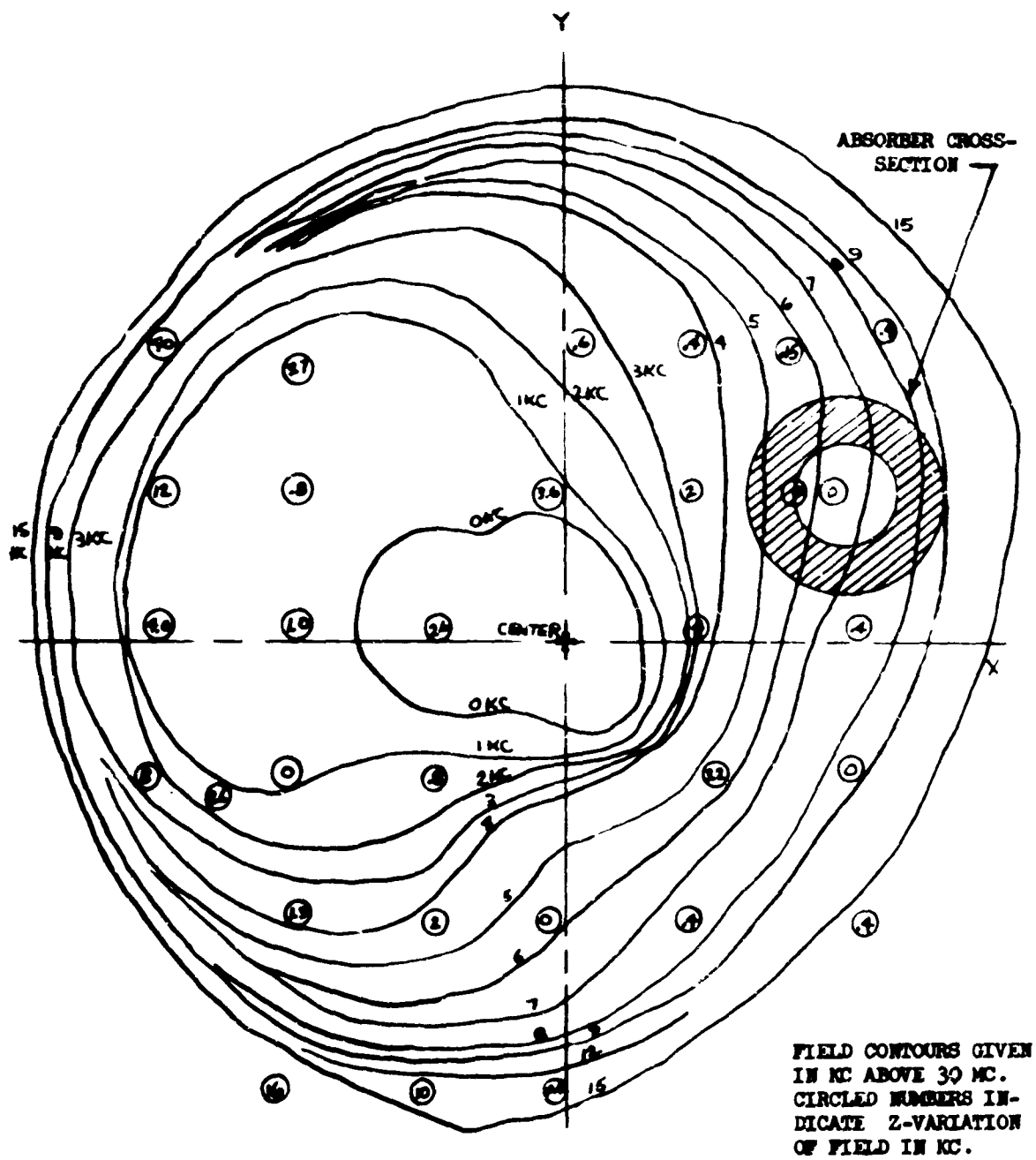


Fig. 25. DC Magnetic Field Contours

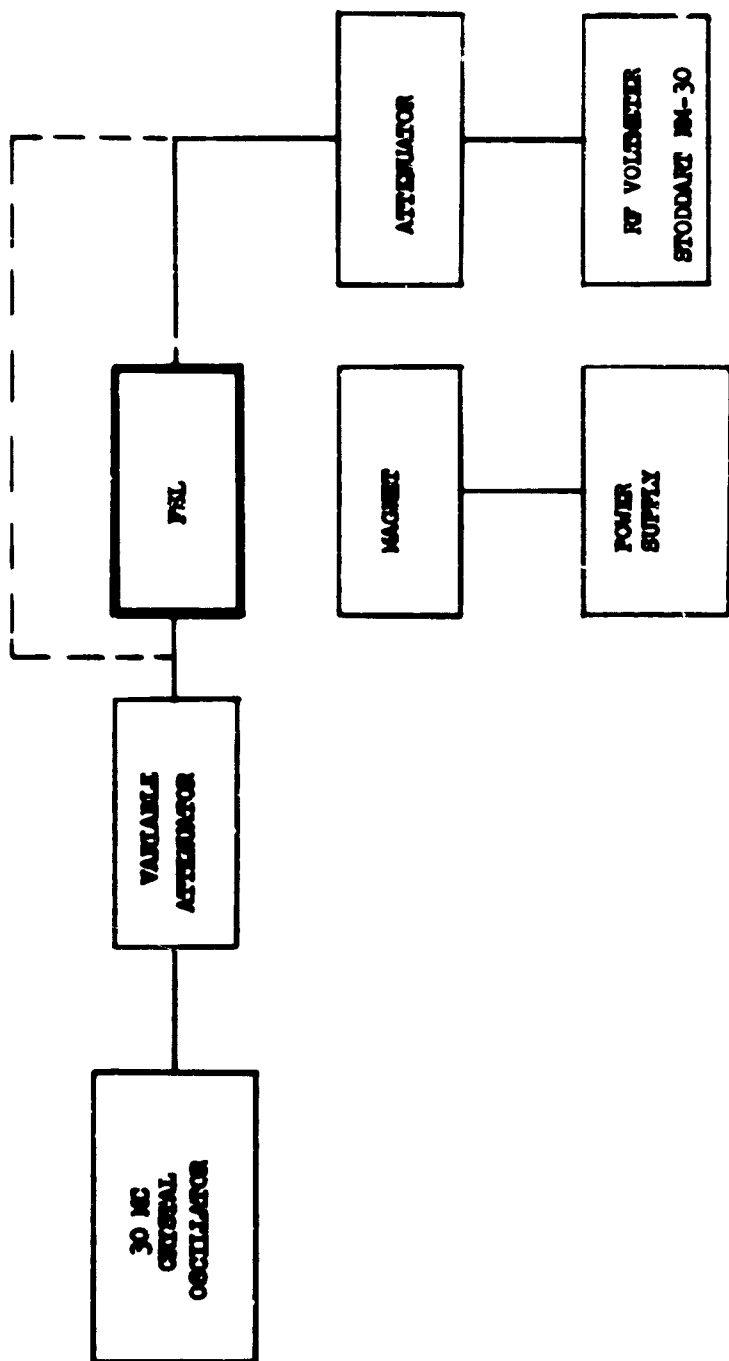


FIGURE 26 BLOCK DIAGRAM OF SYSTEM USED TO MEASURE INSULATION LOSS

The measured values of Q_o , T_1 and T_2 give a theoretical saturation level of -34.5 dbm. The measured saturation level is -36 dbm.

7.4 Selectivity and Intermodulation

The measured values of T_1 and T_2 (0.075 sec) indicate that the small signal selectivity should be 2.1 cps. Selectivity was measured approximately using the technique diagrammed in Fig. 27. A signal with 10% sinusoidal amplitude modulation was applied to the limiter. The input power level was adjusted so that the carrier power was above the limiter saturation level while the two sidebands were below saturation. Selective limiting of the carrier was manifested as an increase in percentage modulation as viewed on an oscilloscope. The modulation frequency was then lowered, bringing the two sidebands closer to the carrier, until the output signal modulation level was reduced to 10%. This occurred at a modulation frequency of 2 cps, which is of the same order as the predicted selectivity.

Intermodulation measurements were made using the setup pictured in Fig. 28. Two battery-powered crystal oscillators were used, one fixed-tuned and one voltage-variable. After passing through variable attenuators, these signals were fed into the limiter and thence into a 30 mc receiver. The 50 kc receiver IF output was fed into a wave analyzer. Absolute input frequency was determined by counting, and frequency difference was measured using the analyzer. The analyzer had a 3 cps selectivity and could be used to measure the frequency and amplitude of intermodulation products for signal spacings between approximately 60 cps and 200 cps.

With the fixed oscillator output power set at saturation and the tunable oscillator 30 db above saturation, only one significant intermodulation component was found.

This component had a frequency of $2\omega_2 - \omega_1$ as predicted by theory, where

ω_1 = fixed oscillator frequency

ω_2 = tunable oscillator frequency.

Intermodulation power was measured at signal separations of 64 cps, 106 cps, 150 cps, and 186 cps. The results are compared with theory in Fig. 29. The worst intermodulation level occurred at a spacing of 64 cps where intermodulation power was

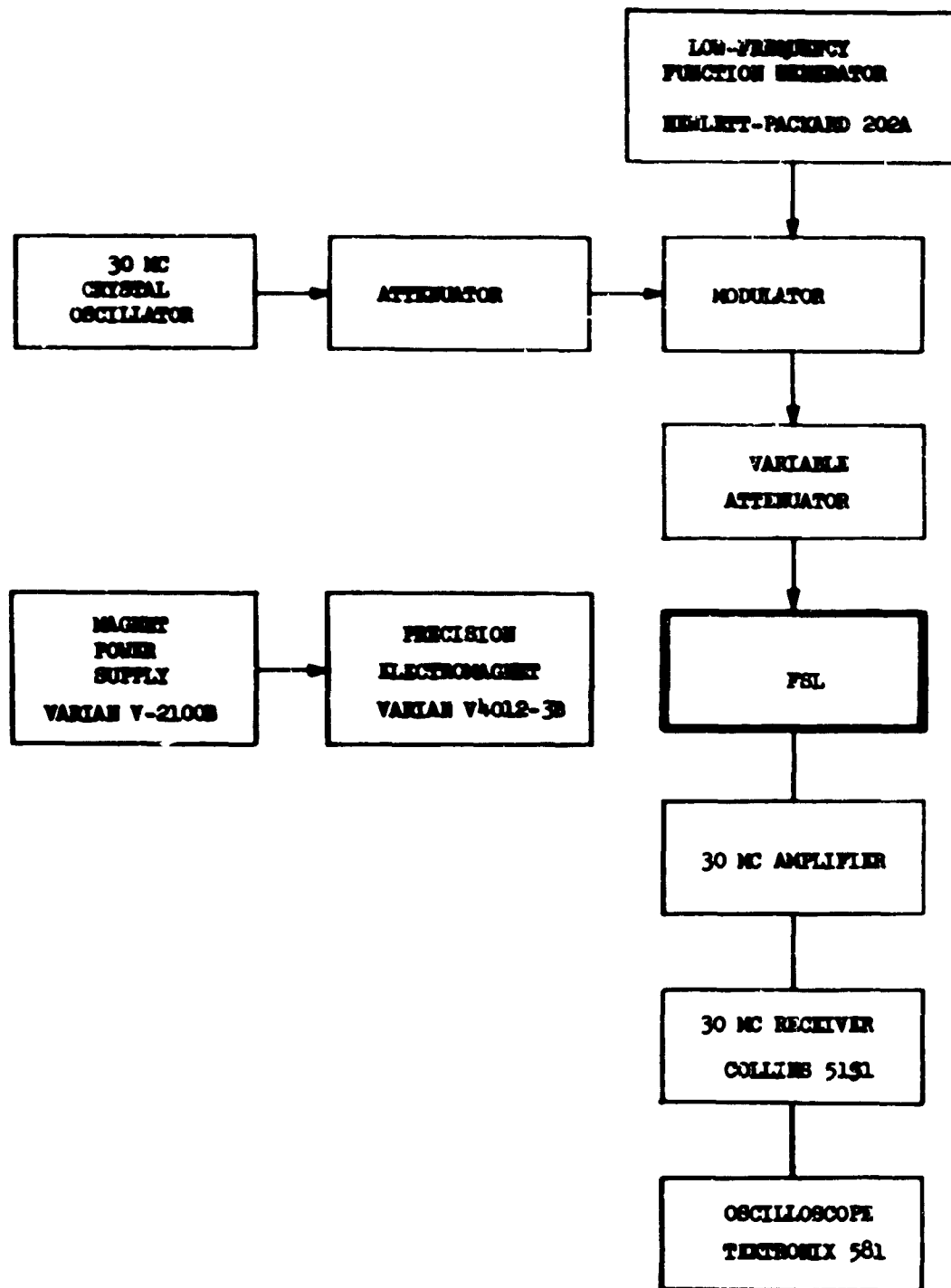


FIGURE 27 BLOCK DIAGRAM OF SYSTEM USED TO MEASURE SELECTIVITY

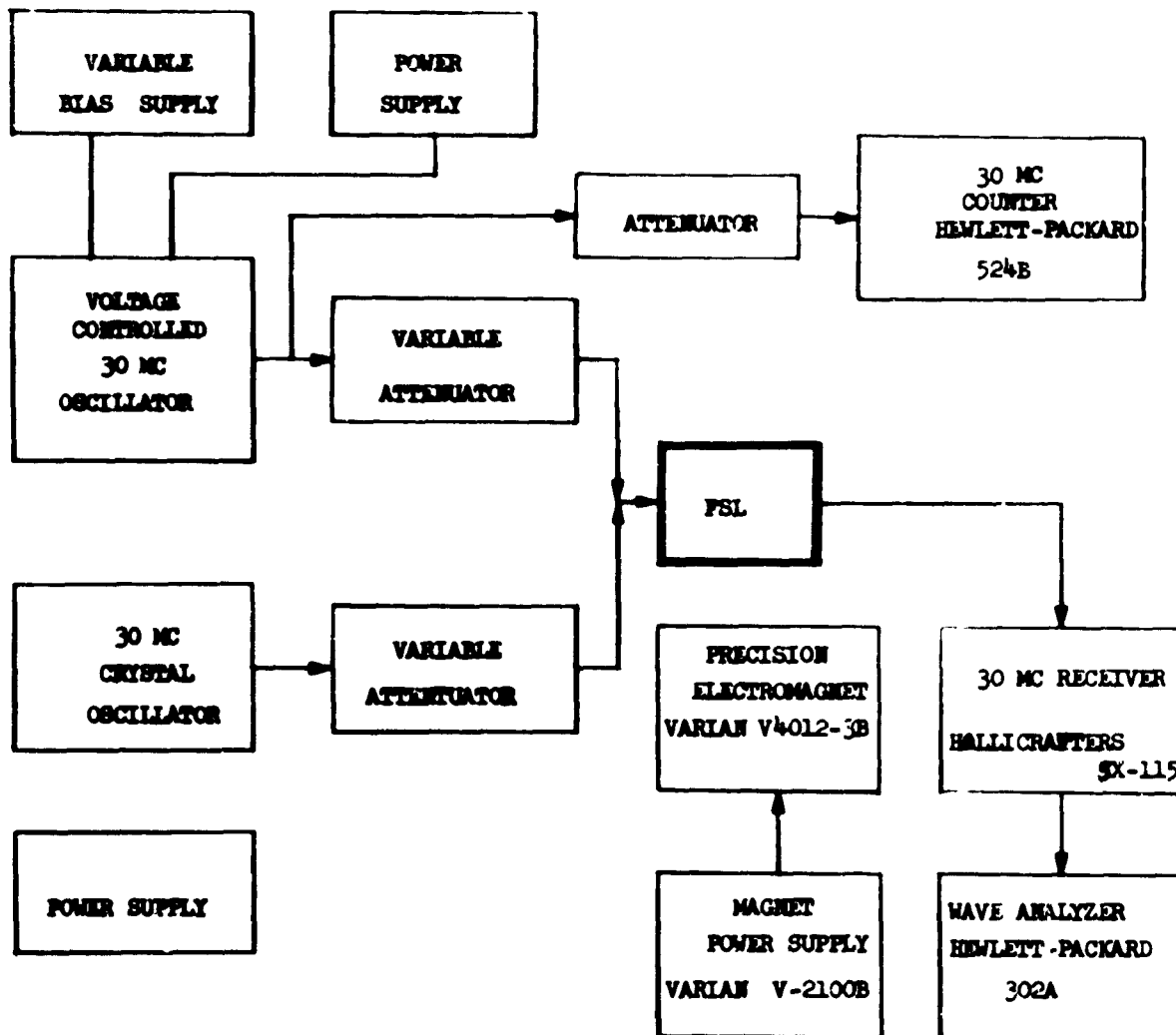


FIGURE 26 BLOCK DIAGRAM OF SYSTEM USED TO MEASURE INTERMODULATION

16 db below signal output level at ω_1 . For spacings beyond 200 cps, limiter intermodulation level was too low to be measured with the present experimental arrangement. As signal spacing was reduced below 60 cps, it was found difficult to hold the frequency spacing accurately, and furthermore the intermodulation component was masked by the much higher fundamental components at ω_1 and ω_2 .

7.5 Limiter Configuration

Fig. 30 shows a photograph of the experimental frequency selective limiter. The absorber and dummy cavities are made of copper, as is the enclosing box. The center conductor length is 1.7 inches. This represents $\frac{1}{230}$ of a free space wavelength at 30 mc; consequently, it was necessary to use a very large (4040 pf) loading capacitor. From left to right in Fig. 30 are shown (1) the ungrounded capacitor plate (0.1 inch copper), (2) the grounded capacitor plate (0.002 inch beryllium copper), (3) a rubber pressure disk, and (4) the cavity lid (0.1 inch copper). A mica sheet, 0.0006 inches thick, is sandwiched between the two capacitor plates, and the cover and pressure disk are used to eliminate air gaps between the capacitor plates and the mica dielectric.

Three detrimental effects result when capacitor air gaps exist:

- 1) An air gap as small as 0.0001 inch can reduce capacity enough to make resonance at 30 mc impossible.
- 2) Air gaps destroy the capacitor symmetry, causing an azimuthal variation in r-f magnetic field. This will degrade both bandwidth and limiting range.
- 3) Air gaps cause capacity to fluctuate with temperature, leading to bridge instability.

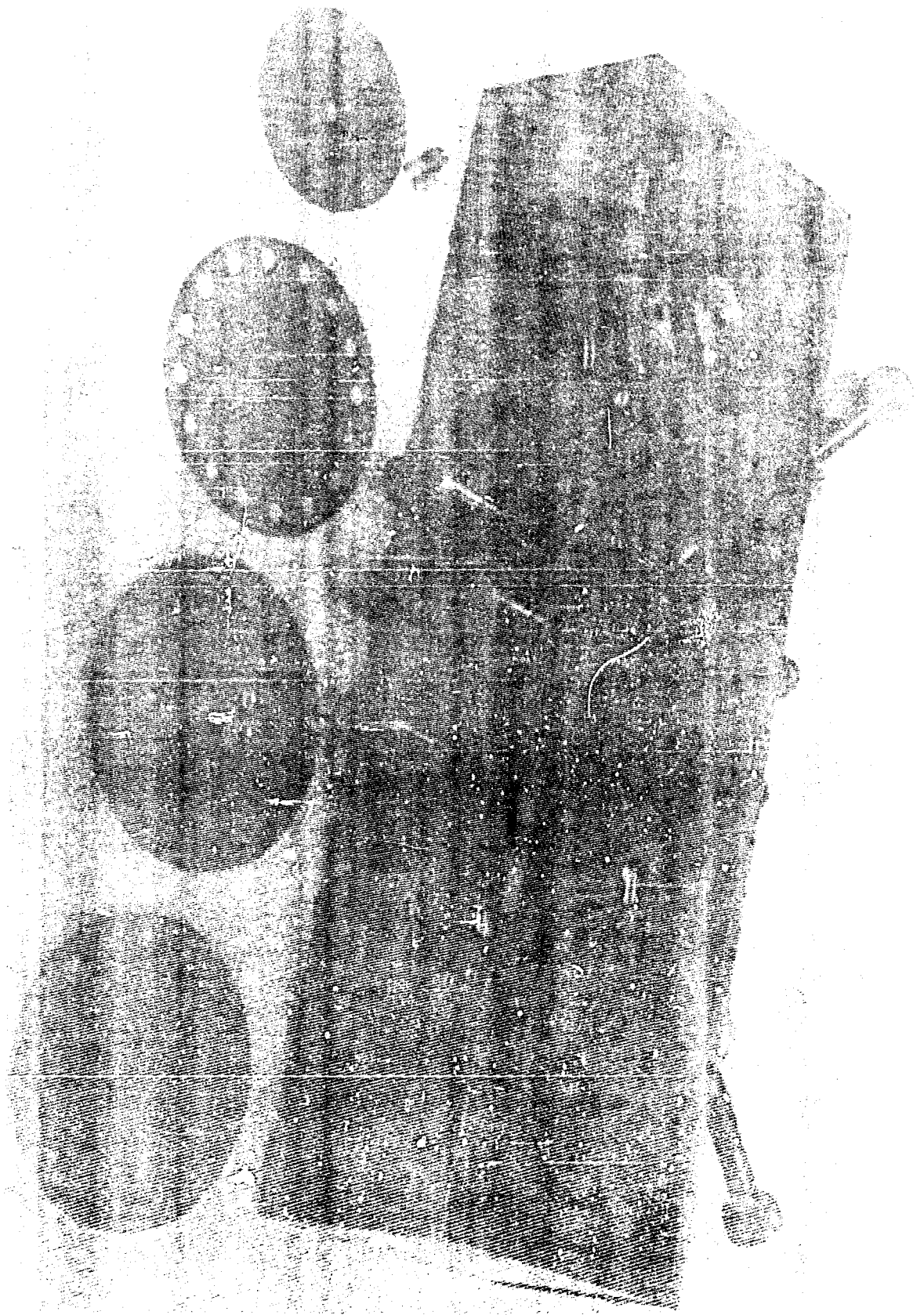


Fig. 30 Frequency selective Limiter

Although the use of a rubber pressure disk greatly reduced the air space between capacitor plates and dielectric, a certain small air gap still exists, as evidenced by a small drift in capacity with temperature. Owing to this drift, it has been possible to maintain a satisfactory bridge balance for only about 5 minutes before readjustment is necessary. It is felt that this drift problem can be eliminated by bonding the capacitor plates directly to the dielectric, thus eliminating all air gaps. Temperature effects could also be reduced by machining the cavities from a metal with a low thermal expansion coefficient, such as Invar. The enclosing copper box should be retained, however, to minimize thermal gradients between the cavities.

The complete bridge circuit is shown in Fig. 31. Resistive bridge balance is adjusted by means of a moveable coil (with series resistor and capacitor) in proximity to the transformer secondary. Copper plungers, visible in Fig. 30, were used to vary the reactive balance, although it was found that these controls also caused an appreciable change in resistive balance. Fine tuning of the cavity resonance was accomplished by means of two 10μ trimmer capacitors. These capacitors could also be used to adjust the reactive balance.

The experimental results confirm the validity of the theoretical analysis. Using this analysis, accurate predictions of device characteristics at other frequencies and of system performance can be made.

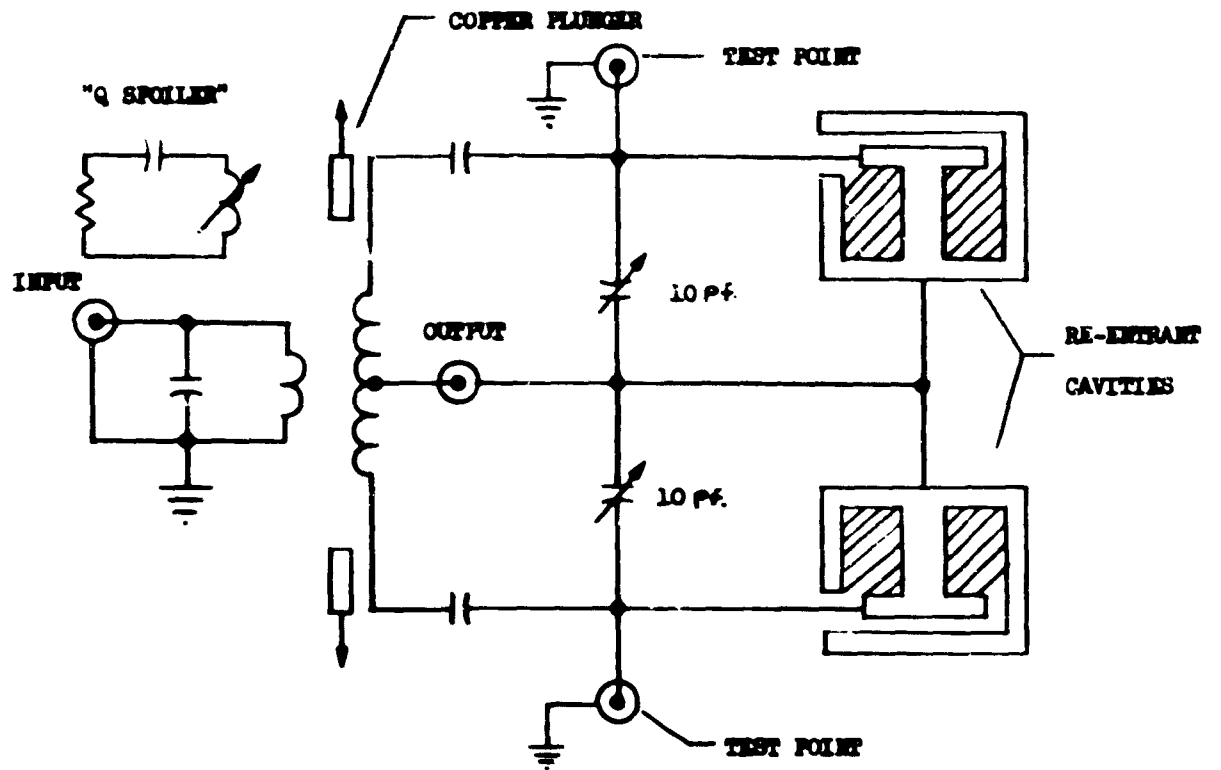


FIGURE 31 COMPLETE LIMITER CIRCUIT

The validity of the bandwidth enhancement (reactive compensation) technique was confirmed. The expected increase in bandwidth was not achieved primarily because the required gradient in dc magnetic field was not used. During this short program it was not possible to devote sufficient time to design or acquire magnet pole pieces that would produce the required magnetic field distribution. Nevertheless, a 20 db improvement in gain-bandwidth product over past models was achieved. Operating with the correct field distribution, the model developed during this program will meet or exceed a 3 kc bandwidth with no modification.

The intermodulation analysis shows that a high amplitude interfering signal which is being limited by as much as 30 db, and which is only 50 cps removed from a desired signal, will generate intermodulation products which are 20 db weaker than the desired signal, and will thus be negligible. This was confirmed by experiment.

The analysis also shows that under these same conditions, the amplitude suppression of the desired signal will be negligible. This, too, was confirmed by experiment.

This study has indicated that this device will provide from 20 to 30 db of suppression to either a cw interfering signal or to a modulated interfering signal with modulating frequencies greater than 30 cps. The limiter displays the unusual property of limiting faster on a high amplitude transient than on a somewhat lower amplitude transient.

The most significant problem encountered during the experimental program was bridge instability. This problem resulted primarily because the electrical characteristics of the cavities were not sufficiently stable with changes in ambient temperature.

This problem can be solved by

- 1) building the cavities out of a thermally stable material such as Invar, and
- 2) eliminating the small air gap between the dielectric and capacitor plates by using vacuum deposition techniques to fabricate the capacitor.

To develop this interference suppression technique further, it is recommended that the following items be investigated:

- 1) The existing cavities should be replaced with cavities with improved thermal stability.
- 2) The existing device should be placed in the properly distributed magnetic field and the bandwidth performance measured.
- 3) The performance of the limiter in a suitable receiving system should be investigated.
- 4) Performance of the limiter with complex signals should be evaluated.
- 5) Methods of reducing the insertion loss such as pumping or cooling should be studied.

This seven-month program has established the feasibility of developing this highly selective limiter. This new device, which is very effective against many types of coherent interference, should provide a valuable addition to the many existing techniques for increasing the jam resistance of communication and radar systems.

BIBLIOGRAPHY

1. Abragam, A., The Principles of Nuclear Magnetism, Clarendon Press, Oxford, 1961.
2. "Frequency Selective Limiter," Technical Proposal to RADC from The Boeing Company, D5-15057, March, 1964.
3. "Hyperselective Limiter," Jackson, D. R., and Orth, R. W., Proc. IEEE, October 1964.
4. "Hyperselective Limiter," Jackson, D. R., and Orth, R. W., presented at the 1964 Electron Device Meeting, Washington, D.C., October 31, 1964.
5. Bloembergen, N., Nuclear Magnetic Relaxation, W. A. Benjamin Co., New York, 1961.
6. Faki, George E., Paramagnetic Resonance, W. A. Benjamin Co., New York, 1962.
7. Ingram, J. E., Spectroscopy at Radio and Microwave Frequencies, Philosophical Library, New York, 1956.
8. Bloembergen, N., et al., Physical Review, 73, No. 7, pp 679-712, 1948.
9. Portis, A. M., Physical Review, 91, No. 5, pp 1071-1078, 1953.
10. Kotzebue, K. L., Trans IRE, M.T.T., pp 516-520, November 1962.
11. Sansalone, F.J., and Spencer, E. G., Trans IRE, M.T.T. -9, No. 3, 1961.
12. Barker, W. A., Reviews of Modern Physics, 34, No. 2, pp 173-185, 1962.

APPENDIX I

IMBALANCE IMPEDANCE OF RE-ENTRANT CAVITY

The object of the following discussion is to determine the reactance contributed to a re-entrant cavity by the paramagnetic material with which it is filled. Let Fig. 32 illustrate an axial view of the cavity which is immersed in a non-uniform dc magnetic field whose gradient (assumed constant) is along the x-axis. The magnetic resonant frequency corresponding to the magnetic field H_c seen at $x = 0$ will be denoted

$$\omega_c = \gamma H_c$$

We can relate a spatial position to a magnetic resonant frequency ω_0 by

$$x = \frac{\omega_0 - \omega_c}{\alpha}$$

where α is a constant of proportionality.

The total power, P_T , absorbed by the spin system from an rf field $H_{rf} = \frac{H_1 b}{r}$ found within the cavity can be expressed as

$$P_T(\omega) = A_1 \int \int \left(\frac{H_1}{r} \right)^2 P(\omega_0) d\omega_0 dy$$

where $P(\omega_0)$ is the absorption line shape (with area arbitrarily normalized to 2) and A_1 is a constant. Since $r^2 = x^2 + y^2$ we have

$$P_T(\omega) = A_1 \int \int \frac{H_1^2 P(\omega_0)}{y^2 + \left(\frac{\omega_0 - \omega_c}{\alpha} \right)^2} d\omega_0 dy$$

The integrand is the product of two functions of ω_0 .

For the case where the line width is much smaller than the spread of magnetic resonant frequencies across the center conductor of the cavity $\frac{1}{T} \ll \alpha b$, the line shape may be considered two delta functions when

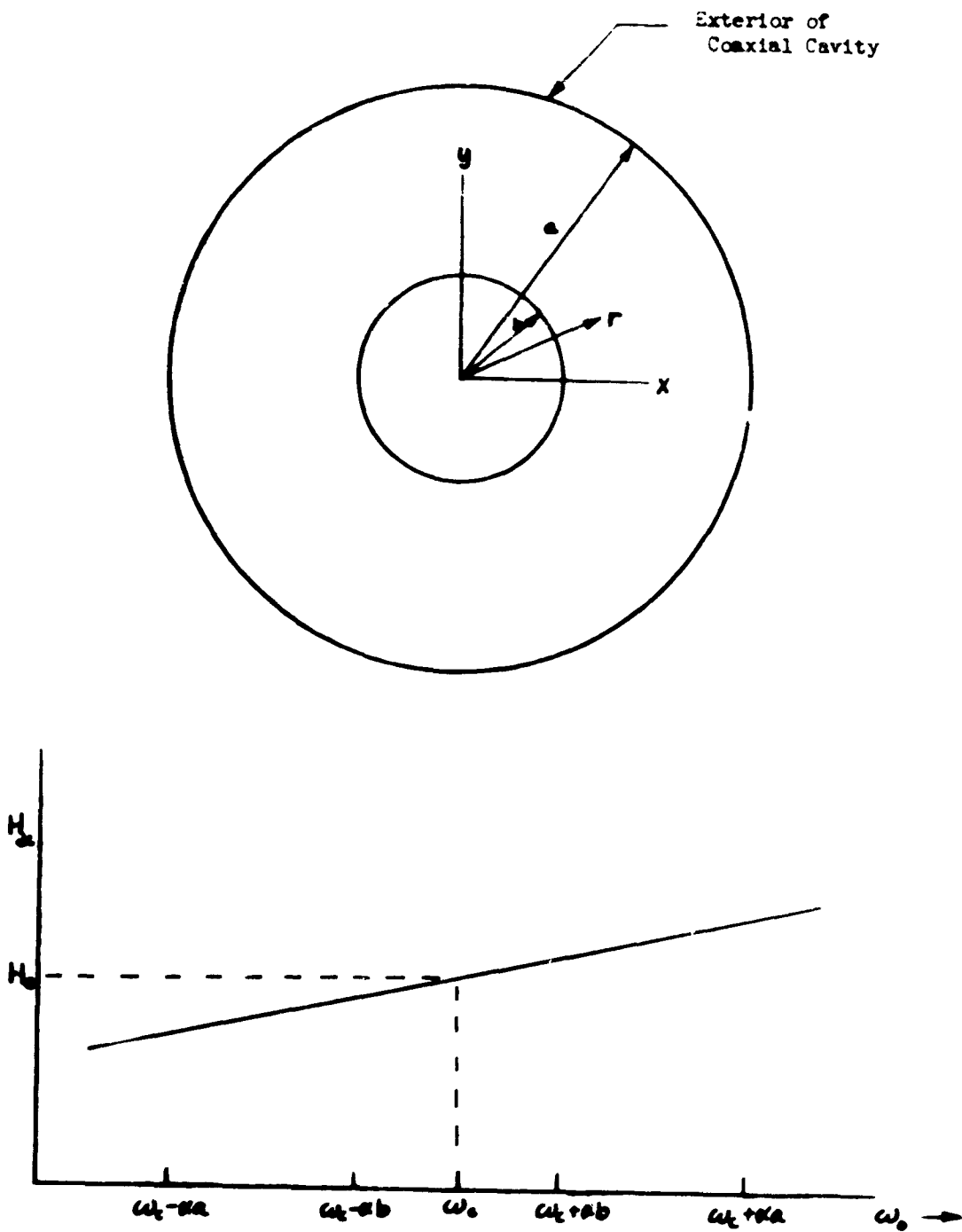


Fig. 32 Cavity and DC Field Configuration

compared to the factor $\frac{1}{r^2}$ (since the latter function varies slowly over the region of integration, changing at most by a factor of $(\frac{1}{2})^2$).

Using $P(\omega_0) \cong \delta(\omega - \omega_0) + \delta(\omega + \omega_0)$, the ω_0 integration then gives

$$P_r(\omega) \cong A_1 \int \frac{H_1^2}{y^2 + (\frac{\omega - \omega_0}{\alpha})^2} dy + A_2 \int \frac{H_2^2}{y^2 + (\frac{\omega + \omega_0}{\alpha})^2} dy \quad (12)$$

where the integration limits depend on the applied frequency ω , and the path of integration is now vertical in the annular region. Along this path of integration,

$$\begin{aligned} r^2 &= y^2 + \left(\frac{\omega - \omega_0}{\alpha}\right)^2 \\ r dr &= y dy \\ dy &= \frac{r dr}{\sqrt{r^2 - \left(\frac{\omega - \omega_0}{\alpha}\right)^2}} \end{aligned}$$

such that

$$P_r(\omega) \cong A_1 \int \frac{H_1^2 dr}{r \sqrt{r^2 - \left(\frac{\omega - \omega_0}{\alpha}\right)^2}} + \left[\text{negligible term from the } -\omega \text{ domain to be evaluated later.} \right]$$

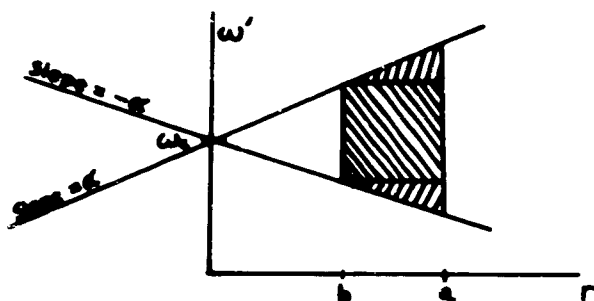
More specifically,

$$P_r(\omega) \cong \begin{cases} 2A_1 \int_{\frac{\omega - \omega_0}{\alpha}}^a \frac{H_1^2 dr}{r \sqrt{r^2 - \left(\frac{\omega - \omega_0}{\alpha}\right)^2}} & \omega_0 - da < \omega < \omega_0 - db \\ 2A_1 \int_b^a \frac{H_1^2 dr}{r \sqrt{r^2 - \left(\frac{\omega - \omega_0}{\alpha}\right)^2}} & \omega_0 + db < \omega < \omega_0 + da \\ 0 & \text{elsewhere} \end{cases} \quad (13)$$

The associated reactance can be found from the Kramers-Kronig relations.

$$X(\omega) = \frac{2A_2}{\pi} \left[\int_{\omega_2 - a}^{\omega_2 - b} \int_b^a \frac{dr d\omega'}{r \sqrt{r^2 - \left(\frac{\omega' - \omega_2}{\alpha}\right)^2} (\omega - \omega')} \right. \\ \left. + \int_{\omega_2 + b}^{\omega_2 + a} \int_b^a \frac{dr d\omega'}{r \sqrt{r^2 - \left(\frac{\omega' - \omega_2}{\alpha}\right)^2} (\omega - \omega')} + \int_{\omega_2 + a}^{\omega_2 + b} \int_{\omega_2 + \omega_0}^a \frac{dr d\omega'}{r \sqrt{r^2 - \left(\frac{\omega' - \omega_2}{\alpha}\right)^2} (\omega - \omega')} \right] \quad (14)$$

Since the integrand is both single valued and identical for each integral, the value of these integrals is determined uniquely by the integrand and the total region of integration in the r, ω' space. The three regions corresponding to the three integrals combine as shown below,



but this integral can be expressed as

$$X(\omega) = \frac{2A_2}{\pi} \int_a^b \int_{\omega_2 - \alpha r}^{\omega_2 + \alpha r} \frac{1}{r \sqrt{r^2 - \left(\frac{\omega' - \omega_2}{\alpha}\right)^2} (\omega - \omega')} d\omega' dr \quad (15)$$

This is the same integral obtained by finding the contribution to the reactance by individual rings of width dr at radius r . The above integral can be completed and for $r > \left| \frac{\omega' - \omega_2}{\alpha} \right|$ the ω' integration gives zero. This means that each ring contributes no reactance to frequencies

such that $|\omega - \omega_c| < \alpha a$ where r is the radius of the ring. Thus, for $|\omega - \omega_c| < \alpha b$, $X(\omega) = 0$. The only contribution to the reactance can come from the "negative-frequency-domain" absorption. (The second integral in expression 12).

The contribution to the reactance due to absorption at "negative frequencies" can be determined by finding the contribution to the reactance at negative frequencies due to absorption at positive frequencies. The integral given in (15) must then be computed in the region $r < \frac{\omega' - \omega_c}{\alpha}$ or $\omega' - \omega_c > \alpha r$. The ω' integral can be completed, leaving

$$\begin{aligned}
 X(\omega) &= \frac{j_2 \alpha}{2} \int_b^a \frac{dr}{r \sqrt{(\omega - \omega_c)^2 - (\alpha r)^2}} & (16) \\
 &= A_2 \alpha \int_{\alpha b}^{\alpha a} \frac{du}{u \sqrt{(\omega - \omega_c)^2 - u^2}} \\
 &= \frac{A_2 \alpha}{\omega - \omega_c} \left[\cosh^{-1} \left| \frac{\omega - \omega_c}{\alpha b} \right| - \cosh^{-1} \left| \frac{\omega - \omega_c}{\alpha a} \right| \right] & (17)
 \end{aligned}$$

Without the integral over r shown in (16) we have the reactance contributed by each ring at r and of width dr ; consequently the expression in (17) is valid for all ω outside $\omega_c \pm \alpha a$.

The reactance at $\omega = -\omega_c$ is

$$\begin{aligned}
 X(-\omega_c) &= A_2 \frac{\alpha}{-2\omega_c} \left[\cosh^{-1} \left| \frac{-2\omega_c}{\alpha b} \right| - \cosh^{-1} \left| \frac{-2\omega_c}{\alpha a} \right| \right] \\
 &\cong -A_2 \frac{\alpha}{2\omega_c} \left[\ln \frac{2\omega_c}{\alpha b} - \ln \frac{2\omega_c}{\alpha a} \right]
 \end{aligned}$$

but $\alpha b = 27(1.5)(10^3)$ and $\alpha = 2.246$ with $\omega_c = 27(30)(10^6)$
 thus,

$$X(-\omega_c) \cong -A_2 \alpha (4.3)(10^{-9})$$

This is also the same reactance contributed (by the absorption at negative ω) to the reactance within the usable band of ω corresponding to the γH_0 found within the center conductor of the coaxial re-entrant cavity.

The reactance seen at $|\omega - \omega_c| = \alpha a$ is

$$\begin{aligned} X(|\omega - \omega_c| = \alpha a) &= A_2 \frac{1}{\alpha} \left[\cosh^{-1} \frac{a}{b} - \cosh^{-1} \frac{a}{a} \right] \\ &= A_2 \alpha (3.25)(10^{-5}) \end{aligned}$$

Thus, the in-band reactance contributed by the absorption at negative frequencies is down by nearly 10^4 from that found at the outside of the coax chamber.

The reactance at frequencies ω corresponding to $\omega_c = \gamma H_0$ for values of H_0 found within the annular region of the coax cavity, but outside the center conductor, is easily found. The reactance at any $\omega_c - \alpha a < \omega < \omega_c - \alpha b$ or $\omega_c + \alpha b < \omega < \omega_c + \alpha a$ would only be contributed by absorptions in rings located at a smaller radius than $\frac{|\omega - \omega_c|}{\alpha}$. The total reactance at any frequency in the above ranges can then be expressed as

$$\begin{aligned} X(\omega) &= \alpha A_2 \int_b^{\frac{\omega - \omega_c}{\alpha}} \frac{dr}{r \sqrt{(\omega - \omega_c)^2 - (\alpha r)^2}} \\ &= A_2 \frac{\alpha}{\omega - \omega_c} \cosh^{-1} \left| \frac{\omega - \omega_c}{\alpha b} \right| \end{aligned}$$

The resulting reactance now has the form

$$X(\omega) = \begin{cases} 0 & -ab < \omega - \omega_c < ab \\ A_2 \frac{d}{\omega - \omega_c} \left[\cosh^{-1} \left| \frac{\omega - \omega_c}{ab} \right| \right] & \begin{array}{l} -da < \omega - \omega_c < -ab \\ ab < \omega - \omega_c < da \end{array} \\ A_2 \frac{d}{\omega - \omega_c} \left[\cosh^{-1} \left| \frac{\omega - \omega_c}{ab} \right|, -\cosh^{-1} \left| \frac{\omega - \omega_c}{da} \right| \right] & |\omega - \omega_c| > da \end{cases}$$

where negative frequency contributions have been neglected. From equation

(13), the corresponding resistance is

$$R(\omega) = \begin{cases} A_2 \frac{d}{\omega - \omega_c} \left[\cos^{-1} \left(\frac{\omega - \omega_c}{da} \right) - \cos^{-1} \left(\frac{\omega - \omega_c}{ab} \right) \right] & -ab < \omega - \omega_c < ab \\ A_2 \frac{d}{\omega - \omega_c} \left[\cos^{-1} \left(\frac{\omega - \omega_c}{da} \right) \right] & \begin{array}{l} -da < \omega - \omega_c < -ab \\ ab < \omega - \omega_c < da \end{array} \\ \sim 0 & |\omega - \omega_c| > da \end{cases}$$

APPENDIX II
OPTIMUM CAVITY DESIGN

In order to determine the best dimensions for the re-entrant cavities to be used in the frequency selective limiter bridge circuit, the criterion should be to maximize the ratio of the power absorbed by the spin system to the power lost in the walls of the cavity. At the same time the length and outer cavity radius will remain fixed (as restricted by the dimensions of the magnet utilized), the magnitude of the inner radius will be varied.

Assuming a TEM mode in a short coaxial cavity (including end plates), the power lost in the walls (P_{walls}) is found to be

$$P_{\text{walls}} = A_2 \left[\frac{L}{a} + \frac{L}{b} + 2 \ln \frac{a}{b} \right] \quad (18)$$

where L = length of cavity

As explained in Appendix I, there is no additional reactance (due to the spins) at magnetic resonant frequencies corresponding to the values of H_0 intercepted by the center conductor of the re-entrant cavity. Furthermore, since any saturation of χ' at one frequency will not change the reactance at that frequency (but will slightly change the reactance at adjoining frequencies) we will neglect the effects of χ' . The power absorbed can be found in the narrow linewidth approximation by evaluation of equation (13).

Defining ω_0 as the resonance frequency corresponding to the H_0 in band center,

$$P_r = \frac{2b}{\delta_1} \frac{2A\rho}{X} \left[\cos^{-1} \frac{X}{a} - \cos^{-1} \frac{X}{b} \right] \quad (19)$$

where $X = \frac{2b}{\delta_1} (\omega - \omega_0)$, and B_1 is a constant

The ratio of this to the wall losses can be maximized for a particular X .

Taking $X \rightarrow 0$

$$P_r = \frac{4 A \rho (a-b)}{B, a}$$

Consequently,

$$\frac{P_r}{P_{wall}} = \frac{4 A \rho (a-b)}{B, a A_s \left(\frac{L}{a} + \frac{L}{b} + 2 \ln \frac{a}{b} \right)} \quad (20)$$

For $\frac{L}{a} = 2$, this is maximum for $\frac{a}{b} = 2.24$; thus typical cavity dimensions can now be found. The design chosen has

$$L = 1.700 \text{ in}$$

$$a = 0.850 \text{ in}$$

$$b = 0.377$$

$$Q_s = 1540$$

$$\epsilon_r = 2.88 = \text{relative dielectric constant .0005 in film used for loading the re-entrant cavity.}$$

Fig. 8 shows the cavity in cross section.

APPENDIX III

DIFFUSION EFFECTS

Brownian Diffusion

We can consider the problem of Brownian diffusion and the resulting limitation on the saturation level and selectivity of the frequency selective limiter by the following method. From a random walk analysis we see that the average squared displacement of a typical molecule is

$$\langle x^2 \rangle = N \lambda^2$$

where

λ = mean path length between collisions

N = number of collisions

By introducing the mobility (m) we obtain

$$\langle x^2 \rangle = 2mkTt$$

Relating the mobility and viscosity we get

$$\langle x^2 \rangle = \frac{2kTt}{3\pi\eta r_0}$$

where

r_0 = effective molecule radius

η = viscosity in poise

t = time during which the observation is taken

Using

$t = 1 \text{ sec.}$

$T = 300^\circ\text{K}$

$k = 1.38 (10^{-23})$

$\eta = 1 \text{ poise} = 1/10 \text{ in mks units}$

$$r_0 = 1 \text{ \AA} \text{ for a worst case}$$

$$\langle x^2 \rangle = 10^{-10} \text{ m}^2$$

The comparison of $\sqrt{\langle x^2 \rangle}$ with the spatial width of a resonance line of 1 cy for a 3 kc bandwidth frequency selective limiter (where the region over which the spin system is distributed is assumed to be about 1 inch) shows that the Brownian motion causes spins to move about 10^{-2} of a line width in a time equal to the spin-lattice relaxation time, thus the effect is negligible.

Spin-Flip Diffusion

An NMR line which is not motionally-narrowed has a line width of about 1 kc. The pertinent relaxation time is then about 10^{-3} seconds. The time for relaxation by mutual spin flips could not be any faster than this value or the line would be determined by the mutual spin-flip rate. Thus if T_m is the mutual spin-flip relaxation time, the magnitude of T_m could be found by finding the time for precessing of one spin in the H field of the adjacent spin. Let r_{nn} be the nuclear-nuclear spacing



between two like nuclei. The field of one due to the other is

$$H = \frac{\mu_n}{r_{nn}^3}$$

This gives

$$T_m = \frac{2\pi \hbar^3}{V \mu_n}$$

Finding r_{nn} from assuming 10^{22} spatial cubes bounded by r_{nn} lines in a cubic centimeter we obtain a propagation rate of 1/20 line width/second for our frequency selective limiter model.

Thus, spin-flip diffusion can also be neglected.

APPENDIX IV - INTERMODULATION

If two sinusoidal signals at frequencies ω_1 and ω_2 are applied to the limiter, intermodulation products will appear at the frequencies $n\omega_1 + m\omega_2$, where n and m are integers. These intermodulation products will, in most cases be insignificantly small, but may become appreciable if ω_1 and ω_2 are very near one another and if the two signals are above the limiter saturation level. To calculate the magnitude of these intermodulation products, Bloch's equations with two sinusoidal driving signals can be used. The two signals will be decomposed into their counter-rotating circularly-polarized components. This allows a great simplification of the problem, since the two circular components at ω_1 and ω_2 rotating opposite the Larmor precession have a negligible effect on the motion of the spin system. To simplify the analysis further, all quantities will be measured from a frame rotating with angular velocity ω_1 in the direction of the Larmor precession. As is shown in Fig. 32 this choice of reference reduces the circularly-polarized RF field at ω_1 to a static field, pointing in the X direction. The circularly polarized field at ω_2 will appear as a vector rotating in the x-y plane with angular velocity $\delta = \omega_2 - \omega_1$. Finally, the DC field, which is assumed to be along the Z-axis, will have the magnitude $H_0 + \frac{\omega_1}{\gamma}$ where H_0 is the value of this field in the non-rotating frame.

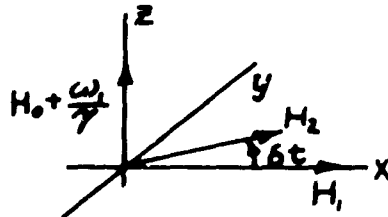


Fig. 32. Magnetic Field Components in Rotating Frame.

Bloch's equations can be written in vector form as

$$\dot{\bar{M}} = \gamma \bar{M} \times \bar{H} - \left[\hat{x} \frac{M_x}{T_2} + \hat{y} \frac{M_y}{T_2} \right] - \hat{z} \frac{M_z - M_0}{T_1} \quad (21)$$

where \hat{x} , \hat{y} , and \hat{z} are the x, y, and z unit vectors, respectively, and \bar{M} is the magnetization of the spin system. When the components of \bar{H} shown in Fig. 32 are substituted in equation (21) the following three equations result:

$$\dot{M}_x = \Delta\omega M_y - \gamma H_2 M_z \sin \delta t - \frac{1}{T_2} M_x \quad (22)$$

$$\dot{M}_y = \gamma H_1 M_z - \gamma H_2 M_z \cos \delta t - \Delta\omega M_x - \frac{1}{T_2} M_y \quad (23)$$

$$\dot{M}_z = \gamma H_2 M_x \sin \delta t - \gamma H_1 M_y - \gamma H_2 M_y \cos \delta t - \frac{1}{T_1} (M_z - M_0) \quad (24)$$

where

$$\Delta\omega = \gamma H_0 + \omega_1$$

From the form of the above equations, it is evident that M_x , M_y , and M_z will be periodic in time with a fundamental angular frequency equal to δ . Accordingly, Fourier expansions of the magnetization components will be written as follows:

$$M_x = \sum_{n=-\infty}^{\infty} M_{xn} e^{jn\delta t}, \quad M_y = \sum_{n=-\infty}^{\infty} M_{yn} e^{jn\delta t}, \quad M_z = \sum_{n=-\infty}^{\infty} M_{zn} e^{jn\delta t} \quad (25)$$

In the rotating frame, the transverse magnetization can be represented by the complex quantity

$$M_{\perp} = M_x + jM_y \quad (26)$$

Note that the magnitude and angle of this complex number are the same as those which the transverse magnetization vector has in the x-y plane. The Fourier expansion of M_{\perp} is

$$M_{\perp} = \sum_{n=-\infty}^{\infty} (M_{xn} + jM_{yn}) e^{jn\delta t} = \sum_{n=-\infty}^{\infty} M_{\perp n} e^{jn\delta t} \quad (27)$$

Each term in this sum corresponds to a component of transverse magnetization rotating with angular velocity $n\delta$, with magnitude and phase angle equal to the magnitude and angle of the corresponding Fourier component of the transverse magnetization vector. Upon transforming back to the non-rotating frame, each of these components will appear as a circularly polarized component of magnetization with angular frequency $\omega_1 + n\delta$. Components for which $n=0$ and 1 correspond to the system response at the two driving frequencies, ω_1 and ω_2 . The lowest order intermodulation components occur for $n = -1$ and $+2$. At this point it is important to recall that M_n is a real quantity and hence

$$M_{2n} = M_{2-n}^*$$

whereas M_n is a complex quantity and, in general

$$M_{2n} \neq M_{2-n}^*$$

A convenient expression involving M_n can be obtained by multiplying equation (23) by j and adding the result to equation (22). The following is obtained:

$$\dot{M}_z = -j\Delta\omega M_z + j\gamma(H_1 + H_2 e^{j\delta t})M_x - \frac{1}{T_2}M_z \quad (28)$$

Using definition (26), equation (28) can be written as follows:

$$\begin{aligned} \dot{M}_z = & \frac{\gamma H_2}{2J} M_z e^{j\delta t} - \frac{\gamma H_2}{2J} M_z e^{-j\delta t} - \frac{\gamma H_1}{2J} (M_z - M_z^*) \\ & - \frac{1}{T_1} (M_z - M_0) \end{aligned} \quad (29)$$

Equations (28) and (29) are sufficient to describe the response of the spin system and will be used as the basis for all that follows.

If the Fourier expansions of M_{\pm} and M_{\pm} are inserted in (28) and (29), terms of like frequency can be equated to give

$$M_{\pm n} = \frac{\gamma H_1 M_{\pm n} + \gamma H_2 M_{\pm n-1}}{n\delta + \Delta\omega - j/T_2} \quad (30)$$

$$M_{\pm n} = \frac{\frac{\gamma H_2}{2J}(M_{\pm 1-n}^* - M_{\pm n}) - \frac{\gamma H_1}{2J}(M_{\pm n} - M_{\pm n}^*) + \frac{M_0}{T_1} \delta_{0n}}{jn\delta + 1/T_1} \quad (31)$$

It is possible to eliminate $M_{\pm n}$ by combining equations (30) and (31) properly. The result is a second-order difference equation with variable coefficients. A series solution has been obtained for this equation, but is too cumbersome to be of immediate practical value. A more tractable solution can be obtained if simplifying assumptions about signal magnitude and frequency separation are introduced. Two such solutions will be obtained here, one which is valid only if the frequency separation, δ , is suitably large, and a second which is only valid if one of the signals is much smaller than the other.

An approximate solution of (30) and (31) will first be obtained, subject to the condition

$$\delta T_2 \gg \gamma^2 T_1 T_2 H_1 H_2 . \quad (32)$$

Remembering that the saturation condition for a circularly polarized field is $\gamma^2 H^2 T_1 T_2 = 1$, condition (32) can be rewritten in the form

$$\delta T_2 \gg \sqrt{P_1 P_2} / P_{sat} \quad (32a)$$

where P_1 and P_2 are the two input powers and P_{sat} is the limiter threshold level.

It is anticipated that the major components of transverse magnetization will be M_{t0} and M_{t1} , the driving frequency components. The major component of \bar{z} -axis magnetization should be the DC coefficient, M_{z0} . The validity of the above assumptions will be examined later. According to equation (30), M_{t0} and M_{t1} can be expressed approximately as

$$M_{t0} = \frac{\gamma H_1 M_{z0}}{\Delta\omega - j/T_2} \quad (33)$$

$$M_{t1} = \frac{\gamma H_2 M_{z0}}{\delta + \Delta\omega - j/T_2} \quad (34)$$

providing $H_1 M_{z0} \gg H_2 M_{z1}$ and $H_2 M_{z0} \gg H_1 M_{z1}$. Setting $n=0$ in (31), (33) and (34) can be substituted to give

$$M_{z0} = \frac{M_0}{1 + \frac{\gamma^2 H_1^2 T_1 T_2}{1 + T_2^2 \Delta\omega^2} + \frac{\gamma^2 H_2^2 T_1 T_2}{1 + T_2^2 (\Delta\omega + \delta)^2}} \quad (35)$$

The first order intermodulation components can be found by setting $n = -1$ and $+2$ successively in equation (30).

$$M_{t-1} = \frac{\gamma H_1 M_{z-1}}{\Delta\omega - \delta - j/T_2} \quad (36)$$

$$M_{t2} = \frac{\gamma H_2 M_{z1}}{\Delta\omega + 2\delta - j/T_2} \quad (37)$$

The assumptions $H_2 M_{z2} \ll H_1 M_{z1}$, $H_1 M_{z2} \ll H_2 M_{z1}$ were used to obtain (36) and (37). M_{z1} can be found by setting $n=1$ in equation (31).

$$M_{z1} = \frac{\frac{\gamma H_1}{2j} M_{t0} - \frac{\gamma H_2}{2j} M_{t1}}{j\delta + 1/T_1} \quad (38)$$

Here, $H_2 M_{t2}$ and $H_1 M_{t-1}$ have been neglected in comparison to $H_2 M_{t0}$ and $H_1 M_{t1}$.

After substituting (33) and (34) in (38),

$$M_{z1} = - \frac{\gamma^2 H_1 H_2 (\delta - 2j/T_2) M_{z0}}{2(\delta - j/T_1)(\Delta\omega + \delta - j/T_2)(\Delta\omega + j/T_2)} \quad (39)$$

Equation (39) can be used to check the assumptions used in deriving (33) and (34), namely, that condition (32) implies

$$\gamma H_1 M_{z1} \ll \gamma H_2 M_{z0}$$

$$\gamma H_2 M_{z1} \ll \gamma H_1 M_{z0}$$

These inequalities can be readily proved using (39) providing T_1 is not appreciably longer than T_2 , a condition which generally holds for a motionally narrowed line. M_{z1} , M_{z-1} , and M_{z2} are third-order intermodulation products. The remaining assumptions used in obtaining (30), (37) and (38) involve neglecting fifth-order products in comparison to the above third-order products and will not be proved.

The intermodulation components of M_z can be found by using (35), (36), (37) and (39)

$$M_{z-1} = - \frac{\gamma^3 H_1^2 H_2 (\delta + \frac{2j}{T_2})(\Delta\omega + \frac{j}{T_2})(\Delta\omega + \delta - \frac{j}{T_2}) M_0}{2(\delta + \frac{j}{T_1})(\Delta\omega - \delta - \frac{j}{T_2})(\Delta\omega - \frac{j}{T_2})(\Delta\omega + \frac{j}{T_2})(\Delta\omega + \delta - \frac{j}{T_2})(\Delta\omega + \delta + \frac{j}{T_2})} \quad (40)$$

$$M_{z2} = - \frac{\gamma^3 H_1 H_2^2 (\delta - \frac{2j}{T_2})(\Delta\omega - \frac{j}{T_2})(\Delta\omega + \delta + \frac{j}{T_2}) M_0}{2(\delta - \frac{j}{T_1})(\Delta\omega + 2\delta - \frac{j}{T_2})(\Delta\omega - \frac{j}{T_2})(\Delta\omega + \frac{j}{T_2})(\Delta\omega + \delta - \frac{j}{T_2})(\Delta\omega + \delta + \frac{j}{T_2})} \quad (41)$$

where

$$T_{21} = \frac{T_2}{\sqrt{1 + \gamma^2 H_1^2 T_1 T_2}}, \quad T_{22} = \frac{T_2}{\sqrt{1 + \gamma^2 H_2^2 T_1 T_2}}. \quad (42)$$

The output voltage of the limiter at any given frequency will be proportional to the volume average of the Fourier component of magnetization at that frequency. Assuming that the distribution of spins per unit frequency range is uniform and that the RF magnetic field is uniform, the output voltage at the frequency $\omega + n\delta$ will be given by

$$V_{\omega, n\delta} = j\beta \int_{-\omega_b + \omega}^{-\omega_a + \omega} M_{\pm n} d\Delta\omega, \quad (43)$$

where ω_a and ω_b are the Larmor frequencies at the edges of the spin distribution, and β is a parameter depending upon the circuit configuration.

The two intermodulation components, $M_{\pm 1}$ and $M_{\pm 2}$, fall off as $\frac{1}{\Delta\omega^3}$ for $\Delta\omega \gg \delta$.

If $\delta \ll \omega_a - \omega_b$, the limits on integral (43) can be extended to $-\infty$

and $+\infty$ and contour integration can be used to evaluate $V_{\omega, -\delta}$ and $V_{\omega, +2\delta}$.

A pole-zero plot for $M_{\pm 1}$ is shown below in Fig. 33, together with the integration contour to be used in evaluating $V_{\omega, -\delta}$.

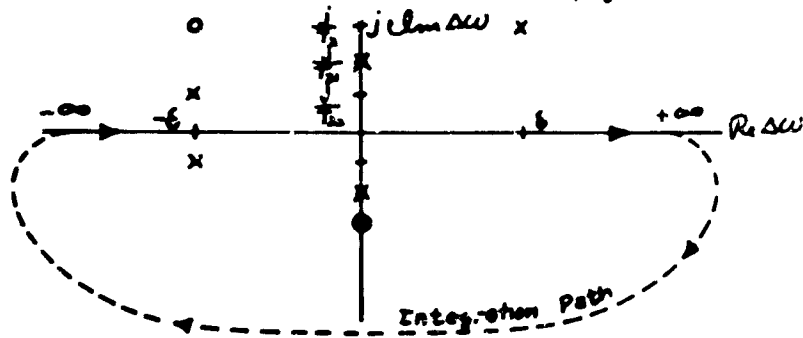


Fig. 33. Pole-Zero Plot

After applying the residue theorem and condition (32), $V_{\omega, -\delta}$ is found to be:

$$V_{\omega, -\delta} = -\frac{\pi\gamma^3 H_1^2 H_2 \beta M_0}{2\delta^2} \left[-\frac{1}{2} + \frac{1}{\sqrt{1 + \gamma^2 H_1^2 T_1 T_2}} + \frac{1}{2\sqrt{1 + \gamma^2 H_2^2 T_1 T_2}} \right] \quad (44)$$

In a like manner, $V_{\omega, \pm 2\delta}$ is found to be

$$V_{\omega, \pm 2\delta} = -\frac{\pi\gamma^3 H_1 H_2^2 \beta M_0}{2\delta^2} \left[-\frac{1}{2} + \frac{1}{2\sqrt{1+\gamma^2 H_1^2 T_1 T_2}} + \frac{1}{\sqrt{1+\gamma^2 H_2^2 T_1 T_2}} \right] \quad (45)$$

In obtaining (44) and (45), it was assumed that $\delta \gg \frac{1}{T_2}$ and $\delta \gg \frac{1}{T_2}$.

This will always be true providing at least one of the signals is near or above saturation; this is the only interesting case so far as intermodulation is concerned and providing condition (3) is satisfied.

The amplitude of the intermodulation products will now be compared to the limiter output for the single signal case. The single signal case has been treated in Appendix IX. In the present notation, output voltage with a single signal applied at ω_1 will be

$$V_{\omega_1} = \frac{j\pi\gamma H_1 M_0 \rho}{\sqrt{1+\gamma^2 H_1^2 T_1 T_2}} \quad (46)$$

Finally, by squaring (44), (45), and (46), the ratio of intermodulation power to signal output power is found to be

$$\frac{P_{\omega, \pm\delta}}{P_{\omega, P_2=0}} = \frac{P_1 P_2 \left(1 + \frac{P_1}{P_{sat}}\right)}{4P_{sat}^2 (\delta T_2)^4} \left[-\frac{1}{2} + \frac{1}{\sqrt{1 + \frac{P_1}{P_{sat}}}} + \frac{1}{2\sqrt{1 + \frac{P_2}{P_{sat}}}} \right]^2 \quad (47)$$

$$\frac{P_{\omega, \pm 2\delta}}{P_{\omega, P_2=0}} = \frac{P_2^2 \left(1 + \frac{P_1}{P_{sat}}\right)}{4P_{sat}^2 (\delta T_2)^4} \left[-\frac{1}{2} + \frac{1}{2\sqrt{1 + \frac{P_1}{P_{sat}}}} + \frac{1}{\sqrt{1 + \frac{P_2}{P_{sat}}}} \right]^2 \quad (48)$$

The assumptions used in deriving (47) and (48) are summarized below.

$$\frac{\sqrt{P_1 P_2}}{P_{sat}} \gg \delta T_2 ; T_1 = T_2 ;$$

$$\frac{P_1 + P_2}{P_{sat}} > 1 .$$

Equation (48) is plotted in Fig. 14 as a function of δ

A solution of equations (49) and (51) will now be obtained for the case where

$$H_2 \gg H_1 \quad (49)$$

If equation (51) is written out for M_{21} and if (49) is substituted in the right-hand side, the following equation results:

$$\begin{aligned} (j\delta + \frac{1}{T_1})M_{21} = \frac{\gamma H_2}{2j} \left[\frac{\gamma H_1 M_{20} + \gamma H_2 M_{21}}{\Delta\omega + j/T_2} - \frac{\gamma H_1 M_{22} + \gamma H_2 M_{21}}{2\delta + \Delta\omega - j/T_2} \right] \\ - \frac{\gamma H_1}{2j} \left[\frac{\gamma H_1 M_{21} + \gamma H_2 M_{20}}{\delta + \Delta\omega - j/T_2} - \frac{\gamma H_1 M_{21} + \gamma H_2 M_{22}}{-\delta + \Delta\omega + j/T_2} \right] \quad (50) \end{aligned}$$

If the fifth-order component, M_{22} , is ignored and if all terms quadratic in H_1 are disposed of, an expression relating M_{21} and M_{20} can be obtained.

$$M_{21} = \frac{\gamma^2 H_1 H_2 (2\delta + \Delta\omega - \frac{j}{T_2}) (\delta - \frac{2j}{T_2}) M_{20}}{2j (j\delta + \frac{1}{T_1}) (\Delta\omega + \delta + \Omega) (\Delta\omega + \delta - \Omega) (\delta + \Delta\omega - \frac{j}{T_2})} \quad (51)$$

$$\Omega = \sqrt{(\delta - \frac{j}{T_2})^2 - \gamma^2 H_2^2} \quad (52)$$

It has been assumed that $T_1 = T_2$. The quantity, Ω , is complex and by convention will be taken as that root of $(\delta - \frac{j}{T_2})^2 - \gamma^2 H_2^2$ which has a positive imaginary part. This choice is arbitrary, since all expressions involving Ω will be unchanged if Ω is replaced by $-\Omega$.

An expression for M_{20} can be readily obtained by setting $H_1 = 0$ in (35), since the assumptions which led to (35) are not in contradiction to condition (49). Written in factored form, M_{20} is

$$M_{20} = \frac{(\Delta\omega + \delta - \frac{j}{T_2})(\Delta\omega + \delta + \frac{j}{T_2}) M_0}{(\Delta\omega + \delta - \frac{j}{T_{22}})(\Delta\omega + \delta + \frac{j}{T_{22}})} \quad (53)$$

The third order intermodulation components, M_{t-1} and M_{t2} are, according to (31),

$$M_{t-1} = \frac{\gamma H_1 M_{z-1} + \gamma H_2 M_{z-2}}{-\delta + \Delta\omega - j/T_2}$$

$$M_{t2} = \frac{\gamma H_1 M_{z2} + \gamma H_2 M_{z1}}{2\delta + \Delta\omega - j/T_2}$$

If $H_2 \gg H_1$, M_{t2} will generally be much larger than M_{t-1} , and can be written approximately as

$$M_{t2} = \frac{\gamma H_2 M_{z1}}{2\delta + \Delta\omega - j/T_2} \quad (54)$$

Combining (51), (53), and (54),

$$M_{t2} = - \frac{\gamma^3 H_1 H_2^2 (\delta - \frac{2j}{T_2}) (\Delta\omega + \delta + \frac{j}{T_2}) M_0}{2(\delta - \frac{j}{T_1}) (\Delta\omega + \delta + \Omega) (\Delta\omega + \delta - \Omega) (\Delta\omega + \delta + \frac{j}{T_2}) (\Delta\omega + \delta + \frac{j}{T_2})} \quad (55)$$

Contour integration can again be used to calculate the limiter intermodulation voltage. The result is

$$V_{\omega_1+2\delta} = - \frac{\pi \beta \gamma^3 H_1 H_2^2 (\delta - \frac{2j}{T_2}) M_0}{2\Omega (\delta - \frac{j}{T_2}) (\Omega + \frac{j}{T_1}) \sqrt{1 + \gamma^2 H_2^2 T_2^2}} \quad (56)$$

If this voltage is compared with the small signal output voltage at ω_1 , when $H_2 = 0$ (see expression (50)), the ratio of intermodulation output power to signal output power (with no large, interfering signal at ω_2) is found to be

$$\frac{P_{\omega_1+2\delta}}{P_{\omega_1}|_{P_2=0}} = \frac{P_2^2 (\delta^2 T_2^2 + 4)}{4 P_{3\omega_1}^2 |\Omega'|^2 (\delta^2 T_2^2 + 1) |\Omega' + j\sqrt{1 + \frac{P_2}{P_{3\omega_1}}}|^2 (1 + \frac{P_2}{P_{3\omega_1}})} \quad (57)$$

where

$$\Omega' = \sqrt{(\delta T_2 - j)^2 - \frac{P_2}{P_{3\omega_1}}} \quad (58)$$

Equation (57) is plotted in Fig. 15 as a function of δ . The only assumptions inherent in (57) are $P_2 \gg P_1$ and $T_1 = T_2$.

In addition to intermodulation, a certain degree of small signal suppression will occur in the limiter. According to (43), the small signal output voltage at ω , is

$$V_{\omega_1} = j\beta \int_{-\omega_b + \omega_1}^{-\omega_a + \omega_1} M_{\pm 0} d\Delta\omega \quad (59)$$

$M_{\pm 0}$, in turn, is approximately given by (see equation (30))

$$M_{\pm 0} = \frac{\gamma H_1 M_{\pm 20}}{\Delta\omega - j/T_2} \quad (60)$$

where the third-order component, $M_{\pm 2-1}$, has been neglected in comparison to the zeroth order component, $M_{\pm 20}$. $M_{\pm 20}$ is a zeroth order component since it is non-zero and equal to M_0 in the absence of H_1 and H_2 . It will be convenient to break the integral (59) into two parts, one part equal to the unsuppressed output voltage and the other part equal to the decrease in small signal voltage due to the presence of a large signal at ω_2 .

$$V_{\omega_1} = j\beta \int_{-\omega_b + \omega_1}^{-\omega_a + \omega_1} \frac{\gamma H_1 M_0}{\Delta\omega - j/T_2} d\Delta\omega + j\beta \int_{-\omega_b + \omega_1}^{-\omega_a + \omega_1} \frac{\gamma H_1 (M_{\pm 20} - M_0)}{\Delta\omega - j/T_2} d\Delta\omega \quad (61)$$

Equation (61) is not entirely rigorous since both integrands should contain an even distribution function, $g(\omega_0)$, to account for reactance compensation. This distribution function has the effect of making the imaginary part of the first term zero over the usable limiter bandwidth. Retaining the real part of the first term and substituting for $M_{\pm 20}$ from (53), (61) becomes

$$V_{\omega_1} = \frac{-\beta \gamma H_1 M_0}{T_2} \int_{-\omega_b + \omega_1}^{-\omega_a + \omega_1} \frac{g(\Delta\omega - \omega_1)}{\Delta\omega^2 + \frac{1}{T_2^2}} d\Delta\omega + j\beta \gamma H_1 H_2^2 \int_{-\omega_b + \omega_1}^{-\omega_a + \omega_1} \frac{g(\Delta\omega - \omega_1) d\Delta\omega}{\left(\Delta\omega - \frac{j}{T_2}\right) \left(\Delta\omega + \delta - \frac{j}{T_2}\right) \left(\Delta\omega + \delta + \frac{j}{T_2}\right)} \quad (62)$$

The distribution function is slowly varying compared to the factor $(\Delta\omega^2 + \frac{1}{T_2})^{-1}$ and hence can be taken outside the first integral and replaced by its value at $\Delta\omega=0$. If $|\delta| \ll \omega_a - \omega_b$, the same thing can be done with the second integral. Both integrands fall off rapidly in comparison to $\frac{1}{\Delta\omega}$, so the limits of integration can be extended to $\pm \infty$. When these integrals are evaluated, V_{ω_1} is found to be

$$V_{\omega_1} = -\pi M_0 \beta \gamma H_1 g(\omega_1) \left[1 - \frac{\gamma^2 H_1^2 T_{22}}{(\frac{1}{T_{21}} + \frac{1}{T_2} - j\delta)} \right] \quad (b3)$$

As before, output power will be normalized to the value of P_{ω_1} when $P_2=0$

$$\frac{P_{\omega_1}}{P_{\omega_1}|_{P_2=0}} = \left| 1 - \frac{P_2}{P_{2sc} \sqrt{1 + \frac{P_2}{P_{2sc}}} \left(1 + \sqrt{1 + \frac{P_2}{P_{2sc}}} - j\delta T_2 \right)} \right|^2 \quad (b4)$$

Equation (b4) is plotted in Fig. 16 as a function of δ .

APPENDIX V

COHERENT INTERFERENCE SUPPRESSION

In order to determine the effectiveness of the Frequency Selective Limiter as an interference suppression device, the mean square error between actual signal voltage and limiter output voltage will be calculated. Because the exact nature of the input signal is unknown, the mean square error must be computed statistically by considering the ensemble of all possible input signals and averaging the mean square error over this ensemble. The i^{th} member of this input ensemble will be denoted $\mathcal{V}_S^i(t) + \mathcal{V}_I^i(t)$ where $\mathcal{V}_S^i(t)$ is the instantaneous signal voltage and $\mathcal{V}_I^i(t)$ is the instantaneous interference voltage. When the ensemble of input voltages is applied to an ensemble of identical limiters, a corresponding ensemble of output voltages, $\mathcal{V}_O^i(t)$ will result. The mean square error is defined as

$$\mathcal{E} = \lim_{N \rightarrow \infty} \frac{1}{N} \sum_{i=0}^N [\mathcal{V}_S^i(t) - \mathcal{V}_O^i(t)]^2 \quad (55)$$

To save space, the ensemble average operation will be denoted by a bar above the averaged quantity, thus

$$\mathcal{E} = \overline{[\mathcal{V}_S^i(t) - \mathcal{V}_O^i(t)]^2} \quad (56)$$

To be a meaningful measure of signal degradation, \mathcal{E} should be zero when there is no interference present and no signal distortion. This can only be so if the quantity $\mathcal{V}_O^i(t)$ is scaled up from the actual limiter output voltage by a factor equal to the small signal voltage loss of the limiter. This convention will be adhered to in the following.

The output voltage, $V_o'(t)$, will contain both signal and interference as well as a variety of intermodulation products. It has been shown in Section 5 that the interaction of signal and interference in the limiter results mainly in the suppression of certain portions of the signal spectrum and that intermodulation products can be neglected. The action of the limiter can be described in this case by a transfer function, $H(\omega)$, which depends upon the input power spectral density. According to the convolution theorem, the instantaneous output voltage can be expressed as

$$V_o'(t) = \frac{1}{2\pi} \int_{-\infty}^{\infty} [V_s'(t-t') + V_I'(t-t')] h(t') dt' \quad (67)$$

where $h(t')$ is the inverse Fourier transform of $H(\omega)$.

$$h(t') = \int_{-\infty}^{\infty} H(\omega) e^{j\omega t'} d\omega \quad (68)$$

Substituting (67) in (66) gives

$$\mathcal{E} = \overline{V_s^2(t)^2} - \frac{1}{\pi} \overline{V_s'(t) \int_{-\infty}^{\infty} [V_s'(t-t') + V_I'(t-t')] h(t') dt'} + \overline{V_o'(t)^2}$$

If the ensemble average is performed before integrating, \mathcal{E} will appear as

$$\mathcal{E} = \overline{V_s^2(t)^2} - \frac{1}{\pi} \int_{-\infty}^{\infty} [\overline{V_s'(t) V_s'(t-t')} + \overline{V_s'(t) V_I'(t-t')}] h(t') dt' + \overline{V_o'(t)^2}$$

The quantity $\overline{V_s'(t) V_s'(t-t')}$ is the autocorrelation function of the desired signal. It is independent of t and will be an even function of t' . The quantity $\overline{V_s'(t) V_I'(t-t')}$ is the cross-correlation between signal

and interference and will be zero since signal and interference are uncorrelated. Using definition (2), \mathcal{E} may now be written as

$$\mathcal{E} = \overline{v_s'(t)^2} - \frac{1}{\pi} \int_{-\infty}^{\infty} \overline{v_s'(t)v_s'(t-t)} \int_{-\infty}^{\infty} H(\omega) e^{j\omega t} d\omega dt + \overline{v_o'(t)^2}$$

Reversing the order of integration,

$$\mathcal{E} = \overline{v_s'(t)^2} - 2 \int_{-\infty}^{\infty} H(\omega) \left[\frac{1}{2\pi} \int_{-\infty}^{\infty} \overline{v_s'(t)v_s'(t-t)} e^{j\omega t} dt \right] d\omega + \overline{v_o'(t)^2} \quad (69)$$

According to the Wiener-Khinchine relation, the quantity in square brackets is proportional to the signal power spectral density, $G_s(\omega)$.

$$R_{in} G_s(\omega) = \frac{1}{2\pi} \int_{-\infty}^{\infty} \overline{v_s'(t)v_s'(t-t)} e^{j\omega t} dt \quad (70)$$

R_{in} = Limiter Input Impedance

The quantity $\overline{v_o'(t)^2}$ is proportional to the total output power, and may be written as the sum of the signal and interference output powers.

$$\overline{v_o'(t)^2} = R_{in} \int_{-\infty}^{\infty} [G_s(\omega) + G_I(\omega)] |H(\omega)|^2 d\omega \quad (71)$$

G_I is the interference power spectral density at the input. Using (70) and (71) and the fact that the imaginary part of $H(\omega)$ is odd while $G_s(\omega)$ is real and even, equation (69) can be written in the form

$$\mathcal{E} = R_{in} \int_{-\infty}^{\infty} |1-H(\omega)|^2 G_s(\omega) d\omega + R_{in} \int_{-\infty}^{\infty} |H(\omega)|^2 G_I(\omega) d\omega \quad (72)$$

The mean square error, when divided by the quantity

$$R_{in} \int_{-\infty}^{\infty} |H(\omega)|^2 d\omega,$$

can be interpreted as an equivalent output interference/signal power ratio.

$$\frac{P_{T0}}{P_{S0}} = \frac{\int_{-\infty}^{\infty} |1-H(\omega)|^2 G_s(\omega) d\omega + \int_{-\infty}^{\infty} |H(\omega)|^2 G_I(\omega) d\omega}{\int_{-\infty}^{\infty} |H(\omega)|^2 d\omega} \quad (73)$$

The mean-square error which corresponds to a given value of P_{I0}/P_{S0} is the same as the error which would result if an amount of interference power, P_{I0} (uncorrelated with the signal), were linearly added to an otherwise undistorted signal with power, P_{S0} . The limiter output will be a reasonably good reproduction of the desired signal for

$$\frac{P_{I0}}{P_{S0}} \ll 1.$$

Equation (73) will now be applied to the case where the input interference is coherent and the desired input signal is below the limiter saturation level. Under these conditions, the transfer function, $H(\omega)$, will be shaped under the influence of the interference power spectrum,

$$G_I(\omega) = \sum_k \frac{1}{2} P_k \delta(\omega - \omega_k) \quad (74)$$

so that $H(\omega)$ is small for frequencies in the vicinity of the ω_k 's. As a first step in determining $H(\omega)$, single frequency CW interference will be considered, that is,

$$G_I = \frac{1}{2} P_k \delta(\omega - \omega_k) + \frac{1}{2} P_k \delta(\omega + \omega_k).$$

This signal will produce saturation of spins in the immediate vicinity of ω_k and will result in a decrease in the susceptibility seen by a second, small signal.

As is shown in Appendix IV, the limiter output voltage due to a small signal at the frequency ω , in the presence of a large signal at ω_2 is

$$V(\omega_1) = -\pi M_0 \beta \gamma H_1 g(\omega_1) \left[1 - \frac{\gamma^2 H_2^2 T_{22}}{\left(\frac{1}{T_{21}} + \frac{1}{T_2} - j\delta\right)} \right] \quad (75)$$

Since H_1 is proportional to the input signal voltage at ω_1 , the voltage transfer function of the limiter can be written as

$$H(\omega) = Ag(\omega) \left[1 - \frac{P_n P_{sat}}{\sqrt{1 + P_n/P_{sat}} \sqrt{1 + P_n/P_{sat}} + 1 - j\delta T_2} \right] \quad (76)$$

where A is a constant. The right-hand term of (76) represents the "hole" burned in the limiter response curve by the signal at ω_1 . This "hole" has a nominal width of

$$\frac{1}{T_2} \sqrt{1 + P_n/P_{sat}} \quad \text{radians/sec.}$$

If the interference signal has more than one frequency component, the effect of additional holes can be approximated by adding terms to $H(\omega)$ as below.

$$H(\omega) = Ag(\omega) \left[1 - \sum_k \frac{P_n/P_{sat}}{\sqrt{1 + P_n/P_{sat}} (\sqrt{1 + P_n/P_{sat}} + 1 - j(\omega_k - \omega)T_2)} \right] \quad (77)$$

This expression is accurate so long as the "holes" do not overlap, that is

$$|\omega_j - \omega_k| > \frac{1}{T_2} \sqrt{\frac{P_n}{P_{sat}}} \quad (78)$$

must hold for all j and k (except $j=k$). Because it has been assumed that there is no small signal voltage drop between the input of the limiter and the point at which the output is measured, the quantity $Ag(\omega)$ in expression (77) must be replaced by unity before $H(\omega)$ is inserted in (73).

For $\omega = \omega_k$, the transfer function $H(\omega)$, as given in (77), does not give the correct value of interference output power. If condition (78) holds, output interference power can be approximated by considering each of the components of interfering power to be independently limited. The total interference output power is then

$$\int_{-\infty}^{\infty} |H(\omega)|^2 G_y(\omega) d\omega = \sum_n \frac{\frac{1}{2} P_n}{1 + P_n/P_{sat}} \quad (79)$$

The first integral in (75) can be evaluated using the method of residues.

First, the complex function, $T(\omega)$, will be defined as follows:

$$T(\omega) = \left[\sum_n \frac{(P_n/P_{sat})(1 + P_n/P_{sat})^{\frac{1}{2}}}{1 + (1 + P_n/P_{sat})^{\frac{1}{2}} j(\omega - \omega_n)T_2} \right] \left[\sum_m \frac{(P_m/P_{sat})(1 + P_m/P_{sat})^{-\frac{1}{2}}}{1 + (1 + P_m/P_{sat})^{\frac{1}{2}} j(\omega - \omega_m)T_2} \right] \quad (80)$$

$T(\omega)$ is equal to $|1 - H(\omega)|^2$ along the real axis of the ω plane and has poles in the upper half plane at

$$\omega = \lambda_n = \omega_n + \frac{j}{T_2} \left[1 + (1 + P_n/P_{sat}) \right]$$

as well as poles in the lower half plane at

$$\omega = \lambda'_m = \omega_m - \frac{j}{T_2} \left[1 + (1 + P_m/P_{sat}) \right]$$

Applying the residu theorem,

$$\int_{-\infty}^{\infty} |1 - H(\omega)|^2 G_y(\omega) d\omega = P_{sat} 2\pi j \sum_n Q(\lambda_n) \left[\frac{\text{Residue of } T(\omega)}{2\pi \omega = \lambda_n} \right]$$

In the above expression, $Q(\omega)$ can be any function which is analytic in the entire upper half plane, whose real part approximates $G_y(\omega)$ on the real axis, and which remains finite as $|\omega| \rightarrow \infty$. The residues of $T(\omega)$ at $\omega = \lambda_n$ can be evaluated approximately as

$$\left[\frac{\text{Residue of } T(\omega)}{\text{at } \omega = \lambda_n} \right] = \frac{(P_n/P_{sat})^2}{2jT_2(1 + P_n/P_{sat})[1 + (1 + P_n/P_{sat})^{\frac{1}{2}}]},$$

providing condition (78) is satisfied.

Equation (73) may now be written in final form as

$$\frac{P_{I0}}{P_{S0}} = Q_0 \frac{\pi}{T_2 P_S} \sum_k Q(\lambda_k) \frac{(P_{k_i}/P_{Sat})^2}{(1 + P_{k_i}/P_{Sat}) [1 + (1 + P_{k_i}/P_{Sat})^2]} + \sum_k \frac{\frac{1}{2} P_{k_i}/P_S}{1 + P_{k_i}/P_{Sat}} \quad (81)$$

where P_S is the total available signal power at the limiter input.

P_{I0}/P_{S0} will be calculated for the model signal and interference spectra shown in Figure 17. For this case,

$$G_I = \frac{1}{2} \frac{P_I}{N} \sum_{k=1}^N \delta(\omega - 2\pi k f_m) + \frac{1}{2} \frac{P_I}{N} \sum_{k=1}^N \delta(\omega + 2\pi k f_m) \quad (82)$$

where N is the number of components of interference power and P_I is the total interference power. In computing P_{I0}/P_{S0} , N in equation (82) should be replaced by M , the number of in-band components. The polynomial Q is simply

$$Q = \frac{P_S}{4\pi B_s}$$

where $2\pi B_s$ is the signal bandwidth in radians per second. From equation

$$(81) \quad \frac{P_{I0}}{P_{S0}} = \left(\frac{M}{2T_2 B_s} \right) \frac{(P_I/N P_{Sat})^2}{(1 + \frac{P_I}{N P_{Sat}}) [1 + (1 + \frac{P_I}{N P_{Sat}})^2]} + M \frac{P_I/N P_S}{1 + P_I/N P_{Sat}} \quad (83)$$

It will be assumed that $2\pi T_2 B_s = 3 \times 10^3$ and that

$$\frac{P_S}{2\pi B_s T_2} = \frac{P_{Sat}}{10}$$

This latter condition states that the signal power available in one line-width is 10 db below the saturation level. Figure 1^a shows the dependence of P_{I0}, P_{S0} upon input interference/signal ratio. P_{I0}/P_{S0} is also plotted for the case where no limiter is used. For this case,

$$\frac{P_{I0}}{P_{S0}} = \frac{P_I}{P_S} .$$

APPENDIX VI TRANSIENT RESPONSE

The object of the following analysis is to obtain the time response of the magnetization of a system of spins, immersed in an inhomogeneous d.c. magnetic field, to transients in the rf magnetic field applied to the spins. The most suitable approach to the problem is to consider that the spin system over a small volume follows the phenomenological equations of Bloch. The nonuniformity in the d.c. field will be included after an expression for the frequency response of one spin has been attained.

First, assume that each spin viewed from a reference frame in the lab follows the following set of (Bloch's) assumptions

$$\begin{aligned}
 \frac{d\bar{M}}{dt} &= \gamma \bar{M} \times \bar{H} \\
 \frac{dM_z}{dt} &= \frac{M_z - M_0}{T_1} \\
 \frac{dM_x}{dt} &= -\frac{M_x}{T_2} \\
 \frac{dM_y}{dt} &= -\frac{M_y}{T_2}
 \end{aligned}
 \tag{84}$$

where \bar{M} = magnetization vector
 M_z = z component of magnetization
 T_1 = transverse relaxation time
 T_2 = longitudinal relaxation time

M_0 = spontaneous magnetization

$$\gamma = \frac{\omega_p}{H_0} = \frac{\omega}{H}$$

\vec{H} = magnetic field

Using a primed set of quantities for those seen from a frame rotating around \hat{z} at ω ($t = t'$) we have the following transformation between the fixed and rotating frames of reference.

$$\begin{aligned} \frac{d\vec{M}'}{dt'} &= \gamma \vec{M}' \times \vec{H} + \vec{M}' \times \vec{\omega} \\ &= \gamma \vec{M}' \times \left(\vec{H} + \frac{\vec{\omega}}{\gamma} \right) \end{aligned} \quad (85)$$

where the magnetization transformations are

$$\begin{aligned} M_x &= M_x' \cos \omega t - M_y' \sin \omega t \\ M_y &= M_y' \cos \omega t + M_x' \sin \omega t \\ M_z &= M_z' \end{aligned} \quad (86)$$

If we consider the case of both a d.c. field $H_0 \hat{z}'$ and a time varying field in the fixed frame, $H_{rf} \hat{x}$, the spins see an effective field H_{eff} of the form

$$\vec{H}_{eff} = H_0 \hat{z}' + H_{rf} \hat{x}' \quad (87)$$

Substituting all components of (86) into (85) we have

$$\frac{d\vec{M}'}{dt'} = \gamma \vec{M}' \times \vec{H}_{eff} - \frac{M_z - M_0}{T_1} \hat{z}' - \frac{M_x'}{T_2} \hat{x}' - \frac{M_y'}{T_2} \hat{y}' \quad (88)$$

Substituting (87) in (86) and considering each component we have in steady state

$$\begin{pmatrix} -\frac{1}{T_2} & \Delta\omega & 0 \\ -\Delta\omega & -\frac{1}{T_2} & -\omega_{rf} \\ 0 & \omega_{rf} & -\frac{1}{T_1} \end{pmatrix} \begin{pmatrix} M_x' \\ M_y' \\ M_z' \end{pmatrix} = \begin{pmatrix} 0 \\ 0 \\ -\frac{M_0}{T_1} \end{pmatrix} \quad (89)$$

where $\Delta\omega = \omega_0 - \omega_{rf}$ and $\omega_{rf} = \gamma H_{rf}$. The solutions to (89) give the steady state magnetization components and any transient solution must approach these values as time increases.

The steady-state components of magnetization are

$$M_x' = - \frac{\Delta\omega \omega_{rf} M_0 T_2^2}{1 + \omega_{rf}^2 T_1 T_2 + (T_2 \Delta\omega)^2} \quad (90)$$

$$M_y' = \frac{\omega_{rf} T_2 M_0}{1 + \omega_{rf}^2 T_1 T_2 + (T_2 \Delta\omega)^2} \quad (91)$$

$$M_z' = M_0 = \frac{[1 + (\Delta\omega T_2)^2] M_0}{1 + \omega_{rf}^2 T_1 T_2 + (T_2 \Delta\omega)^2} \quad (92)$$

Bloch's equations become questionable in low H_0 or high H_{rf} fields.

$$H_0 \cong \frac{1}{\gamma T_2} \quad \text{or} \quad H_{rf} \cong H_0$$

In these cases one can use¹ Bloch's equations, but should use $T_1 = T_2 = T$

Consider an rf magnetic field of the form

$$H_{rf}(t) = H_{rf} \cos \omega t \quad U(t) \quad (93)$$

where $U(t)$ is a unit step such that

$$U(t) = \begin{cases} 0 & t < 0 \\ 1 & t \geq 0 \end{cases} \quad (94)$$

1. Chapter III p. 53 or Chapter 12 Abragam

This transient in $H_{np}(t)$, could alternately be expressed as

$$H_{np}(t) = \begin{cases} H_n \omega_1(t) t \\ \text{where } \omega_1(t) = \omega_1 U(t) \end{cases} \quad (95)$$

For this special case of a unit step input in $H_{np}(t)$; we are able to use the usually impossible approach of solving the inhomogeneous differential equations of Bloch by using Laplace Transforms. For simplicity, let the following identifications hold:

$$\mathcal{L}\{M_x'(t)\} = m_x(s)$$

$$\mathcal{L}\{M_y'(t)\} = m_y(s) \quad (96)$$

$$\mathcal{L}\{M_z'(t)\} = m_z(s)$$

$$\omega_1(t) = \omega_1 U(t)$$

$$\omega_{np} = \nu H_p$$

The reason that the system of equations is solvable by a Laplace Transform approach for the particular case of a unit step in H_{np} is interesting to note. With the above notational identification, Equation (88) becomes

$$\begin{aligned}
\dot{M}_x' &= -\frac{M_x'}{T_2} + \Delta\omega M_y' \\
\dot{M}_y' &= -\Delta\omega M_x' - \frac{M_y'}{T_2} - \omega_{rf} M_z' \\
\dot{M}_z' &= \omega_{rf} M_y' - \frac{M_z' - M_0}{T_1}
\end{aligned} \tag{97}$$

Notice that $M_z' - M_0$ represents the displacement of the z component of magnetization from the initial magnetization M_0 . If we let $V = M_z' - M_0$, (97) becomes

$$\begin{aligned}
\dot{M}_x'(t) &= -\frac{M_x'}{T_2} + \Delta\omega M_y' \\
\dot{M}_y'(t) &= -\Delta\omega M_x' - \frac{M_y'}{T_2} - \omega_{rf} V - \omega_{rf} M_0 \\
\dot{V}(t) &= \omega_{rf} M_y' - \frac{V}{T_1}
\end{aligned} \tag{98}$$

Taking the Laplace transform we have

$$\begin{aligned}
s m_x(s) &= -\frac{m_x(s)}{T_2} + \Delta\omega m_y(s) \\
s m_y(s) &= -\Delta\omega m_x(s) - \frac{m_y(s)}{T_2} - \omega_{rf} v(s) - \omega_{rf} M_0 \\
s m_z(s) &= \omega_{rf} m_y(s) - \frac{v(s)}{T_1}
\end{aligned} \tag{99}$$

r in matrix notation

$$\begin{pmatrix} -\frac{1}{T_2} - s & \Delta\omega & 0 \\ -\Delta\omega & -\frac{1}{T_2} - s & -\omega_1 \\ 0 & \omega_1 & -\frac{1}{T_1} - s \end{pmatrix} \begin{pmatrix} m_x(s) \\ m_y(s) \\ v(s) \end{pmatrix} = \begin{pmatrix} 0 \\ \frac{\omega_{rf} M_0}{s} \\ 0 \end{pmatrix} \quad (100)$$

The solutions will be the response of the spin system (no spread in magnetic field) to a unit step of rf magnetic field at ω_1 . Note that the values of s are the eigenvalues of the steady-state matrix (that is, to the corresponding matrix in the steady-state solution). These values of s are the characteristic frequencies of the system. The similar eigenvalue problem results by solving (98) where the form in the rotating system is $\dot{A} = B A + C$ (as matrices). The solution is of the form e^{Bt} if B is diagonal in the system chosen. If B is in a diagonal representation, the diagonal elements are the eigenvalues and the relation to (100) is apparent.

The complete transform solution to (100) is then

$$m_x(s) = \frac{\Delta\omega M_0 (s + \frac{1}{T_1}) \omega_{rf}}{s \mathcal{L}} \quad (101)$$

$$m_y(s) = \frac{\omega_{rf} (s + \frac{1}{T_2}) (s + \frac{1}{T_1}) M_0}{s \mathcal{L}} \quad (102)$$

$$v(s) = \frac{\omega_{rf}^2 M_0 (s + \frac{1}{T_2})}{s \mathcal{L}} \quad (103)$$

$$\mathcal{L} = - \left(\frac{1}{T_2} + s \right)^2 (s + \frac{1}{T_1}) - \omega_{rf}^2 (s + \frac{1}{T_2}) - (\Delta\omega)^2 (s + \frac{1}{T_1}) \quad (104)$$

$$\mathcal{L} = - (s + a_1) \left[(s + a_2)^2 + a_3^2 \right] \quad (105)$$

where a_3 is not necessarily real.

The magnetization components will have the following partial fraction expansions

$$\frac{A_1}{s + a_1} + \frac{B_1 (s + a_2) + C_1}{(s + a_2)^2 + a_3^2} + \frac{D_1}{s} \quad (106)$$

The inverse transforms for a homogeneous dc field have components of the form

$$A_2 e^{-a_1 t} + B_2 e^{-a_2 t} \cos a_3 t + \frac{C_2}{a_3} e^{-a_2 t} \sin a_3 t + D_2 U(t) \quad (107)$$

where the first three terms are the transient response and the last term is the steady state response all seen in the rotating frame.

For simplicity let us assume $T_1 = T_2 = T$

Thus,

$$m_y(s) \cong \frac{-(s + \frac{1}{T}) M_0 \omega_{rf}}{s \left[(s + \frac{1}{T})^2 + \omega_{rf}^2 + (\Delta\omega)^2 \right]} \quad (108)$$

$$m_x(s) \cong \frac{-\Delta\omega M_0 \omega_{rf}}{s \left[(s + \frac{1}{T})^2 + \omega_{rf}^2 + (\Delta\omega)^2 \right]} \quad (109)$$

$$v(s) = \frac{-\omega_{rf}^2 M_0}{s \left[(s + \frac{1}{T})^2 + \omega_{rf}^2 + (\Delta\omega)^2 \right]} \quad (110)$$

To account for the spread in dc magnetic field across the spin system we must sum the contributions of all spins to the frequency response. Consider a configuration such that we have a uniform magnetic field gradient and a uniform number of spins per unit volume such that the spontaneous magnetization is M_0 . As a result of the non-uniform magnetic field we then have a spread in the poles indicated by (28), (29) and (30).

Considering only the y component of magnetization, the steady state and transient responses can be separated by a partial fraction expansion as in (11).

$$M_y(s) = \frac{-\frac{1}{T} M_0 \omega_{rf}}{\frac{1}{T} s + \omega_{rf}^2 + (\Delta\omega)^2} \left[\frac{1}{s} - \frac{s + \frac{\omega}{T}}{(s + \frac{1}{2})^2 + \omega_{rf}^2 + (\Delta\omega)^2} \right] - \frac{M_0 \omega_{rf}}{(s + \frac{1}{2})^2 + \omega_{rf}^2 + (\Delta\omega)^2} \quad (11)$$

The $1/s$ term represents the steady-state magnetization as seen in the rotating coordinate system. The poles of the remaining transient terms are at $s = -\frac{1}{2} \pm \sqrt{\omega_{rf}^2 + (\Delta\omega)^2}$, and the position depends upon the dc magnetic field. If we assume that the magnetic field has a constant gradient and that the spin density in each interval of magnetic field is constant, we have a set of poles along the lines indicated below.

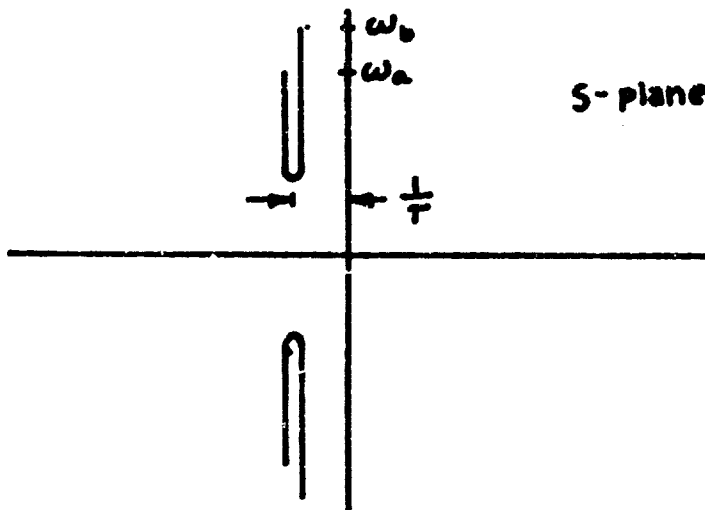


FIGURE 34 POLES IN S-PLANE

To find out for the spread in a magnetic field over the spin system, we integrate along the lines of poles shown in Fig. 34; thus

$$\begin{aligned}
 m_y(s) = & -\frac{1}{T} M_0 \omega_{rf} \int \frac{1}{\frac{1}{T} s + D^2} \left\{ \frac{1}{s} + \frac{\frac{1}{T} - jD}{2jD(s + \frac{1}{T} + jD)} - \frac{\frac{1}{T} + jD}{2jD(s + \frac{1}{T} - jD)} \right\} \\
 & \frac{D dD}{(j\sqrt{D^2 - \omega_{rf}^2})} + M_0 \omega_{rf} \int \left\{ \frac{-\frac{1}{2jD}}{s + \frac{1}{T} + jD} \right. \\
 & \left. + \frac{\frac{1}{2jD}}{s + \frac{1}{T} - jD} \right\} \frac{D dD}{(j\sqrt{D^2 - \omega_{rf}^2})} \quad (11)
 \end{aligned}$$

where $D = \sqrt{\omega_{rf}^2 + \Delta\omega^2}$

$$\begin{aligned}
 m_y(s) = & M_0 \omega_{rf} \int_{\omega_a = \omega_0}^{\omega_b = \omega_0} \left[\frac{-\frac{1}{T} D}{\sqrt{D^2 - \omega_{rf}^2} (D^2 + \frac{1}{T} s)} - \frac{\frac{1}{T} (\frac{1}{T} - jD) + (D^2 + \frac{1}{T} s)}{(2jD)(D^2 + \frac{1}{T} s)(s + \frac{1}{T} + jD)\sqrt{D^2 - \omega_{rf}^2}} \right. \\
 & \left. + \frac{\frac{1}{T} (\frac{1}{T} + jD) + (D^2 + \frac{1}{T} s)}{2j(D^2 + \frac{1}{T} s)(s + \frac{1}{T} - jD)\sqrt{D^2 - \omega_{rf}^2}} \right] dD \quad (113)
 \end{aligned}$$

but at $\omega_0 = \omega_a$, $D = \sqrt{\omega_{rf}^2 + (\omega_0 - \omega)^2} = D_a$

similarly at $\omega_0 = \omega_b$, $D = \sqrt{\omega_{rf}^2 + (\omega_0 - \omega)^2} = D_b$

Thus

$$m_y(s) = - \frac{M_0 \omega_{rf}}{\gamma} \int_{D_a}^{\omega_{rf}} [\quad] dD + M_0 \omega_{rf} \int_{\omega_{rf}}^{D_b} [\quad] dD \quad (114)$$

The first term in (113) has an inverse transform which corresponds to a unit step in magnetization at $t=0$ and is thus just the steady state

$$| \text{steady state } M_y' | = \left| - \frac{M_0 \omega_{rf}}{\gamma} \int_{D_a}^{D_b} \frac{D}{\sqrt{D^2 - \omega_{rf}^2} (D^2 + \frac{1}{2})} dD \right| \quad (115)$$

Define

$$G(D) = \begin{cases} 0 & D < -D_b \\ -1 & -D_b \leq D < -D_a \\ -2 & -D_a \leq D < -\omega_{rf} \\ 0 & -\omega_{rf} \leq D < \omega_{rf} \\ 2 & \omega_{rf} \leq D < D_a \\ 1 & D_a \leq D \leq D_b \\ 0 & D_b \leq D \end{cases}$$

Then we can write the transient portion of (114) as

$$m_y(s) \Big|_{\text{transient}} = \int_{-\infty}^{\infty} G(D) M_0 \omega_{rf} \frac{\frac{1}{2}(\frac{1}{2} + jD) + D^2 + \frac{1}{2}}{2j(s + \frac{1}{2} - jD) \sqrt{D^2 - \omega_{rf}^2} (D^2 + \frac{1}{2})} dD \quad (116)$$

but $s = j\omega'$ where ω' is the parameter for the frequency spectrum of the resulting response; thus (116) becomes

$$m_y(s) \Big|_{\text{transient}} = M_0 \omega_{rf} \int_{-\infty}^{\infty} G(D) \frac{\frac{1}{2}(\frac{1}{2} + jD) + D^2 + \frac{1}{2}}{\sqrt{D^2 - \omega_{rf}^2} (D^2 + \frac{1}{2}) \left(-\omega' + \frac{1}{2} + D \right)} dD \quad (117)$$

But (117) is actually the convolution of the transform, for example (116) and one shown as (119). $m_y(\omega') = f(\omega) * p(\omega)$

$$\frac{M_0 \frac{\omega \cdot t}{2}}{s \left[D - \omega' + \frac{1}{2} \right]} \equiv f(\omega' - \omega) \quad (118)$$

$$s \frac{G(\omega) \frac{1}{2} \left(\frac{1}{2} + s \right) + D^2 + \frac{1}{2}}{\sqrt{D^2 - \omega \cdot \frac{1}{2}} \left(D^2 + \frac{1}{2} \right)} \equiv p(\omega) \quad (119)$$

The inverse transform of the transient portion becomes

$$M_y'(t) \Big|_{\text{transient}} = \frac{1}{2\pi} \int_{-\infty}^{\infty} f(\omega) * p(\omega) e^{s\omega t} d\omega \quad (120)$$

$$= \frac{1}{2\pi} \int_{-\infty}^{\infty} \int_{-\infty}^{\infty} f(\omega' - \omega) p(\omega) e^{s\omega t} d\omega' d\omega \quad (121)$$

$$= \frac{1}{2\pi} \int \int f(\omega' - \omega) e^{s(\omega' - \omega)t} d\omega' p(\omega) e^{s\omega t} d\omega \quad (122)$$

$$= 2\pi F(s) P(s) \quad (123)$$

The transient solution is the product of the inverse transforms of $f(\omega)$ and $p(\omega)$ as shown in (123).

From (116),

$$f(\omega) = - \frac{M_0 \omega \cdot t}{2s \left(D - \frac{1}{2} \right)} \quad (124)$$

Thus taking the inverse Fourier transform we get

$$F(t) = -\frac{M_0 \omega_p}{2} e^{-\frac{t}{T}} \quad (125)$$

This illustrates that the transient magnetization response of the spin system to a step in rf energy has an exponential decay at $\frac{1}{T}$. The inverse transform of (119) is

$$\begin{aligned} P(t) &= \frac{1}{2\pi} \int_{-\infty}^{\infty} G(\omega) \left[\frac{\frac{1}{2}(\frac{1}{2} + iD)}{\sqrt{D^2 - \omega_p^2} (D^2 + \frac{1}{4})} + \frac{1}{\sqrt{D^2 - \omega_p^2}} \right] e^{-i\omega t} d\omega \\ &= \frac{1}{\pi} \int_{\omega_p}^{\infty} G(\omega) \left[\frac{\frac{1}{2} \sin \omega t + \frac{1}{2} D \cos \omega t}{\sqrt{D^2 - \omega_p^2} (D^2 + \frac{1}{4})} + \frac{\sin \omega t}{\sqrt{D^2 - \omega_p^2}} \right] d\omega \quad (126) \end{aligned}$$

Thus using the definition of $G(\omega)$ we have

$$\begin{aligned} P(t) &= -\frac{1}{\pi} \int_{\omega_p}^{D_0} \left\{ \frac{\frac{1}{2} \sin \omega t + \frac{1}{2} D \cos \omega t}{\sqrt{D^2 - \omega_p^2} (D^2 + \frac{1}{4})} + \frac{\sin \omega t}{\sqrt{D^2 - \omega_p^2}} \right\} d\omega \\ &\quad - \frac{1}{\pi} \int_{D_0}^{\infty} \left\{ \frac{\frac{1}{2} \sin \omega t + \frac{1}{2} D \cos \omega t}{\sqrt{D^2 - \omega_p^2} (D^2 + \frac{1}{4})} + \frac{\sin \omega t}{\sqrt{D^2 - \omega_p^2}} \right\} d\omega \quad (127) \end{aligned}$$

The only assumption up to equation (127) was that ω was $\omega_a < \omega < \omega_b$

Assume that $\omega_p \gg \frac{1}{2}$ then (127) becomes

$$\begin{aligned} P(t) &= -\frac{1}{\pi} \int_{\omega_p}^{D_0} \left(\frac{\frac{1}{2} \sin \omega t}{D^2 \sqrt{D^2 - \omega_p^2}} + \frac{\frac{1}{2} \cos \omega t}{D \sqrt{D^2 - \omega_p^2}} \right) d\omega \\ &\quad - \frac{1}{\pi} \int_{\omega_p}^{\infty} \frac{\sin \omega t}{\sqrt{D^2 - \omega_p^2}} d\omega + \frac{1}{\pi} \int_{D_0}^{\infty} \frac{\sin \omega t}{\sqrt{D^2 - \omega_p^2}} d\omega \quad (128) \\ &\quad + \frac{2}{\pi} \int_{D_0}^{\infty} \frac{\sin \omega t}{\sqrt{D^2 - \omega_p^2}} d\omega - \frac{1}{\pi} \int_{D_0}^{D_0} \left(\frac{\frac{1}{2} \sin \omega t}{D^2 \sqrt{D^2 - \omega_p^2}} + \frac{\frac{1}{2} \cos \omega t}{D \sqrt{D^2 - \omega_p^2}} \right) d\omega \end{aligned}$$

Assume $D_0 \gg \omega_{p0}$, then the terms of (128) become

$$-\frac{1}{\pi} \int_{\omega_{p0}}^{\infty} \frac{\sin D\tau}{\sqrt{D^2 - \omega_{p0}^2}} dD = \frac{1}{\pi} \sqrt{\frac{\pi}{2}} \sqrt{\frac{\pi}{2}} J_0(\omega_{p0} t)$$

and

$$\frac{1}{\pi} \int_{D_0}^{\infty} \frac{\sin D\tau}{\sqrt{D^2 - \omega_{p0}^2}} dD \approx \frac{1}{\pi} \int_{D_0\tau}^{\infty} \frac{\sin D\tau}{D\tau} dD\tau$$

and

$$\frac{1}{\pi} \int_{D_0}^{D_0\tau} \frac{\sin D\tau}{\sqrt{D^2 - \omega_{p0}^2}} dD \approx \frac{1}{\pi} \int_{D_0\tau}^{D_0\tau} \frac{\sin D\tau}{D\tau} dD\tau$$

and

$$\begin{aligned} -\frac{1}{\pi} \int_{D_0}^{D_0\tau} \left(\frac{\frac{1}{2} \sin D\tau}{D \sqrt{D^2 - \omega_{p0}^2}} + \frac{\frac{1}{2} \cos D\tau}{D \sqrt{D^2 - \omega_{p0}^2}} \right) dD &= -\frac{1}{\pi} \int_{D_0}^{D_0\tau} \left(\frac{\frac{1}{2} \sin D\tau}{D^2} + \frac{\frac{1}{2} \cos D\tau}{D^2} \right) dD \\ &= -\frac{1}{\pi} \left[\frac{t^2}{\pi^2} \left(-\frac{\sin D\tau}{2(D\tau)^2} - \frac{\cos D\tau}{2D\tau} - \frac{1}{2} \int \frac{\sin D\tau}{D\tau} dD\tau \right) \right. \\ &\quad \left. + \frac{t}{\pi} \left(-\frac{\cos D\tau}{D\tau} - \int \frac{\sin D\tau}{D\tau} dD\tau \right) \right]_{D_0\tau}^{D_0\tau} \\ &= \frac{1}{\pi} \left[\frac{t^2}{\pi^2} \left(\frac{\sin D_0\tau}{2(D_0\tau)^2} - \frac{\sin D_0\tau}{2(D_0\tau)^2} + \frac{\cos D_0\tau}{2D_0\tau} \right. \right. \\ &\quad \left. \left. - \frac{\cos D_0\tau}{D_0\tau} + \frac{1}{2} \int_{D_0\tau}^{D_0\tau} \frac{\sin D\tau}{D\tau} dD\tau \right) \right. \\ &\quad \left. + \frac{t}{\pi} \left(\frac{\cos D_0\tau}{D_0\tau} - \frac{\cos D_0\tau}{D_0\tau} + \int_{D_0\tau}^{D_0\tau} \frac{\sin D\tau}{D\tau} dD\tau \right) \right] \end{aligned}$$

Using;

$$\sqrt{\frac{2}{\pi}} J_0(\omega_{np} t) = \sqrt{\frac{2}{\pi}} \int_{\omega_{np}}^{\infty} \frac{\sin x t}{\sqrt{x^2 - \omega_{np}^2}} dx$$

or

$$\begin{aligned} \int_0^t J_0(\omega_{np} t) dt &= \frac{2}{\pi} \int_{\omega_{np}}^{\infty} \frac{1}{\sqrt{x^2 - \omega_{np}^2}} \int_0^t \sin x t dt dx \\ &= -\frac{2}{\pi} \int_{\omega_{np}}^{\infty} \left\{ \frac{\cos \omega_{np} t}{x \sqrt{x^2 - \omega_{np}^2}} - \frac{1}{x \sqrt{x^2 - \omega_{np}^2}} \right\} dx \end{aligned}$$

but

$$\frac{2}{\pi} \int_{\omega_{np}}^{\infty} \frac{1}{x \sqrt{x^2 - \omega_{np}^2}} dx = -\frac{1}{\omega_{np}}$$

thus

$$\int_0^t J_0(\omega_{np} t) dt = -\frac{2}{\pi} \int_{\omega_{np}}^{\infty} \frac{\cos \omega_{np} t}{D \sqrt{D^2 - \omega_{np}^2}} dD + \frac{1}{\omega_{np}}$$

Similarly

$$\begin{aligned} \iint_0^t J_0(\omega_{np} t) dt &= -\frac{2}{\pi} \int_{\omega_{np}}^{\infty} \frac{1}{D \sqrt{D^2 - \omega_{np}^2}} \int_0^t \cos \omega_{np} t dt dD + \int_0^t \frac{1}{\omega_{np}} dt \\ &= -\frac{2}{\pi} \int_{\omega_{np}}^{\infty} \frac{\sin \omega_{np} t}{D^2 \sqrt{D^2 - \omega_{np}^2}} dD + \frac{t}{\omega_{np}} \end{aligned}$$

If we assume the limits on the first terms in (12) can be extended to $D = \infty$ without changing the value, we get for all

$$\begin{aligned}
 P(t) &= -J_0(\omega_{rf}t) + \frac{2}{\pi} \int_{D_0 t}^{\infty} \frac{\sin D t}{D t} dD + \frac{1}{\pi} \int_{D_0 t}^{D_0 t} \frac{\sin D t}{D t} dD \\
 &\quad + \frac{1}{\pi} \int_0^t \int_0^t J_0(\omega_{rf}t) dt dt + \frac{1}{\pi} \int_0^t J_0(\omega_{rf}t) dt - \frac{t}{\omega_{rf} T} - \frac{t}{\omega_{rf} T} \\
 &\cong -J_0(\omega_{rf}t) + \frac{1}{\pi} \int_0^t \int_0^t J_0(\omega_{rf}t) dt dt + \frac{1}{\pi} \int_0^t J_0(\omega_{rf}t) dt - \frac{t}{\omega_{rf} T} - \frac{1}{\omega_{rf} T}
 \end{aligned} \tag{129}$$

For $M_y(t)$ we then have (ω within band $D = \sqrt{\omega_{rf}^2 + (\Delta\omega)^2}$)

$$\begin{aligned}
 M_y(t > 0) &\cong -\frac{M_0 \omega_{rf}}{2} \left\{ \left| \frac{1}{\pi} \int_{\omega_0 - \omega_{rf}}^{\omega_0 + \omega_{rf}} \frac{dD}{(D^2 - \omega_{rf}^2)(D^2 + \frac{1}{T^2})} \right| U(t) + e^{-\frac{t}{T}} \left(-J_0(\omega_{rf}t) \right. \right. \\
 &\quad \left. \left. + \frac{1}{\pi} \int_0^t \int_0^t J_0(\omega_{rf}t) dt dt + \frac{1}{\pi} \int_0^t J_0(\omega_{rf}t) dt \right. \right. \\
 &\quad \left. \left. - \frac{t}{\omega_{rf} T} - \frac{1}{\omega_{rf} T} \right) \right\}
 \end{aligned} \tag{130}$$

The steady-state term can be further simplified by using $D \gg \frac{1}{T}$

which is true for $\omega_{rf} \gg \frac{1}{T}$ or the situation corresponding to saturation of the spin system.

$$\frac{1}{\pi} \int_{\omega_0 - \omega_{rf}}^{\omega_0 + \omega_{rf}} \frac{D}{\sqrt{D^2 - \omega_{rf}^2} (D^2 + \frac{1}{T^2})} dD \cong \int_{\omega_0 - \omega_{rf}}^{\omega_0 + \omega_{rf}} \frac{dD}{D \sqrt{D^2 - \omega_{rf}^2}}$$

$$\begin{aligned} \frac{1}{T\pi} \int_{\omega_0=\omega_a}^{\omega_b=\omega_0} \frac{D dD}{\sqrt{D^2-\omega_1^2} (D^2+\frac{1}{T^2})} &\cong \frac{1}{T\pi\omega_1} \operatorname{Sec}^{-1} \frac{D}{\omega_1} \Bigg|_{\omega_0=\omega_a}^{\omega_b=\omega_0} \\ &\cong \frac{1}{T\pi\omega_1} \left[\operatorname{Sec}^{-1} \frac{\sqrt{\omega_1^2+(\omega-\omega_0)^2}}{\omega_1} \right. \\ &\quad \left. - \operatorname{Sec}^{-1} \frac{\sqrt{\omega_1^2+(\omega-\omega_a)^2}}{\omega_1} \right] \end{aligned}$$

Thus we have

$$\begin{aligned} M_y'(t>0) &\cong -\frac{M_0}{2T\pi} \left[\operatorname{Sec}^{-1} \frac{\sqrt{\omega_{rf}^2+(\omega-\omega)^2}}{\omega_{rf}} - \operatorname{Sec}^{-1} \frac{\sqrt{\omega_{rf}^2+(\omega-\omega_a)^2}}{\omega_{rf}} \right] U(t) \\ &\quad - \frac{M_0\omega_{rf}}{2} e^{-\frac{t}{T}} \left[-J_0(\omega_{rf}t) + \frac{1}{T^2} \int_0^t \int_0^t J_0(\omega_{rf}t) dt dt \right. \\ &\quad \left. + \frac{1}{T} \int_0^t J_0(\omega_{rf}t) dt - \frac{t}{\omega_{rf}T^2} - \frac{1}{\omega_{rf}T} \right] \quad (131) \end{aligned}$$

The transient terms far outweigh the steady-state terms.

In a similar manner we can find $M_x'(t)$. From equation (131) we get

$$M_x(s) = -\frac{\Delta\omega M_0 \omega_{rf}}{(\omega_{rf}^2 + \Delta\omega^2 + \frac{1}{T^2})} \left[\frac{1}{s} - \frac{(s + \frac{2}{T})}{(s + \frac{1}{T})^2 + \omega_{rf}^2 + \Delta\omega^2} \right] \quad (132)$$

or ignoring the steady state portion we have

$$\begin{aligned} m_x(s) \Big|_{\text{transient}} &= \frac{M_0\omega_{rf}(\pm 1)\sqrt{D^2-\omega_{rf}^2}}{D^2 + \frac{1}{T^2}} \left[\frac{\frac{1}{T} - jD}{-2jD} + \frac{\frac{1}{T} + jD}{2jD} \right] \quad (133) \\ D &= \sqrt{\omega_{rf}^2 + \Delta\omega^2} \end{aligned}$$

After accounting for the spread in the field we have

$$\begin{aligned}
 m_y(s) \Big|_{\text{transient}} &= \int \frac{M_0 \omega r_f}{D^2 + \frac{1}{T^2}} \left\{ \frac{\frac{1}{T} - jD}{2j(s + \frac{1}{T} + jD)} + \frac{\frac{1}{T} + jD}{2j(s + \frac{1}{T} - jD)} \right\} dD \\
 &= \int \frac{M_0 \omega r_f}{2(D^2 + \frac{1}{T^2})} \left\{ \frac{\frac{1}{T} - jD}{\omega' + D - \frac{j}{T}} - \frac{\frac{1}{T} + jD}{\omega' - D - \frac{j}{T}} \right\} dD \\
 &= \int_{-D_b}^{-D_a} \frac{M_0 \omega r_f}{2(D^2 + \frac{1}{T^2})} \left\{ \frac{\frac{1}{T} + jD}{\omega' - D - \frac{j}{T}} \right\} dD - \int_{D_a}^{D_b} \frac{M_0 \omega r_f}{2(D^2 + \frac{1}{T^2})} \left\{ \frac{\frac{1}{T} + jD}{\omega' - D - \frac{j}{T}} \right\} dD
 \end{aligned}$$

Defining

$$G'(D) = \begin{cases} -1 & D_a \leq D < D_b \\ +1 & -D_b \leq D < -D_a \\ 0 & \text{elsewhere} \end{cases}$$

we can write

$$m_y(s) \Big|_{\text{transient}} = \frac{M_0 \omega r_f}{2} \int_{-\infty}^{\infty} \frac{G'(D) (\frac{1}{T} + jD)}{(D^2 + \frac{1}{T^2})(\omega' - D - \frac{j}{T})} dD$$

again identifying

$$P(D) = \frac{j G'(D) (\frac{1}{T} + jD)}{D^2 + \frac{1}{T^2}}$$

and

$$f'(D) = \frac{M_0 \omega r_f}{2j(-D + \frac{j}{T})}$$

Equation (135) is again the convolution of (136) and (137). Following (123)

$$F'(t) = -\frac{M_0 \omega r_f}{2} e^{-t/T}$$

$$P'(t) = \frac{1}{2\pi} \int_{-\infty}^{\infty} \frac{j G'(D) (\frac{1}{T} - jD)}{D^2 + \frac{1}{T^2}} e^{jDt} dD$$

$$= \frac{1}{\pi} \int_{D_a}^{D_b} \frac{\frac{1}{T} \sin Dt - D \cos Dt}{D^2 + \frac{1}{T^2}} dD$$

Using the same approximations as before we can neglect $P'(t)$ as compared to the $M_y'(t)$ in (129).

Consequently, the transverse and longitudinal magnetization components in the rotating coordinate system can be approximated as

$$M_x' \hat{x}' + M_y' \hat{y}' \cong \hat{y}' \frac{M_0 \omega_{rf}}{2} e^{-\frac{t}{T}} J_0(\omega_{rf} t) \quad (13\epsilon)$$

for the response to a unit step in CW.

Had other than a uniform spin distribution per unit Larmor frequency interval been assumed, the $G(s)$ indicated in (116) and $G'(s)$ in (135), which are proportional to the distribution functions, would be modified. If the distribution were symmetrical and if the same H_{rf} was seen by each spin, the resultant M_x' would still be negligible compared to M_y' .

APPENDIX VII — CHARACTERISTICS OF ABSORBING SAMPLE

The behavior of a system of protons immersed in a d. c. magnetic field has been studied extensively (References 1, 3, 4, and 5). It can be shown that the steady-state magnetic susceptibility, X_{total} , of such a system has real and imaginary parts given by

$$X'(\omega) = \frac{T_2^2 N_0 \gamma^2 \hbar^2 \omega (\omega_0 - \omega)}{8kT \left[1 + T_2^2 (\omega - \omega_0)^2 + 1/4 \gamma^2 H_1^2 T_1 T_2 \right]}$$

$$X''(\omega) = \frac{T_2 N_0 \gamma^2 \hbar^2 \omega}{8kT \left[1 + T_2^2 (\omega - \omega_0)^2 + 1/4 \gamma^2 H_1^2 T_1 T_2 \right]}$$

where $X_{\text{total}} = X' - jX''$

- ω = $2\pi f$, f = applied frequency
- ω_0 = $2\pi f_0$, f_0 = resonant frequency of proton system
- N_0 = number of protons/cc
- γ = gyromagnetic ratio (2.675×10^4 rad/sec/gauss for protons)
- T_1 = spin-lattice relaxation time in seconds
- T_2 = transverse relaxation time in seconds
- H_1 = rf magnetic field strength
- k = Boltzmann's constant
- T = absolute temperature in °K

Equations 139 and 140 are written in centimeter-gram-second units. These units will be used throughout except that the results of some numerical calculations will be presented in meter-kilogram-second units for ease of interpretation.

The above equations are applicable to systems of weakly interacting magnetic dipoles immersed in uniform d. c. magnetic fields. The dependence of X' and X'' on applied frequency is shown in Figure 35 for weak rf magnetic fields.

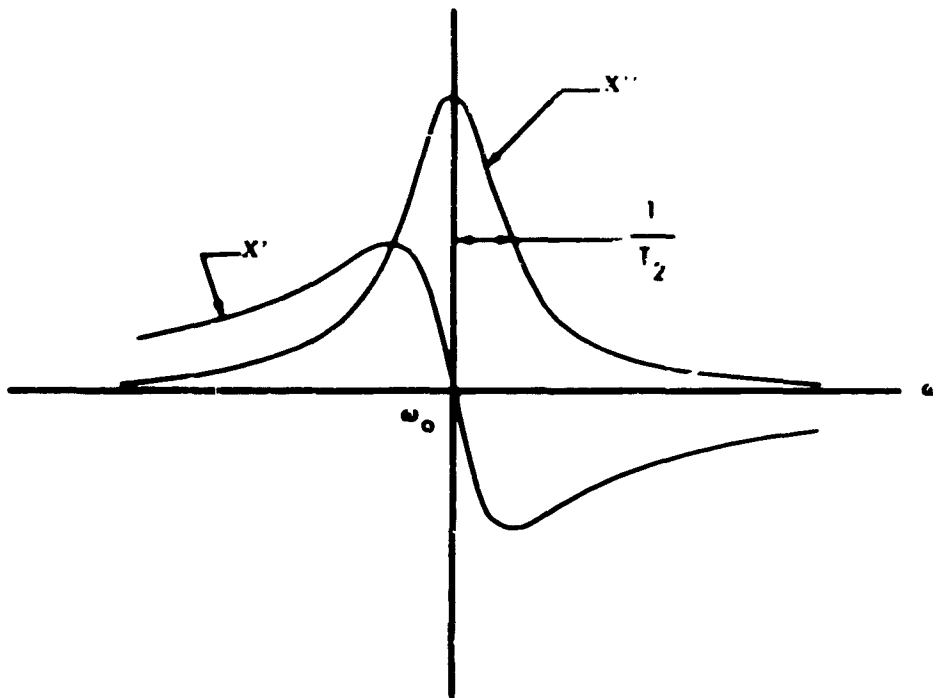


FIGURE 35. SUSCEPTIBILITY OF SYSTEM OF PROTONS IN UNIFORM MAGNETIC FIELD VS FREQUENCY

X'' has the Lorentzian line shape common to many resonant systems and is a measure of power dissipated in the spin system. X' is a measure of the energy storage capability of the spin system (i.e., it is the lossless part of X_{total}). The half maximum width of X' is $2/T_2$ rad/sec where T_2 is referred to as the transverse relaxation time. T_2 is dependent on the amount of interaction between neighboring dipoles of the system; in viscous liquids this interaction is large and may cause T_2 to be as short as 10^{-3} second; in nonviscous liquids, T_2 may be as long as 100 seconds.

Maximum absorption occurs when a time-varying magnetic field, H_1 , is applied perpendicular to the d.c. magnetic field; this orientation has been assumed in the derivation of Equations 139 and 140. The saturation effect will occur as the quantity $1/4\gamma^2 H_1^2 T_1 T_2$ becomes appreciable compared to unity. An important parameter in determining saturation level is T_1 , the spin-lattice relaxation time. T_1 can be thought of as the time required for the spin system to come into thermal equilibrium with the "lattice" of molecules making up the absorbing substance. In nonviscous liquids, T_1 will be approximately equal to T_2 , while in viscous liquids T_1 may be much longer than T_2 . When H_1^2 exceeds the saturation level, two effects are noted: First, the magnitudes of X' and X'' decrease owing to the decreased effectiveness of the resonance absorption; second, a broadening of the resonance line occurs. This latter phenomena is termed "saturation broadening." Equations 139 and 140 show that the broadened linewidth is

$$\frac{2}{T_2} \sqrt{1 + 1/4\gamma^2 T_1 T_2 H_1^2} \quad \text{rad/sec}$$

Equations 139 and 140 are valid only for the case of a completely homogeneous d.c. magnetic field. That is, it is assumed that every proton has the same resonant frequency. The frequency selective limiter used as an inhomogeneous magnetic field, however, so that new formulas for the magnetic susceptibility must be found. Following the method of Bloembergen (Reference 5) and Portis (Reference 9), the total susceptibility in an inhomogeneous field may be found by summing the contributions of protons having a distribution of resonant frequencies. If $g(f_0) df_0$ is the number of spins per unit volume with resonant frequency between f_0 and $f_0 + df_0$, then the real and imaginary parts of susceptibility will be given by

$$X'(\omega) = \frac{\pi T_2^2 N_0 \gamma^2 h^2 \omega}{4kT} \int_0^{\infty} \frac{g(f_0) (f_0 - \omega) df_0}{1 + (2\pi T_2)^2 (f_0 - \omega)^2 + 1/4\gamma^2 H_1^2 T_1 T_2} \quad (141)$$

$$X''(\omega) = \frac{T_2 N_0 \gamma^2 \hbar^2 \omega}{8 k T} \int_0^\infty \frac{g(f_0) df_0}{1 + (2\pi T_2)^2 (f_0 - f)^2 + 1/4 \gamma^2 H_1^2 T_1 T_2} \quad (142)$$

The above integrations are equivalent to an averaging of the susceptibility over the sample volume. The result must be interpreted not as the actual value of susceptibility at every point within the sample, but rather as an effective or average susceptibility.

Integrals 141 and 142 can be evaluated exactly if $g(f_0)$ is assumed to be a simple rectangular function such that

$$g(f_0) = \begin{cases} 0 & f_1 > f_0 > f_2 \\ \frac{N_0}{f_2 - f_1} = \frac{N_0}{B} & f_1 < f_0 < f_2 \end{cases} \quad (143)$$

where $g(f_0)$ is normalized so that

$$\int_0^\infty g(f_0) df_0 = N_0 \quad (144)$$

In all that follows, it will be assumed that $f_2 > f_1$. The quantity $B = f_2 - f_1$ will be referred to as the bandwidth of the limiter, to be distinguished from the quantity $2/T_2$, the nuclear resonance linewidth (in radians/sec).

For rectangular $g(f_0)$, Equations 141 and 142 become:

$$X' = \frac{N_0 \gamma^2 \hbar^2 f}{16 k T B} \ln \left[\frac{1 + \frac{\gamma^2}{4} H_1^2 T_1 T_2 + (2\pi T_2)^2 (f_2 - f)^2}{1 + \frac{\gamma^2}{4} H_1^2 T_1 T_2 + (2\pi T_2)^2 (f_1 - f)^2} \right] \quad (145)$$

$$X'' = \frac{N_0 \gamma^2 \hbar^2 f}{8 k T B \sqrt{1 + \frac{\gamma^2}{4} H_1^2 T_1 T_2}} \tan^{-1} \left[\frac{2\pi T_2 B}{\sqrt{1 + \frac{\gamma^2}{4} H_1^2 T_1 T_2} + \frac{(2\pi T_2)^2 (f_1 - f)(f_2 - f)}{\sqrt{1 + \frac{\gamma^2}{4} H_1^2 T_1 T_2}}} \right] \quad (146)$$

Figure 36 shows the shape and relative magnitude of X' and X'' for the case $T_1 = T_2 = \frac{100}{2\pi B}$. (i.e., for a case where the linewidth is one hundredth of the bandwidth). X' and X'' have the same order of magnitude, but X' cuts off much more slowly outside the bandpass region. X' and X'' have widely different saturation levels. As can be seen from Equation 146, X'' will begin to saturate when

$$\frac{\gamma^2}{4} H_1^2 T_1 T_2 \sim 1 \quad (147)$$

Equation A-7 shows that X' saturates when

$$\frac{\gamma^2}{4} H_1^2 T_1 T_2 \sim 1 + (2\pi T_2)^2 B^2 \quad (148)$$

Using the value $2\pi T_2 B = 10^2$ as a typical case, the rf magnetic field required to saturate X' is 100 times greater than that needed to saturate X'' . A more detailed study would also show that the saturation of X' corresponds to saturation of the entire sample rather than saturation of a small localized volume. This effect can be explained schematically as in Figure A-3, which shows the superimposed contributions to X' . Figure A-4 shows in a similar fashion how X'' is produced. Because of the long "tails" in Figure 37, significant contributions from protons will be made to X' at any frequency over the entire sample volume; consequently, it is necessary to saturate the entire sample in order to saturate X' . X'' , on the other hand, saturates selectively. Owing to the sharp cutoff of individual particle absorptions, significant contributions will be made to X'' only by protons having resonant frequencies close to the applied frequency. Thus, it is only necessary to saturate a small fraction of the total sample volume to saturate X'' . This frequency selective action is essential to the operation of the limiter.

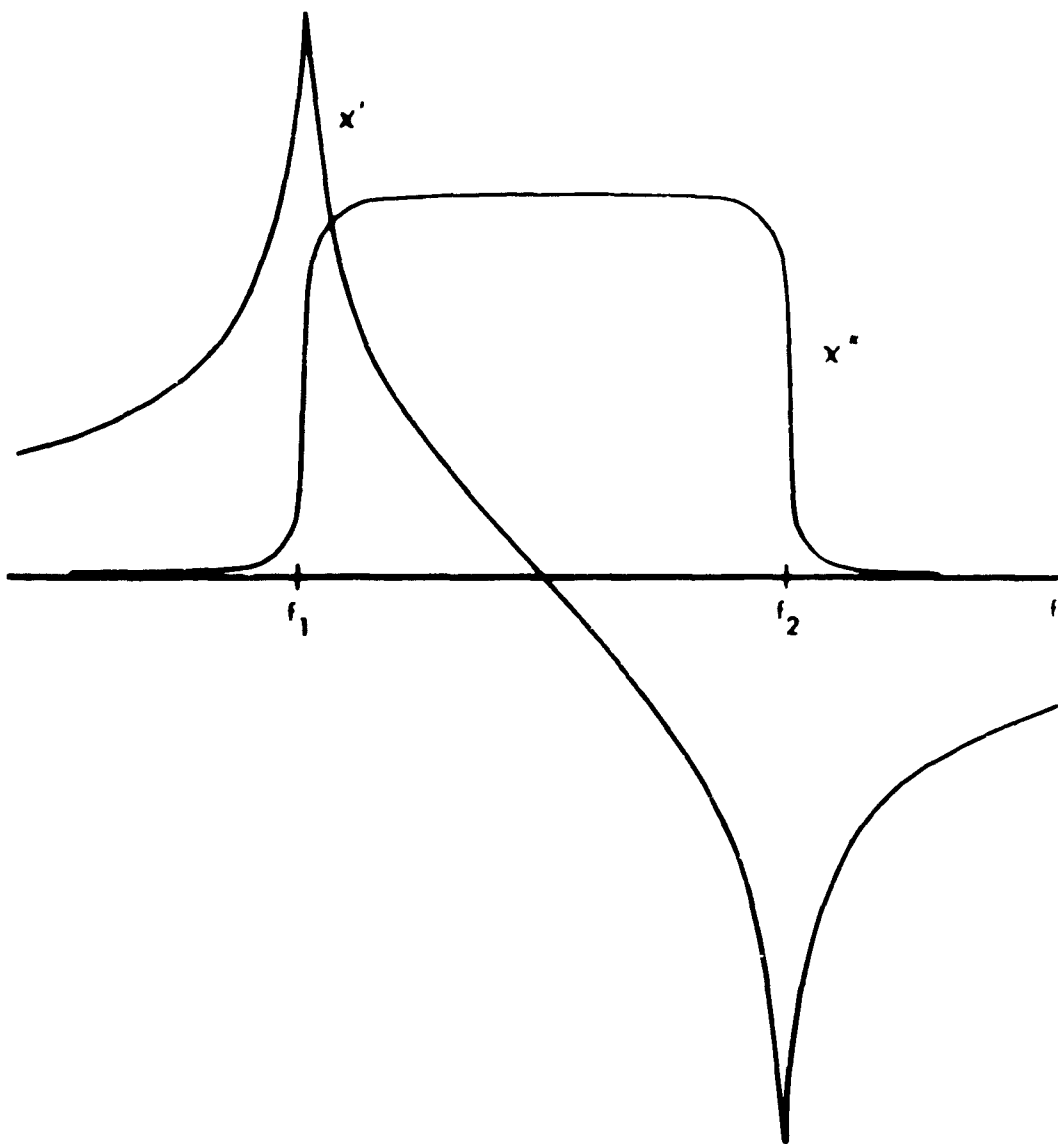


FIGURE 36. SUSCEPTIBILITY VS FREQUENCY FOR INHOMOGENEOUS BROADENING

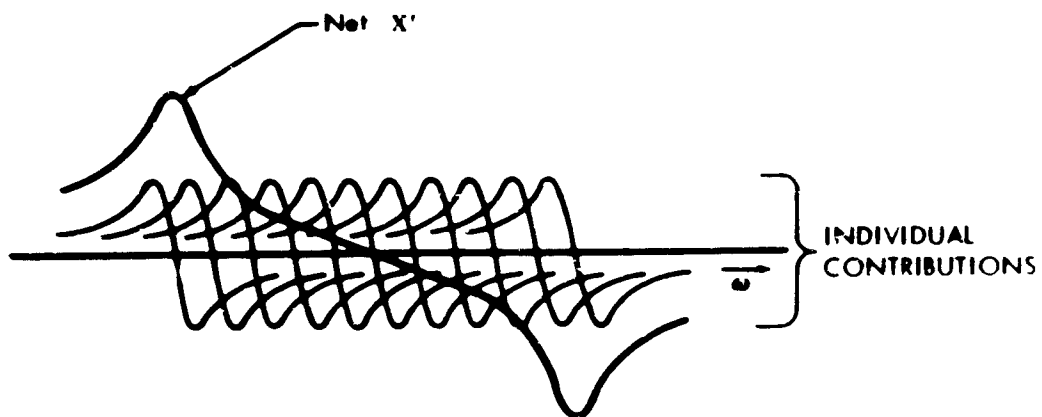


FIGURE 37. CONTRIBUTIONS OF INDIVIDUAL PROTONS TO X'

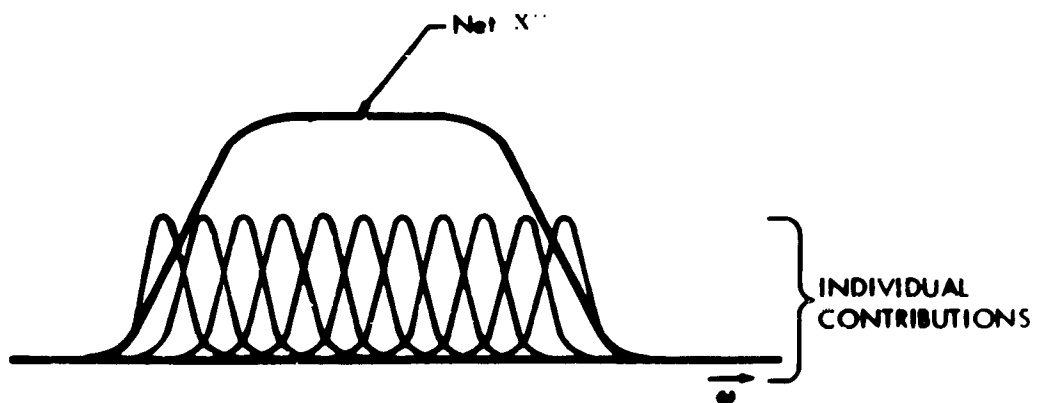


FIGURE 38. CONTRIBUTIONS OF INDIVIDUAL PROTONS TO X''

APPENDIX VIII - COUPLING TO SAMPLE

Magnetic coupling to the absorbing sample is accomplished using an rf coil, as shown in Figure 59. This coil is the source of the rf magnetic field, H_1 , and so is oriented with its axis perpendicular to the d.c. magnetic field, H_0 , to obtain maximum absorption. To further enhance absorption, the coil is series-tuned by means of capacitor, C . The presence of the absorbing sample within this coil will change its inductance from some value, L_0 , to a new value given by

$$L = L_0 \left[1 + 4\pi \xi (X' - jX'') \right] \quad (149)$$

The quantity in square brackets is the effective relative permeability of the absorbing sample. The dimensionless parameter ξ is included to account for nonperpendicular alignment of H_1 , and incomplete filling of the coil with absorbing material. ξ is referred to as the fill factor and will range from a value of unity for a completely filled coil with $H_1 \perp H_0$ to a value of zero for an empty coil.

Coupling effectiveness can be deduced by finding the change, Z_a , in coil impedance to be expected when the absorbing sample is introduced. With no magnetic resonance absorption, the total impedance will be

$$Z_0 = j\omega L_0 + R_0 + \frac{1}{j\omega C}$$

where R_0 is the series resistance of the coil due to copper losses. The fractional impedance change is

$$\frac{Z_a}{Z_0} = \frac{j\omega L_0 \left[1 + 4\pi \xi (X' - jX'') \right] - j\omega L_0}{j\omega L_0 + R_0 + \frac{1}{j\omega C}}$$

$$\frac{Z_a}{Z_0} = \frac{\omega L_0 \xi (X'' + jX')}{j\omega L_0 + R_0 + \frac{1}{j\omega C}}$$

The reason for tuning the absorbing coil is now evident. If C is chosen so that $\omega = 1/\sqrt{L_0 C}$, the denominator will attain its smallest magnitude and Z_a/Z_0 will be maximized.

For this tuned case, $Z_0 = R_0$ and

$$\frac{X_a(\omega)}{R_0} = \frac{4\pi\omega L_0 \xi X'(\omega)}{R_0} = 4\pi \xi Q_0 X'(\omega) \quad (150)$$

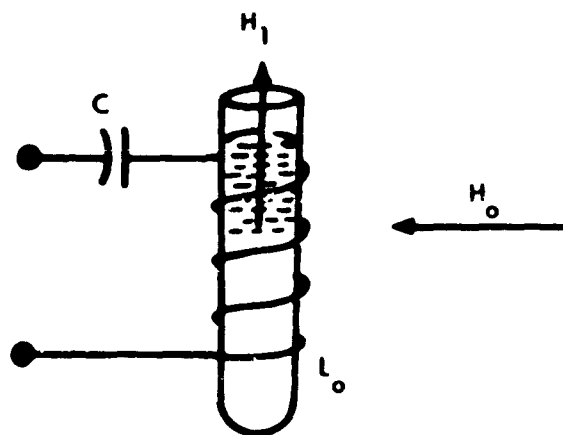


FIGURE 39. MAGNETIC COUPLING TO ABSORBING SAMPLE

$$\frac{R_a(\omega)}{R_0} = \frac{4\pi\omega L_0 \xi X''(\omega)}{R_0} = 4\pi \xi Q_0 X''(\omega) \quad (151)$$

where $Z_a = R_a + jX_a$. The real part of Z_a is proportional to X'' and is selectively saturable, as is X'' . The imaginary part of Z_a , like X' , is not selectively saturable.

To couple effectively to the absorbing sample, the parameter $\omega L_0/R_0$ should be large. This quantity is the unfilled Q of L_0 and will hereafter be denoted Q_0 . The magnitude of R_a/R_0 will now be calculated using the following typical values in Equation 151

$$\xi = 1/2$$

$$Q_0 = 300$$

$$f = 30 \text{ Mc}$$

$$B = 3 \text{ kc centered at } 30 \text{ Mc}$$

$$T = 293^\circ\text{K}$$

$$\gamma^2 H_1^2 T_1 T_2 \ll 1 \text{ (below saturation)}$$

$$N_0 = 6.5 (10^{22}) \text{ protons/cc (for a typical hydrocarbon liquid)}$$

$$\frac{R_a}{R_0} = 9.5 (10^{-3})$$

This small fractional impedance change shows that coupling to the spin system is rather weak. This weak coupling is a central problem in limiter development since, as will be shown in the next section, weak coupling leads to high insertion loss. Without changing material, the most effective way to improve this coupling appears to be by cooling the absorbing sample. As can be seen from Equations 145 and 146, a reduction in temperature, T , by a certain factor will cause an increase in both X' and X'' by the same factor; hence, an increase in Z_a/R_0 . Cooling to liquid nitrogen temperature, for example, would increase Z_a/R_0 by a factor of 3.8. The major difficulty in operating at these temperatures lies in finding an absorbing substance with sufficiently long T_2 . Since long transverse relaxation times are found only in liquids, the absorbing material must have an extremely low freezing point. Propane offers promise as an absorber at low temperatures with a freezing point of 86°K. This freezing point might be lowered still further by the addition of a dissimilar organic substance.

A significant improvement in coupling can be realized with a special cooling method known as electron pumping or dynamic polarization (References 1 and 7). This method (discussed later) uses an absorbing sample exhibiting both proton and electron spin resonance (liquid ammonia with dissolved sodium, for example). If the electron spin system is saturated using a microwave source, it is found that the effective temperature of the proton spin system may be

greatly reduced, increasing Z_A/R_0 by a factor as great as 480. Such an improvement would substantially reduce limiter insertion loss. For this reason, it is proposed that a study of the electron-pumped limiter be undertaken as part of the first-year program.

APPENDIX IX - LIMITING CHARACTERISTICS

The frequency-selective limiter circuit is basically an rf bridge, one arm of which contains an absorbing substance. To ensure symmetry, the opposing bridge arm is constructed identically, even to the point of containing a substance identical to that of the absorbing arm. The only difference is that this dummy arm is not immersed in a d. c. magnetic field. A typical limiter circuit is shown in Figure 40.

In analyzing the limiter circuit, as few restrictions as possible will be imposed on the exact circuit configuration used. In a later section, the analysis will be restricted to specific circuits, and numerical results will be obtained.

Figure 41 depicts a general bridge circuit with a generator of internal impedance, R_g , connected to the input port, and with a load resistance, R_L , connected to the output port. Such a two-port circuit will possess a voltage transfer function, $A(\omega, Z_u)$, that is a rational function of both frequency, ω , and the imbalance impedance, Z_u , introduced in one arm.

$$A(\omega, Z_u) = \frac{V_L(\omega, Z_u)}{V_g} \quad (152)$$

Expanding $A(\omega, Z_u)$ in a power series in Z_u about the point $Z_u = 0$ yields:

$$A(\omega, Z_u) = A(\omega, 0) + \left. \frac{\partial A}{\partial Z_u} \right|_{Z_u=0} Z_u + \frac{1}{2} \left. \frac{\partial^2 A}{\partial Z_u^2} \right|_{Z_u=0} Z_u^2 + \dots$$

The first term in this series is identically zero. This follows from the definition of Z_u . If the imbalance impedance is zero, the bridge must be balanced; hence $A(\omega, 0) = 0$. If Z_u is sufficiently small, $A(\omega, Z_u)$ can be approximated accurately by the second term in the above series, from which the overall insertion loss can be calculated as follows:

$$\begin{aligned} L &= \frac{\text{Available Generator Power}}{\text{Power Dissipated in } R_L} \\ &= \frac{V_g^2 / 4 R_g}{|V_g A(\omega, Z_u)|^2 / R_L} \\ &= \frac{R_L}{4 R_g \left| \frac{\partial A}{\partial Z_u} \right|_{Z_u=0}^2 |Z_u|^2} \end{aligned}$$

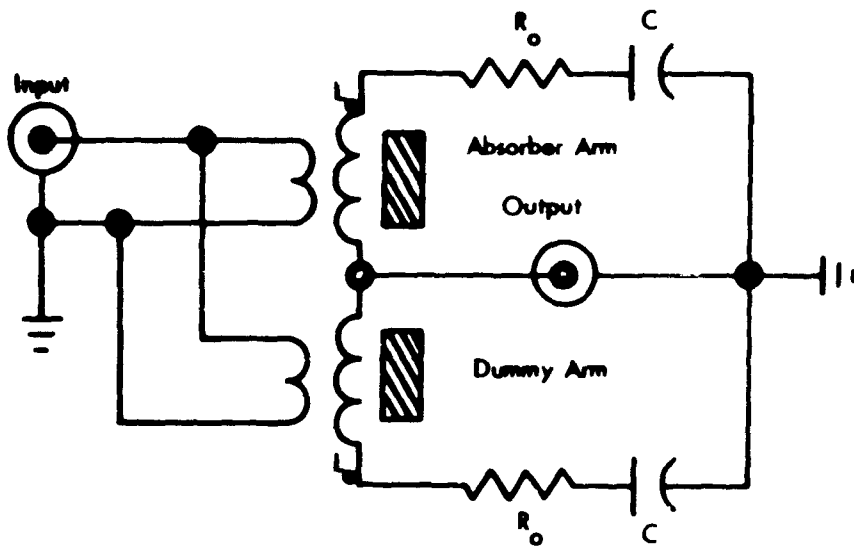


FIGURE 40. TYPICAL LIMITER CIRCUIT

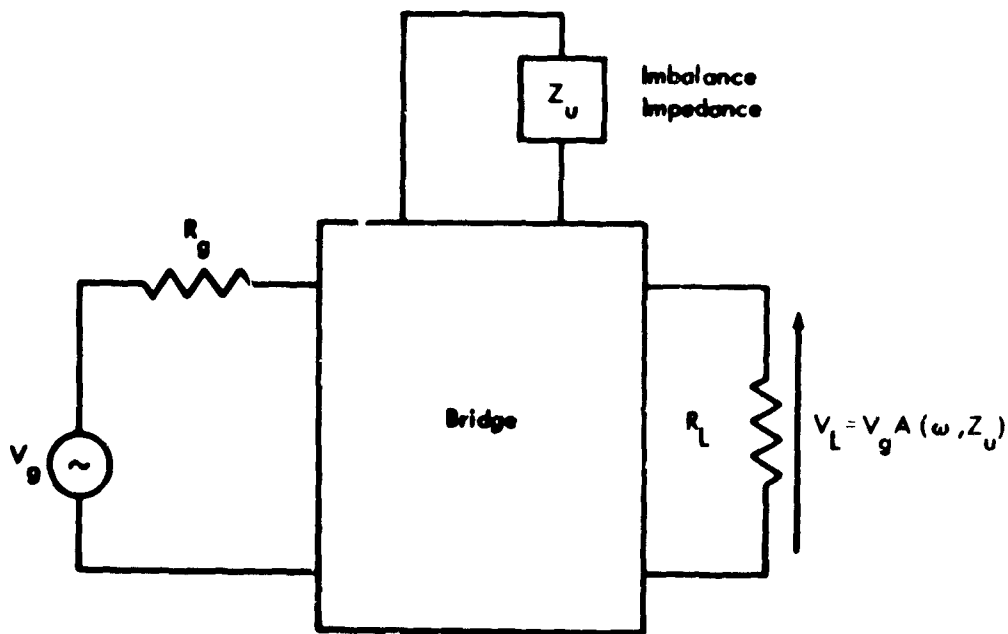


FIGURE 41. GENERAL BRIDGE CIRCUIT

This is a convenient form for L in that all imbalance effects, whether due to proton resonance or simply to imperfect bridge construction, are lumped in the factor $\frac{1}{|Z_u|^2}$. The factor $\frac{R_L}{4R_g \left| \frac{\partial A}{\partial Z_u} \right|_{Z_u=0}^2}$ is a function of frequency only and independent of Z_u .

To obtain selective limiting action over the entire bandwidth, bridge imbalance should depend only on R_B (i.e., $Z_u = R_B$). This condition can be met only if the effect of the imaginary part of Z_B is somehow cancelled. The details of how this effect can be cancelled will be deferred until later in this Appendix. For now, it will be assumed that bridge imbalance is due to both R_B and X_B , so that insertion loss is given by

$$L = \frac{R_L}{4R_g \left| \frac{\partial A}{\partial Z_u} \right|_{Z_u=0}^2 |Z_B|^2} \quad (153)$$

L may be written alternately as

$$L = L_0 \left| \frac{X_B''}{X'' + jX'} \right|^2 \quad (154)$$

L_0 and X_B'' are the small-signal values of L and X'' at midband, where $X' = 0$. Setting $f = 1/2 (f_1 + f_2)$ (midband),

$$L_0 = \frac{R_L}{4R_g \left| \frac{\partial A}{\partial Z_u} \right|_{Z_u=0, f = \frac{1}{2}(f_1 + f_2)}^2 |R_B|^2} \quad (155)$$

and, from Equation 146,

$$X_B'' = \frac{2N_0 \gamma^2 B^2 f}{8kTB} \quad (156)$$

It has been assumed in the derivation of Equation 154 that the quantity

$$\left. \frac{\partial A(\omega, Z_u)}{\partial Z_u} \right|_{Z_u=0}$$

is constant over the limiter bandwidth, so that it may be replaced by its midband value (as in Equation 155). This assumption is valid, provided the bandwidth of the bridge circuitry is much greater than the actual limiter bandwidth, B .

All experimental circuits constructed to date have met this requirement, the latest model having $B = 10$ kc with a bridge bandwidth of 150 kc.

The field, H_1 , within the absorbing coil will be proportional to the generator voltage, V_g , except for the small nonlinear perturbation in coil impedance due to proton resonance. To a good approximation, then, the parameter $1/4 \gamma^2 H_1^2 T_1 T_2$ will be proportional to available generator power, P_g .

$$P_g = P_{sat} \frac{1}{4} \gamma^2 H_1^2 T_1 T_2 \quad 157$$

The constant of proportionality, P_{sat} , will be referred to as the saturation power, since the condition $P_g = P_{sat}$ is equivalent to the saturation condition for X'' (see Equation 147).

Using Equations 146, 154, and 157, and assuming X' to be constant (unsaturated), output power can be found as a function of input power:

$$P_L = \frac{P_g}{L} = \frac{P_g}{L_s} \left[\frac{1}{1 + \frac{P_g}{P_{sat}}} \cdot \left(\frac{X'}{X''} \right)^2 \right] \quad 158$$

Equation 158 is plotted in Figure 42 for various values of the ratio X'/X'' . These curves show that best limiting action is obtained when X'/X'' is small. Because X' cannot be saturated at reasonable power levels, it causes a bridge imbalance, and leak-through results.

In addition to causing leak-through, uncompensated X' will also produce power-dependent phase shift. The first-order expansion of the voltage transfer function is

$$A(\omega, Z_a) = \left. \frac{\partial A}{\partial Z_u} \right|_{Z_u = 0} Z_a$$

If $\left. \frac{\partial A}{\partial Z_u} \right|_{Z_u = 0}$ can be considered constant over the limited bandwidth, phase

shift will be equal to the angle of the complex absorption impedance, Z_a . Z_a is proportional to $X' + jX''$; therefore, the phase shift angle, θ , must be given by

$$\theta = \tan^{-1} \frac{X'}{X''}$$

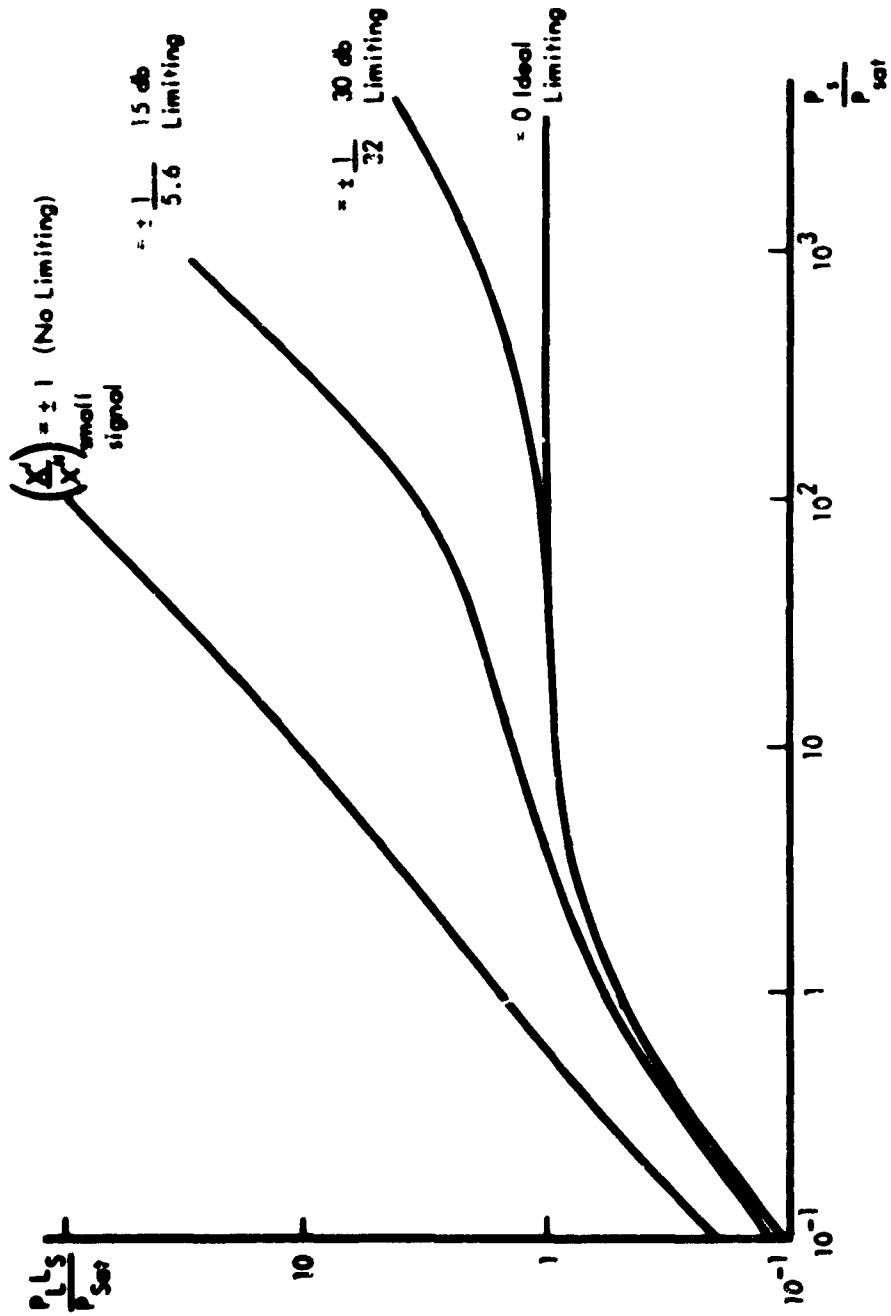


FIGURE 42. NORMALIZED OUTPUT POWER VS NORMALIZED INPUT POWER FOR VARYING DEGREES OF REACTIVE BRIDGE IMBALANCE.

Using Equations 146 and 157, θ can be written as a function of P_B .

$$\theta = \tan^{-1} \left[\frac{X'}{X_B} \sqrt{1 - \frac{P_B}{P_{sat}}} \right] \quad (159)$$

As shown in Figure 43, this phase shift is smallest when X'/X_B is small and increases with input power level. The maximum phase shift that can occur is 90 degrees.

The bridge imbalance attributable to X' is a result of the difference in saturation level of X' and X'' . X' saturates at a significantly higher level because of the broadness of the contributing proton line shapes. Saturation of X' at any frequency corresponds to the saturation of X'' throughout the entire volume; moreover, the bridge will not be balanced when selective saturation of X'' is obtained. The deleterious effect of X' can be minimized by two methods

- 1) Cancellation of X' after AM detection.
- 2) Reduction of X' through sample shaping.

The first technique uses a bridge circuit with a relatively large imbalance resistance in one arm. If this resistance is denoted by R_u , total imbalance impedance will be

$$Z_u = R_u + 4\pi \xi Q_0 R_0 X'' + j 4\pi \xi Q_0 R_0 X'$$

Since bridge output voltage is proportional to Z_u , the detected output will be proportional to $|Z_u|$. If $R_u \gg 4\pi \xi Q_0 R_0 X''$, $4\pi \xi Q_0 R_0 X'$, then $|Z_u| \approx R_u + 4\pi \xi Q_0 R_0 X''$.

Thus, the detected output is independent of X' for large resistive imbalance. The detected bridge output voltage, proportional to Z_u , contains an undesired component due to R_u . This term can be eliminated by subtracting from the detected bridge output a second unlimited, detected output of magnitude just sufficient to cancel the leak-through due to R_u . If this is done, the final output will be proportional to X'' and will display frequency selective limiting action. This technique results in loss of phase information.

The second technique uses sample shaping techniques to minimize X' , and involves no loss of phase information. By careful control of field inhomogeneity and sample shape, the distribution function, $g(f_0)$, can be altered, and, in turn, X' and X'' will be altered. To minimize the effect of X' while maintaining a relatively strong absorption, the ratio X'/X_B should be minimized. The degree to which this ratio must be minimized depends on the limiting range desired. For example, Figure 42 shows that a minimum limiting range of 15 db will be obtained for $X'/X_B < 1/5.6$. If a 30-db range is desired, X'/X_B must be less than $1/32$. In the case of the uncompensated limiter, the effect of these

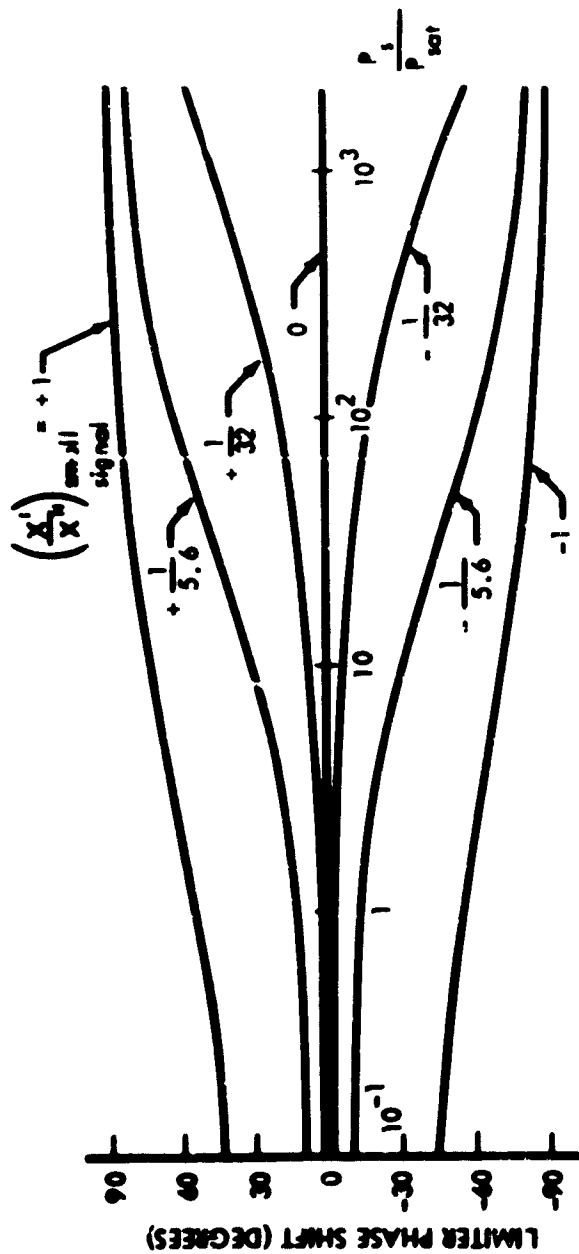


FIGURE 43. PHASE SHIFT VS NORMALIZED INPUT POWER FOR VARYING DEGREES OF REACTIVE BRIDGE IMBALANCE

restrictions is to reduce usable bandwidth. Figure 36 shows that the criterion $X'/X_0'' < 1/5.6$ is satisfied by the uncompensated limiter over only a small range of frequencies near band center. This usable range is approximately 0.25 B, so that 75 percent of the total bandwidth is wasted in this case.

A good portion of this wasted bandwidth can be regained through sample shaping techniques. As an illustration of this method, consider the distribution function shown in Figure 44 (solid line). The uncompensated rectangular distribution function assumed in the preceding appendixes is also shown in Figure 44 (dotted line) for comparison. The new distribution function has "rabbit ears" positioned near the band edges, which give rise to compensating reactances. X' and X'' can be calculated exactly for this distribution using Equations 141 and 142. It is found that the relation $X'/X_0'' < 1/5.6$ is satisfied over a range of frequencies of 0.5 B. This represents an increase in usable bandwidth over the uncompensated case by a factor of 2. The form assumed in Equation 44 was chosen arbitrarily and by no means represents an optimum case. A theoretical investigation into the optimum form for $g(f_0)$ is to be made as part of the proposed program.

Figure 45 shows one possible means of obtaining the "rabbit ear" distribution function. As shown in this figure, the absorbing liquid is contained in a rectangular resonator that can be recognized as a foreshortened, capacitively loaded, transmission line section. An inhomogeneous d.c. field is applied parallel to the center conductor axis. The strength of this field increases linearly in the direction of the long dimension of the resonator, yielding a distribution of protons versus field strength that is greatest in the low- and high-strength regions and somewhat reduced in the intermediate-strength region. Recalling the linear relationship between field strength and Larmor frequency, this gives a distribution function of the form shown in Figure 44, which is greatest in the low- and high-frequency regions.

$g(f)$ = Number of Resonant Particles per
Unit Frequency Interval per Unit Volume

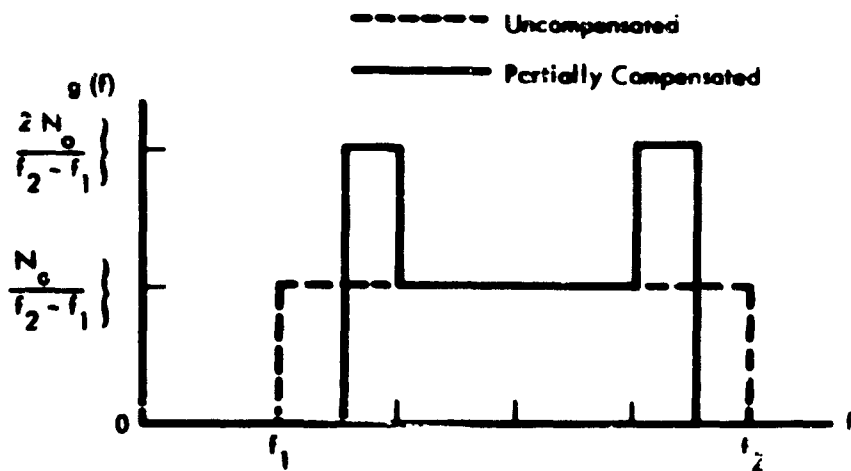
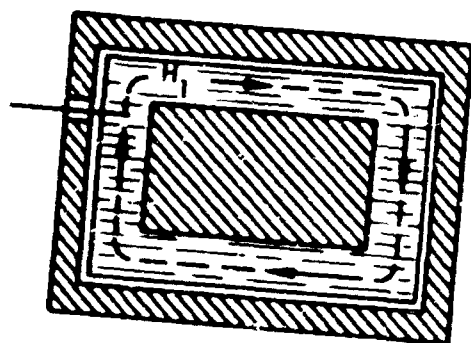


FIGURE 44. EXAMPLE DISTRIBUTION FUNCTION GIVING PARTIAL
COMPENSATION OF X'



SECTION A-A

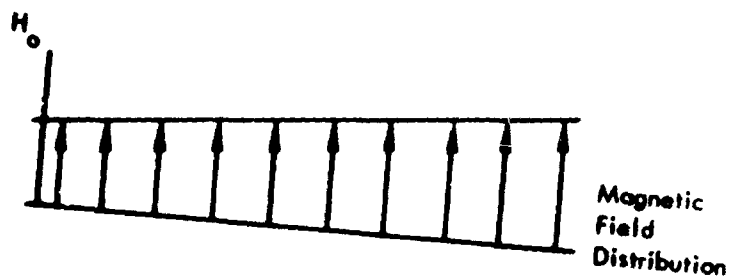
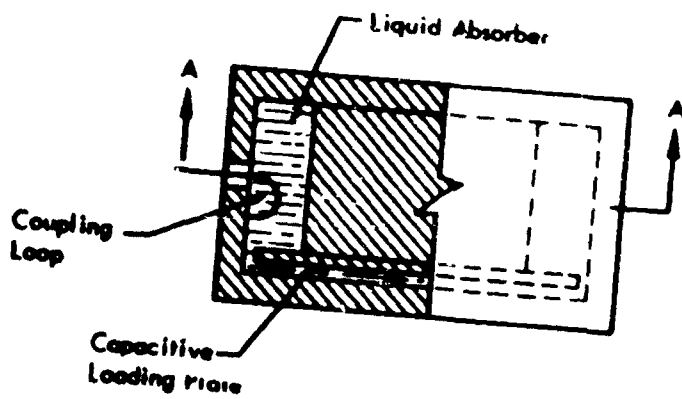


FIGURE 45. RESONATOR ASSEMBLY GIVING THE DISTRIBUTION FUNCTION OF FIGURE 44

APPENDIX X — SATURATION LEVEL

Saturation of the limiter begins as available input power, P_a , approaches the saturation power, P_{sat} . As defined, P_{sat} is a constant of proportionality between P_a and $1/4 \gamma^2 H_1^2 T_1 T_2$. H_1^2 is directly related to the power dissipated in the spin system by the expression

$$\text{Power Dissipated in Spin System} = P_a = \xi \omega X'' H_1^2 V,$$

where V is the volume of the absorber coil. P_a , in turn, is related to the power dissipated in R_o by the ratio R_a/R_o :

$$P_a = \frac{R_a}{R_o} P(\text{dissipated in } R_o). \quad (160)$$

For $R_a \ll R_o$, the power dissipated in R_o is (see Figure D-1):

$$P(\text{dissipated in } R_o) = I^2 R_o = \frac{V_R'}{R_g' + R_o}{}^2 R_o = P_{in} \frac{2 R_g' R_o}{(R_g' + R_o)^2}$$

Combining this result with Equation 160, the desired connection between P_a and H_1^2 is obtained:

$$H_1^2 = \frac{P_a}{\xi V \omega X''} \frac{2 R_g' R_o}{(R_g' + R_o)^2}$$

Substituting for R_a from Equation 151 gives

$$H_1^2 = \frac{P_a}{V \omega} \frac{2 R_g' R_o Q_o}{(R_g' + R_o)^2}$$

Finally, using Equation 157:

$$P_{sat} = \frac{2 V (R_g' + R_o)^2}{R_g' R_o Q_o \gamma^2 T_1 T_2}$$

When R_g' is adjusted to give minimum insertion loss ($R_g' = 1/2 R_o$), P_{sat} is given by

$$P_{sat} = \frac{9 \omega V}{Q_o \gamma^2 T_1 T_2} \quad (161)$$

Equation 162 is valid only for the case of high insertion loss. For $f = 30$ Mc, $V = 5$ cc, $Q_0 = 300$, and $T_1 = T_2 = 1$ second, as is common in many hydrocarbon liquids.

$$P_{\text{sat}} = 0.04 \text{ erg/sec, or } -54 \text{ dbm}$$

This is a much lower saturation level than is obtainable in ferrite limiters. Low saturation levels such as this are essential, however, if the limiter is to serve its function of reducing large interfering signals to the level of weaker desired signals. P_{sat} can be controlled over a wide range through suitable choice of T_1 and T_2 . An upper limit is set on P_{sat} by the degree of selectivity desired and the allowable absorber volume. Taking 100 cps as the largest useful selectivity, and 50 cc as the largest practical absorbing volume, maximum P_{sat} will be on the order of -4 dbm at 30 Mc with $Q_0 = 300$.

Lowest values of P_{sat} will be achieved using nonviscous liquids such as benzene. Benzene has $T_1 = T_2 = 20$ seconds and will have a saturation power on the order of -40 dbm. One difficulty in attaining such low saturation levels as this will be the presence of convection currents and molecular diffusion in the absorbing sample. These matter-transport mechanisms make it difficult to obtain local saturation of the sample because of the continuous replacement of saturated spins with unsaturated ones. The net effect of either diffusion or convection would be to increase P_{sat} and, at the same time, to reduce selectivity because the fraction of saturated sample volume is increased. For a completely stationary absorber, the fraction of volume saturated for input powers on the order of P_{sat} will be approximately $1/\pi T_2 B$. Matter transport will become important when the rate of spin replacement approaches the thermal relaxation rate, $1/T_1$. Equivalently, it may be said that P_{sat} will be significantly increased if an appreciable number of molecules leave the fractional volume $V/\pi T_2 B$ within a time interval of T_1 seconds. For benzene, with $B = 3$ kc, this fractional volume is on the order of $V/180,000$, and T_1 is approximately 20 seconds, so that ordinary convection currents are important. To combat convection and diffusion effects, the liquid absorber can be trapped in a porous nonparamagnetic substance that inhibits long-range fluid motion. This measure is only necessary, however, when long relaxation times are used.

APPENDIX XI — SELECTIVITY AND INTERMODULATION

If a strong signal above threshold is applied to either a diode or parametric limiter, the response of the limiter to other signals is disabled over the entire passband. The response of a frequency selective limiter, on the other hand, is disabled only for frequencies in the immediate vicinity of the strong signal. The minimum frequency separation that can exist between a small and large signal without interaction of the two is referred to in this proposal as the limiter selectivity.

Intermodulation will occur whenever the protons that resonate at the frequency of one signal are saturated by an adjacent large signal. If f is the frequency of the large signal, protons with resonant frequencies within $1/2$ linewidth of f will experience appreciable saturation. From Equation 140 it can be seen that the half linewidth is $1/2\pi T_2 \sqrt{1 + \frac{1}{4} \gamma^2 H_1^2 T_1 T_2}$ cps; this quantity, then, is the limiter selectivity. Using Equation C-6, the selectivity becomes:

$$\text{selectivity} = \frac{1}{2\pi T_2} \sqrt{1 + \frac{P_s}{P_{\text{sat}}}}$$

At saturation, selectivity will be on the order of $1/2\pi T_2$, and will increase slowly as P_s increases, becoming proportional to $\sqrt{P_s}$ for $P_s \gg P_{\text{sat}}$.

The most important parameter in determining selectivity is T_2 , the transverse relaxation time. For $T_2 = 1$ second, selectivities on the order of a few cycles may be expected. This extremely small figure becomes quite noteworthy when compared with the selectivity of the ferrite limiter, which is on the order of megacycles.

A quantitative analysis of intermodulation is to be undertaken as part of the 7-month program. It is proposed to study the interaction (in the limiter) of two signals as a function of frequency separation and signal strength. The analysis should reveal the degree of signal suppression due to an adjacent saturating signal and should also disclose the frequency and amplitude of intermodulation products.

APPENDIX XII—NOISE FIGURE OF THE LIMITER

Since the frequency selective limiter is essentially a passive element, the available output noise is essentially kTB , where T corresponds to the limiter temperature when no noise is supplied to the input terminals. The noise figure is then

$$F = \frac{\text{available noise output (with } kTB \text{ at input)}}{kTB \text{ (gain of limiter)}}$$
$$= \frac{kTB}{kTBG_1} = \frac{1}{G_1} = L_s$$

In cascade with a second stage, the overall noise figure becomes

$$F_{12} = F_1 + \frac{F_2 - 1}{G_1} = L_s + L_s F_2 - L_s = L_s F_2$$

$$(F_{12})_{db} = (L_s)_{db} + (F_2)_{db}$$

The overall noise figure of two stages (F_{12}) is the sum in decibels of the insertion loss of the limiter as first stage and the noise figure (F_2) of the second stage.